ÉCOLE POLYTECHNIQUE
FÉDÉRALE DE LAUSANNE

January 2018

Master Project report

Land cover classification of the semi-arid Namibian savanna

BACCHILEGA Beatrice
Master in Environmental Engineering and Science
Specialization: Monitoring and Modeling of the Environment

Supervision: Dr. JOOST Stéphane & PARKAN Matthew
Expert: Dr. REINHARD Friedrich

ABSTRACT

The vegetation of semi-arid savanna landscapes relies on the fragile equilibrium between rainfall, grazing and fires [Trodd and Dougill, 1998]. For a sustainable management of their farms, farmers need to take into account this delicate equilibrium and correctly balance the amount of animals and the available food and water resources. These two quantities are estimated every year at the end of the growing season (end of May) to define the yearly management plans [Reinhard, 2017].

Ground based techniques for animal counting and biomass estimation are long and time consuming processes that can hardly provide a good coverage of the farm [Reinhard, 2017]. Farmers are now more and more looking towards remote sensing techniques to overcome the field work and achieve both these tasks.

The main goal of this project was to classify the soil cover in Kuzikus Wildlife Reserve, in the north-eastern Kalahari region of Namibia, in order to provide an estimate of the food availability for wildlife at the end of the growing season. Ultra-high resolution UAV images and coarse resolution satellite images were classified using both supervised and unsupervised classification techniques.

Random Forest and Support Vector Machine supervised classifiers gave encouraging results and the research showed the great potential of UAV and satellite imagery for biomass estimation. Used together, these two complementary types of data allow to have both a detailed plant species recognition and a general overview of the study area.

ACKNOWLEDGMENTS

I would like to thank Stéphane Joost, for the supervision of the project and advice on the drafting of the report, and Friedrich Reinhard, manager of Kuzikus Wildlife Reserve, for the precious information about wildlife management and flora in the reserve.

Many thanks go to Matthew Parkan, who also supervised the project and gave suggestions about the most appropriate algorithms and analysis to perform and valuable programming advice.

A special thanks goes to Drone Adventures, without which I would not have had the opportunity to go to Kuzikus Wildlife Reserve to collect part of the data of the project and live a unique experience.

I am also grateful to the Kuzikus' staff for the warm welcome in the reserve. In particular to Gous Gammo Divia, the San [Boden, 2009] who guided us around for the mappings and gave valuable information about animals' life and behavior.

I would also like to thank the SAVMAP consortium, who provided part of the dataset.

A final thanks go to the LASIG laboratory for welcoming me into their team and the chats during the morning breaks.

CONTENTS

CHAPTER 1

INTRODUCTION

1.1 Context and Problematics

Semi arid savannas are ecoregions that mostly develop in regions with hot semi arid climates in the tropics and subtropics. They are most commonly found in Africa, South Asia and Australia, but also in some areas of Europe, North and South America. Those regions are characterized by hot summers, warm to cold winters and few precipitation [Peel et al., 2007]. Because of this particular climate, herbaceous vegetation dominates, with some scattered shrubs and trees.

Semi-arid savannas vegetation relies on the fragile equilibrium between rainfall, grazing and fires [Trodd and Dougill, 1998]. After each rain season, vegetation regrows and is grazed by animals. During the dry season, it can be destroyed by occasional fires. Shrubs are a stable and resistant type of vegetation which usually wins the competition against grasses [Trodd and Dougill, 1998]. After fires, though, grasses recover faster, which helps maintaining the equilibrium between the two.

While rainfall and fires act mostly on the short term, grazing can affect the dynamics of the vegetation on the long term and break this equilibrium.

When in the late 1800's Europeans settled in the tropics and sub-tropics, they introduced domestic cattle and sheep [Walker et al., 1981]. The introduction of those mammals, whose population rapidly increased and exceeded the maximum size sustainable by the environment (carrying capacity), significantly reduced the number of indigenous mammalian herbivores and their predators [Walker et al., 1981].

These events caused radical changes in the vegetation of the semi-arid savannas. Cattle and sheep do not eat shrubs and prefer perennial grasses. The overstocking of those mammals and the fencing of farms caused high grazing pressure. Together with sufficient rain and reduction of the frequency of fires, this led to a decrease in the perennial grasses cover, in favor of annual grasses and shrubs. Even with a significant decrease of grazing pressure, the reestablishment of perennial grasses may take decades [Walker et al., 1981],[Joubert et al., 2008].

The phenomenon of "excessive expansion of bush at the expense of other plant species, especially grasses" [De Klerk, 2004] is called *bush encroachment*. It causes an "imbalance of the grass:bush ratio, a decrease in biodiversity, and a decrease in carrying capacity" [De Klerk, 2004].Trodd and Dougill [1998] recognize it as "the most widespread ecological problem affecting semi-arid range lands utilized for cattle grazing". The increase in domestic livestock, poor range land management practices and the exclusion of occasional fires are the most important causes that contributed to this phenomenon. The decrease in wild herbivores populations (indigenous browsers and grazers), replaced by livestock, and the consequent increase of pressure on the grass layer created a favorable environment for bushes and shrubs. Perennial grasses lost their com-

petitive advantage [De Klerk, 2004]. Moreover, the introduction of domestic livestock pushed farmers to suppress fires, which used to play an important role in maintaining the equilibrium of semi-arid savannas vegetation [De Klerk, 2004]. As grass recovers faster than shrubs, one tool to reestablish the equilibrium could be controlled fires [Joubert et al., 2008]. Grasses use water in the top soil layers, while bushes and shrubs the one in deeper layers. In overgrazed areas, the lower grass cover allows water to easily percolate in the deeper soil layers, favoring bush encroachment [Reinhard, 2017]. In Namibia, this phenomenon is estimated to affect up to 45 millions ha of land with negative consequences on agricultural productivity and groundwater [De Klerk, 2004]. The central, eastern and north-eastern regions are the most affected. Blackthron (*Acacia mellifera*), Sickle bush (*Dichrostachys cinerea africana*) and Three thorn (*Rhigozum trichotomum*) are the main species causing bush encroachment.

Farmers need to take into consideration this delicate equilibrium between vegetation and grazing for a sustainable management of their farms. Two points are important, in particular for wildlife farms: a) Estimating the carrying capacity (i.e. available food and water resources) and b) Estimating wild animal population numbers by species.

Every year, at the end of the growing season (end of May), farmers estimate the fodder availability for the year and consequently adapt their management plan. They have to pay attention to correctly balance the amount of wildlife and the food available. If the food and water resources are not enough, three choices are available to maintain the balance: translocate animals to other areas, hunting or introducing predators [Bothma and Toit, 2010].

Estimating the amount of food and animals is a long and complicated task. Ground-based analysis can hardly provide a good coverage of the spatial patterns of the vegetation and animal counting is often done using an helicopter, causing disturbances to the wildlife [Reinhard, 2017]. The use of remote sensing is a new promising technique to help farmers achieving both this tasks. Thanks to airborne imagery, it is possible to get a high spatial and temporal cover of large areas in relatively short time and without the need to directly access them.

Amongst these new possibilities, satellite imagery is freely available at resolutions down to 10-15 meters and provides a good overview of the temporal evolution of the land cover over the 30 past years. It can be useful to provide a general understanding of land cover change dynamics and help estimate the quantity of fodder available for the next year [Reinhard, 2017]. For more precise analysis, commercially available low altitude Unmanned Aerial Vehicles (UAV) can be used to produce very high resolution (sub-decimeter) imagery. The use of UAVs can be combined with sensors like RGB, multispectral, hyperspectral or thermal in order to retrieve different information from images. However, their limited endurance restricts them to map much smaller areas than those that can be covered with manned aircrafts or satellites. More and more studies are being developed on how to use satellite or UAVs imagery for quality and quantity of forage estimation or animal counting [Ramoelo et al., 2012], [Rey et al., 2017]. The information obtained from these two types of imagery is complementary.

Farmers are more and more interested into these new technologies. Kuzikus Wildlife Reserve, in Namibia, for example, is part of a project that aims at developing an innovative land monitoring strategy using ultra-high resolution photographic imaging from drones [SAVMAP, 2017].

1.1.1 Kuzikus Wildlife Reserve

In the south-eastern Kalahari region of Namibia, Kuzikus Wildlife Reserve has been for over 70 years a cattle and sheep natural reserve (figure 1.1). Since 1964, it was one of the first farms to slowly restore into a wildlife reserve by reintroducing locally extinct species and allowing wild animals to reproduce. Today, this 10,300 ha large reserve (figure 1.2), is a hot spot for ecological integrity and biodiversity and hosts more than 3000 individuals from more than 40 mammals and reptiles species, more than 90 insects species and 200 birds species [Kuzikus, 2017], [Kuzikus,

2018].

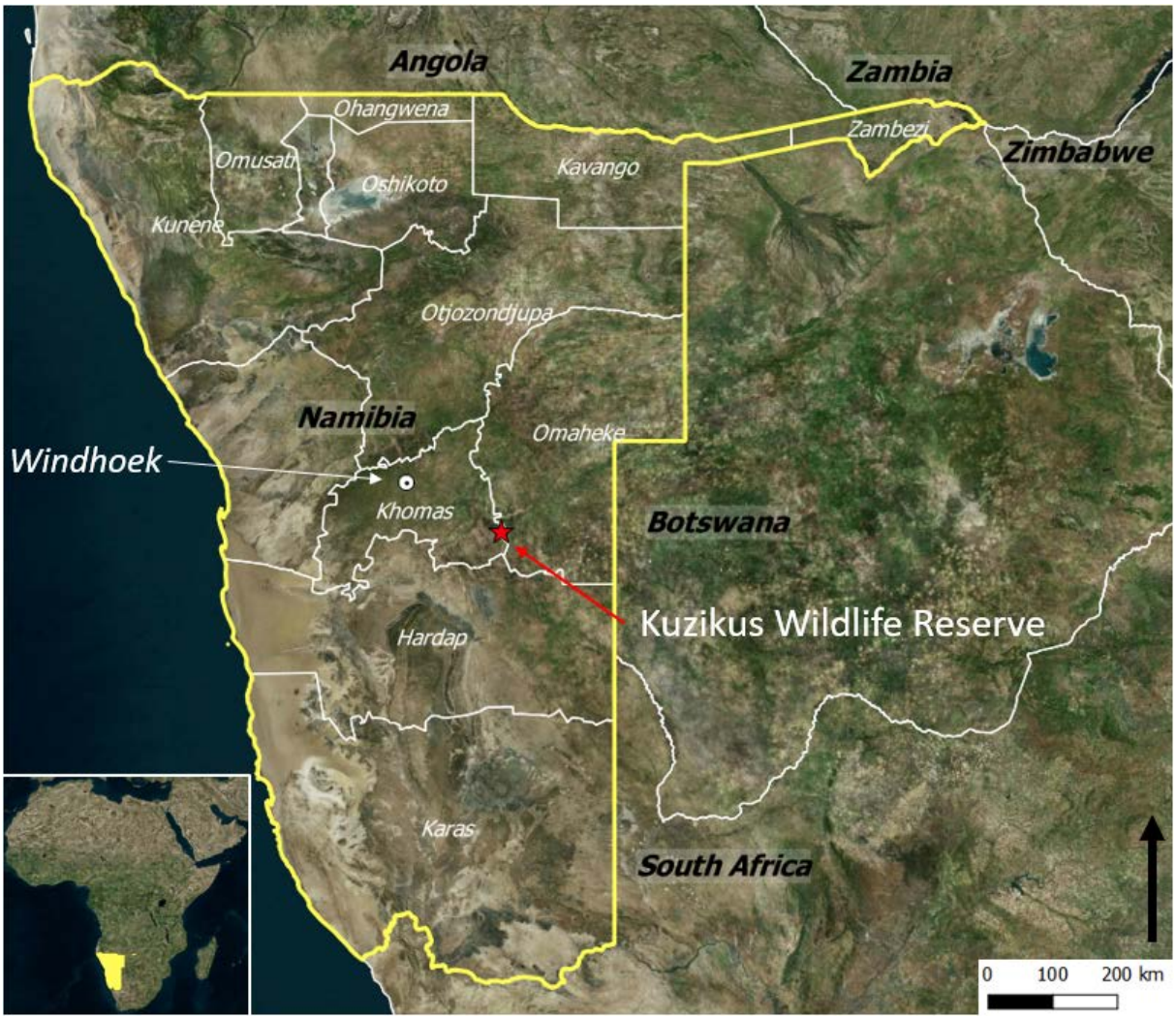

Figure 1.1: Location of Kuzikus Wildlife Reserve, in Namibia [DigitalGlobe, 2018], [Hijmans, 2018]

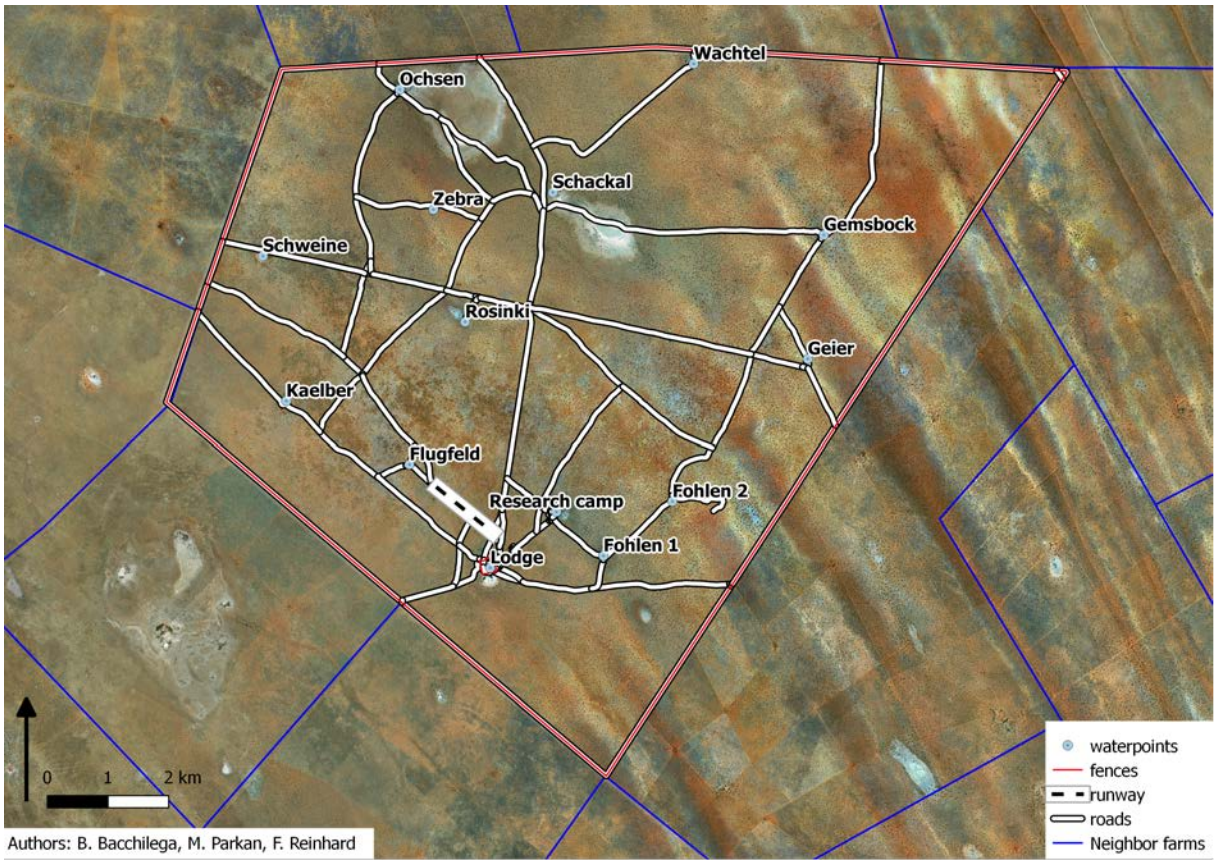

Figure 1.2: Kuzikus Wildlife Reserve [DigitalGlobe, 2018], [SAVMAP, 2017]

1.1.2 Animal-Vegetation relations

In Kuzikus, animals are not fenced within the reserve. It these conditions, it is difficult to establish a good strategy for grass cover and farmers need to constantly control the game number by "mimicking the function of predators and droughts [Kuzikus, 2018]. This, other than being a sustainable way of meat production, helps avoiding overgrazing and maintaining the equilibrium between food and animals [Reinhard, 2017], [Kuzikus, 2018], [Robinson and Bennett, 2004].

We can distinguish between three types of animals:

- Pure grazers: eat only grass. Some examples are the Burchell's Zebra (*Equus quagga burchellii*), the Gnu (*Connochaetes gnou and C. taurinus*), the Blesbok (*Damaliscus albifrons*) and the Hartebeest (*Alcelaphus buselaphus*).
- Pure browsers: eat only bushes, trees and trunks. Between them, the Greater Kudu (*Tragelaphus strepsiceros*), the Giraffe (*Giraffa camelopardalis giraffa*) and the Black Rhinoceros (*Diceros bicornis bicornis*).
- Both grazers and browsers, like the Common Eland (*Taurotragus oryx*), the Springbok (*Antidorcas marsupialis*), the Gemsbok (*Oryx gazella*) and the Impala (*Aepyceros melampus*).

Most of the animals in the reserve are pure grazers or both grazers and browsers. Thus, it is important to correctly estimate the available amount of grass at the end of the rain season (January-May).

Grasses can be annual or perennial and have different roles in the diet of the animals. Figure 1.3 shows their phenological stages. Perennial grasses are the most important plants for grazers. They survive droughts, live more than one year and just need some humidity to start getting

green. This generally happens at the beginning of October, at the end of the dry season (May-December). Their peak is in April. This rapid growth at the beginning of the rain season gives them an advantage over annual grasses [van Langevelde et al., 2016].

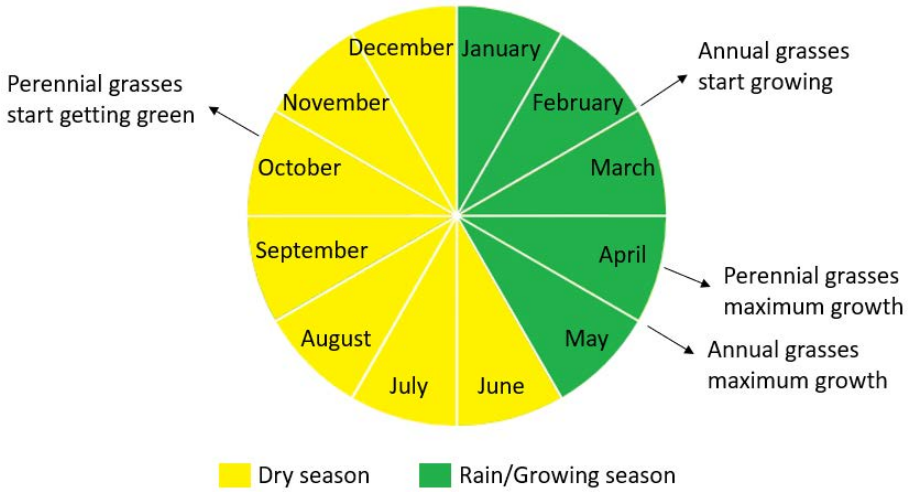

Figure 1.3: Phenological stages of perennial and annual grasses [Bacchilega, 2018].

Perennial grasses put energy in the roots, growing slowly and forming a strong root system. They are sensitive the first year and the more they grow, the more resistant they become. The Long-awned grass (*Aristida stipitata*) (figure 1.4a) is an abundant and nutritious grass. The best perennial plant that can be found in Kuzikus is the Silky Bushman grass (*Stipagrostis uniplumis*) (figure 1.4b). This plant is good for cattle and sheep and also beneficial for wildlife. It is rare because it is the first to be eaten by animals.

(a) The Long-awned grass **(b)** The Silky Bushman grass

Figure 1.4: a) The Long-awned grass (*Aristida stipitata*) [Strohbach, 2014] and (b) The Silky Bushman grass (*Stipagrostis uniplumis*) [Juergens, 2005].

Annuals plants, on the other hand, germinate year after year. They start growing in February/March, after a certain threshold of rain is reached, and are at their maximum height at the end of April/beginning of May. This type of plant put energy in the aerial structures, growing higher and faster than perennial plants. The Kalahari sourgrass (*Schmidtia kalahariensis*) is a nutritious annual grass for wildlife.

As animals prefer the fresh growing grasses than the older ones, it is difficult for them to grow high. Perennial plants die sooner if they are not grazed at all [Reinhard, 2017]. In low grazing pressure areas, the cover of perennial grasses is large, but when density of herbivores increases it decreases in favor of annual grasses. The seeds of perennial grasses germinate rapidly with the arrival of the first rains, but they have a low longevity. On the other hand, seeds of

annual grasses persist more in the ground, facilitating the transition from perennial to annual grasses [van Langevelde et al., 2016], [Tessema et al., 2016].

Grasses excepted, the Velvit raisin (*Grevia flava*) is a shrub that produces valuable food for animals and the Buffalo thorn (*Ziziphus mucronata*) is a nutritious tree [Reinhard, 2017].

1.2 Goal and objectives

The main goal of the project is to classify the land cover in Kuzikus, using a combination of satellite and aerial imagery, in order to provide a rough estimation of the quantity of food available for animals at the end of the growing season.

One part of the project concerns the analysis of ultra-high resolution images from UAVs. The main objectives for this part are:

- Differentiate trees, bushes and grasses from soil at the end of the growing season and at the end of the dry season with different classification algorithms.
- Use the classification results to estimate the forage quantity available for the wildlife in the same periods.

Another part of the project concerns satellite imagery. The main objectives for this part are:

- Classify two images - one at the end of the growing season and one at the end of the dry season - in order to differentiate grasses and higher vegetation from soil.
- Use the classification results to estimate the amount of grass in the reserve in those periods.
- Analyze the temporal evolution of the Difference Vegetation Index (DVI) in some areas of the reserve and one neighbor farm to detect some trends.

1.3 Methodology

Plant recognition on the ground is quite simple, but from remote images it is challenging. Depending on the image spatial resolution, it is possible to distinguish different patterns on the ground.

To distinguish trees and different species of bushes and grasses from ground, drone images taken in May 2015 with spatial resolutions between 3 and 7 cm are used. Three classification algorithms (K-means, Support Vector Machine and Random Forest) are tested using RGB (Red Green Blue) and NIR (Near infrared) images together with elevation data, vegetation indexes, principal component analysis (PCA) and textures to differentiate the classes over some small areas of the reserve. Then, the three classification methods are compared to manually delineated reference land cover classes and the results obtained from the best one used to estimate the forage quantity.

The distinction between perennial and annual plants is not straightforward when many plants are green, but this task is easier at the end of the dry season when only perennial plants start flowering and becoming green (figure 1.5). For this reason, a drone flight campaign was carried out in October 2017 with the aim of better differentiating those plants, in particular grasses.

Figure 1.5: Freshly green perennial grass in the typical red sand soil in Kuzikus Wildlife Reserve [Bacchilega, 2017]

The second type of data used is satellite imagery. Sentinel-2 images have a spatial resolution of 10 m (for bands B2, B3, B4 and B8) [ESA, 2017a], but one single image covers the whole extent of the reserve. This larger coverage allows to get a general overview of the vegetation cover in Kuzikus and the neighboring farms. One Sentinel-2 image dating May 2017 and one image dating October 2017 are used to classify the land cover in Kuzikus and estimate the amount of vegetation.

As the main advantage of satellite data is their high temporal resolution, another element of this research is to analyze the temporal evolution of the DVI over two and a half years (from August 2015 to November 2017). A few patches of grass and fields in Kuzikus and one neighbor farm are analyzed during the same period and compared with rain data measured on water points in Kuzikus and provided by the manager of the reserve [Reinhard, 2017]. Finally, the evolution of DVI for each pixel of the image is computed over one year (November 2016-November 2017).

At the end, drone and satellite results are compared to try to determine if some common and useful information can be extracted to facilitate the long term exploitation of satellite images to estimate the fodder quantity.

The structure of the report is the following: chapter 2 is a review of literature about vegetation classification and forage quantity estimation; chapter 3 describes the data; chapter 4 presents the methods used for classification, forage estimation and temporal analysis; chapter 5 illustrates the results and chapter 6 discusses them; chapter 7 concludes and gives perspectives for future works.

CHAPTER 2

STATE OF THE ART

2.1 Land cover classification

In the literature, different approaches to classify and map plant species can be found. These approaches can be applied to a range of images types with different spatial resolutions, number of spectral bands, radiometric resolutions and renewal periods. The use of high spatial resolution (sub-metric) imagery is the most common approach and many studies report satisfactory results [Michez et al., 2016]. The use of lower spatial resolution (decametric) imagery offers a good alternative solution when the patches of mapped species are bigger than the spatial resolution of the satellite image [Michez et al., 2016]. Many authors suggest that not only the spatial resolution is important, but that also the time period and phenological stage of the targeted plants play an important role in the classification [Michez et al., 2016].

When classifying different plant species, questions often arise about whether to use a pixel or an object based approach, which kind of algorithm is the best and which features help in the classification.

With the increase in spatial resolution, single pixels do not represent the characteristics of classification targets anymore. This causes the spectral variability inside the class to increase and the classification accuracy to decrease, causing the salt and pepper effect, where individual pixels are classified differently from their neighbors [Yu et al., 2006]. Object based classification techniques group similar pixels into homogeneous objects through segmentation, then classify objects instead of pixels. This approach allows to consider textural, shape and spatial relationships between pixels in addition to spectral information [Juel et al., 2015]. Many studies found that this technique improves the performances of classification [Juel et al., 2015],[Yu et al., 2006]. Yu et al. [2006], for example, used an object based approach to map 43 vegetation alliances over 72 ha in Point Reyes National Seashore, California, using high-resolution airborne remote sensing images from DAIS sensor.

Unsupervised classifiers define the class of belonging of pixels or segments according to similarity measurements, without needing examples of classes provided by the user. Supervised classifiers, on the other hand, use training data-sets to train the classifier and probability models to assign pixel or segments to a class [Mafanya et al., 2017]. Their ability to learn the characteristics of target classes from descriptors given by the user and to identify them in previously unseen data makes them more robust than unsupervised models [Belgiu and Drăguţ, 2016]. These two types of classifiers are compared in a study from Mafanya et al. [2017], who evaluated the accuracy of pixel and object based supervised and unsupervised classifiers for mapping *Harrisia Pomanensis* using 3.65 cm spatial resolution images from UAVs and found that object-based supervised methods gave the best accuracy.

Random Forest (RF) and Support Vector Machine (SVM) are popular supervised classifiers for remotely sensed data [Belgiu and Drăguţ, 2016]. Random Forest is well known because of its ability to handle high dimensional datasets [Michez et al., 2016], [Belgiu and Drăguţ, 2016], [Juel et al., 2015] and its high resistance to noisy variables [Michez et al., 2016], [Juel et al., 2015]. It uses a bagging technique (resample with replacement) to build a forest of classification trees with high variance among individual decision trees, becoming a stable and robust model insensitive to overfitting [Michez et al., 2016],[Belgiu and Drăguţ, 2016]. Moreover, it can be used to select the most relevant features for classification, allowing to reduce the high dimensionality of remote sensing data [Yu et al., 2006], [Belgiu and Drăguţ, 2016]. Many authors apply and recommend this procedure, because it decreases the dimensionality of data, simplifying the model, and increases the accuracy of the classification [Belgiu and Drăguţ, 2016], [Ghosh and Joshi, 2014]. The algorithm, though, is reported by many studies to be not transferable to new areas: the overall accuracy decreases when it is trained on different study areas [Belgiu and Drăguţ, 2016],[Juel et al., 2015]. The RF classifier has been successfully used with satellite imagery to map insect defoliation levels using RapidEye images, boreal forest habitats using WorldView-2 imagery, biomass using Landsat temporal data, to identify tree health using IKONOS data, and to map tree canopy cover and biomass using uni-temporal Landsat-8 imagery [Belgiu and Drăguţ, 2016]. Studies also report the use of RF in the classification of UAVs data. Michez et al. [2016], for example, found satisfactory results mapping riparian species from UAV derived aerial imagery using RF algorithm and segmentation and Juel et al. [2015] used it to map fine scale coastal vegetation in Denmark.

Support Vector Machine (SVM) is a non-parametric classifier which divides classes using hyperplanes that fit the training dataset [de Morsier, 2017]. It became popular in machine learning because of its efficiency in handling large input data and the higher accuracy compared to techniques like maximum likelihood or decision trees classifiers [Colgan et al., 2012]. SVM can also handle the non-linear separation of classes by transforming data into a higher dimensionality feature space using kernels: similarity functions over pairs of data [de Morsier, 2017]. This classifier has successfully been applied to predict tree species in deciduous and tropical forests from hyperspectral and LIDAR data [Colgan et al., 2012], [Baldeck et al., 2014].

According to Belgiu and Drăguţ [2016], RF and SVM classifiers are equally reliable. The first performs slightly better for high dimensional input data and is faster. The second performs generally better in objects based analysis, but seems to be more sensitive to input features and less user friendly in terms of parameter settings. Ghosh and Joshi [2014] found higher classification accuracies (94%) with SVM object based classifier than RF while attempting to classify bamboo patches using WorldView 2 imagery in West Bengal, India, using both pixel and object based approaches. Burai et al. [2015] tested the applicability of SVM and RF to classify extremely fine scale mosaics of several vegetation types in the Pannonian basin. They tried to classify 20 vegetation classes using images acquired from an AISA EAGLE II hyperspectral sensor, which has 128 contiguous bands (400-1000 nm) of 5 nm bandwidth and 1m spatial resolution. SVM classifier provided the highest accuracies [Burai et al., 2015].

Concerning features to be used in the classification, many authors report that image bands derivatives and ancillary data are usually helpful to differentiate between spectrally inseparable vegetation classes [Yu et al., 2006]. The most used features, other than multispectral bands, are textures [Ghosh and Joshi, 2014], [Belgiu and Drăguţ, 2016], topographic features such as elevation data, slope or aspect [Yu et al., 2006], [Belgiu and Drăguţ, 2016], geometric features [Yu et al., 2006], principal components [Ghosh and Joshi, 2014] or statistical features like means, standard deviations or quantiles of some variables [Juel et al., 2015].

To summarize, object based approaches and supervised classification methods allow to achieve better results, and Random Forest and Support Vector Machine are among the most used and successful classifiers. Ancillary data and band derivatives help in the distinction between classes. High resolution UAV or satellite imagery is preferred to coarse resolution satellite

imagery.

2.2 Biomass estimation

Grass quantity and quality are important information for the management and planning of grazing resources and to understand the dynamics of herbivores' populations [Ramoelo et al., 2012]. For decades, this information has been acquired by biomass sampling. Now, "remote sensing techniques have the potential to overcome the physical restriction that limits large scale ecological surveys" [Smith et al., 1990], offering multispectral images in the visible, NIR and others regions of the spectrum to study vegetation patterns at regional and global scales [Smith et al., 1990].

Literature about biomass estimation from UAVs or manned aircrafts imagery is scarce, more is available for images derived from satellites like RapidEye, Sentinel-2, Landsat or MODIS.

Vegetation indexes derived from satellites, such as the Normalized Difference Vegetation Index (NDVI), are now "commonly used by ecologists as a proxy for vegetation productivity" [Borowik et al., 2013] at different temporal and spatial scales. NDVI values are high for green vegetation because it has a high reflectance in the NIR and absorbs light in the visible. Values are lower for senescent or dry vegetation and soils because they have a higher absorption in the NIR [Borowik et al., 2013].

Borowik et al. [2013] studied whether NDVI is a good predictor of forage availability in semi-open landscape in eastern Poland using MODIS images. Coherently with other studies, they found a positive relation between the two variables, with a stronger correlation occurring in summer. Thus, suggesting that the usefulness of NDVI to predict above ground biomass depends on the season.

Another study, conducted by Ramoelo et al. [2012] using 6.5 m resolution RapidEye images taken at peak productivity in North eastern South Africa, found that vegetation indexes alone yielded poor results in estimating biomass. However, combining them with ancillary variables like altitude, slope, aspect, distance to river, temperature and precipitation improved the estimation.

In an article from Moleele et al. [2001] the authors try to determine whether green browse biomass can be quantified in a bush encroached semi arid rangeland in south-east Botswana, using vegetation indexes and transforms from Landsat data. Their work shows the limitations of those indexes in the assessment of the herbaceous layer in this kind of landscape. Other studies state that quantifying the vegetation cover in semi arid rangelands with Landsat imagery is difficult because of the spectral dominance of the background soil [Smith et al., 1990], [Giri et al., 2013].

A lot is found in the literature about biomass estimation using small footprint LIDAR (LIght Detection And Ranging) coupled with manned aircrafts, which, according to some studies, give accurate estimates [Vaglio Laurin et al., 2014]. This surveying method consists of measuring the distance of a target by illuminating it with a pulse laser light and measuring the time taken to the pulse to reach it, be reflected and come back to its source [Bluesky, 2017].

The combination of this technology with hyperspectral data is now considered one of the most accurate remote sensing methods for biomass mapping [Vaglio Laurin et al., 2014]. Hyperspectral data alone have already been used to directly estimate leaf canopy and grassland biomass [Vaglio Laurin et al., 2014].

CHAPTER 3

DATA

3.1 Drone data

Kuzikus Wildlife Reserve has a vast amount of ultra-high resolution images taken from drones. In May 2014, May 2015 and October 2017 the SAVMAP consortium [SAVMAP, 2017], [Rey et al., 2017], [Ofli et al., 2016], did several flight campaigns in Kuzikus with the aim of characterizing the vegetation and wildlife status in the reserve. Orthomosaics, point clouds and elevation models have been obtained after processing raw images taken by different sensors: RGB, NIR, Red Edge (RE), MultiSpectral (MS) and Thermal InfraRed (TIR). In all three campaigns, aerial photographies were acquired with fixed wings drones produced by senseFly SA [senseFly, 2017a] and further processed with Pix4D photogrammetry software [Pix4D, 2017].

The flight campaign of October 2017 took place to map the reserve at the end of the dry season with RGB and MS sensors. In order to get as much overlap as possible with the existent dataset, the new acquisition campaign was based on the ones from 2014 and 2015. During the campaign, we tried to always fly the two sensors over the same areas at the same time (or with the least possible time shift). This choice aimed at avoiding different shadow effects between RGB and MS images and consequently facilitating the combination of the two images during classification. More than 2740 hectares were mapped in five days (October 15 - October 21) with the help of Gous Gammo Divia, a San [Boden, 2009], and Dr. Reinhard, the managing director of Kuzikus, who guided us in the reserve (figure 3.1).

Figure 3.1: SAVMAP team, flight campaign 2017 [Bacchilega, 2017].

For this project, only a few RGB and NIR images with corresponding point clouds or elevation models from May 2015 and October 2017 are used for classification. Figures 3.2 and 3.3 show the footprints of all 2015 and 2017 acquisitions over Kuzikus with RGB, NIR and MS sensors and tables 3.1 and 3.2 give the details of the flight campaigns. In 2015, 6831 images were acquired with RGB and NIR sensors within 42 flights. In 2017, 18540 images were acquired within 37 flights. The selection of data is detailed in chapter 4.1.

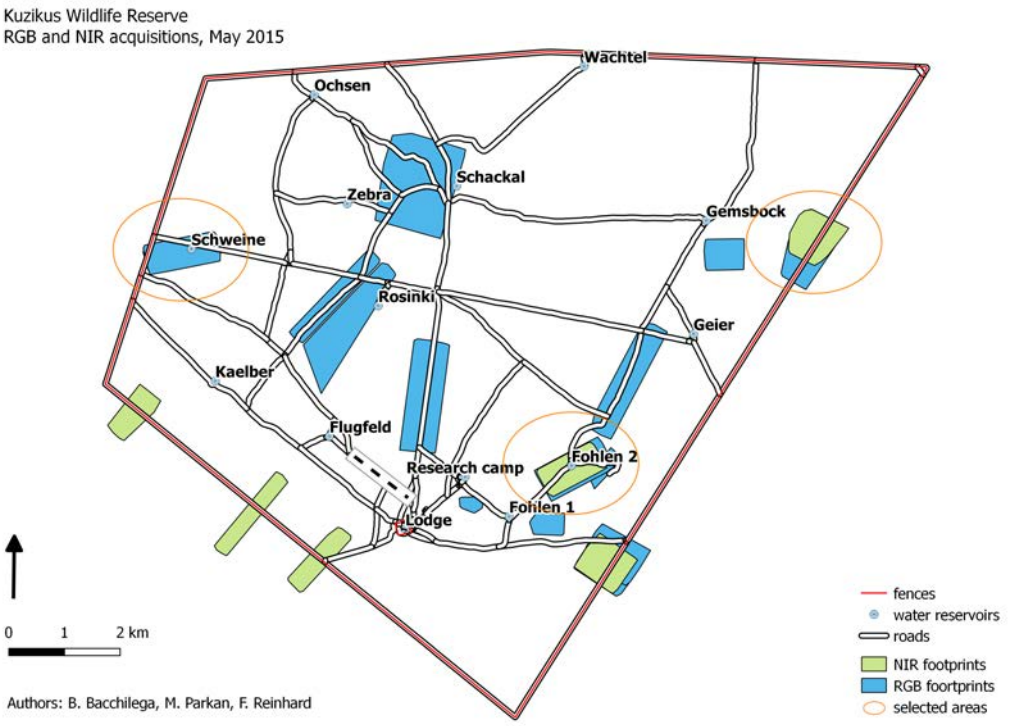

Figure 3.2: Mapped areas with NIR and RGB sensors during the 2015 flight campaign [SAVMAP, 2017]

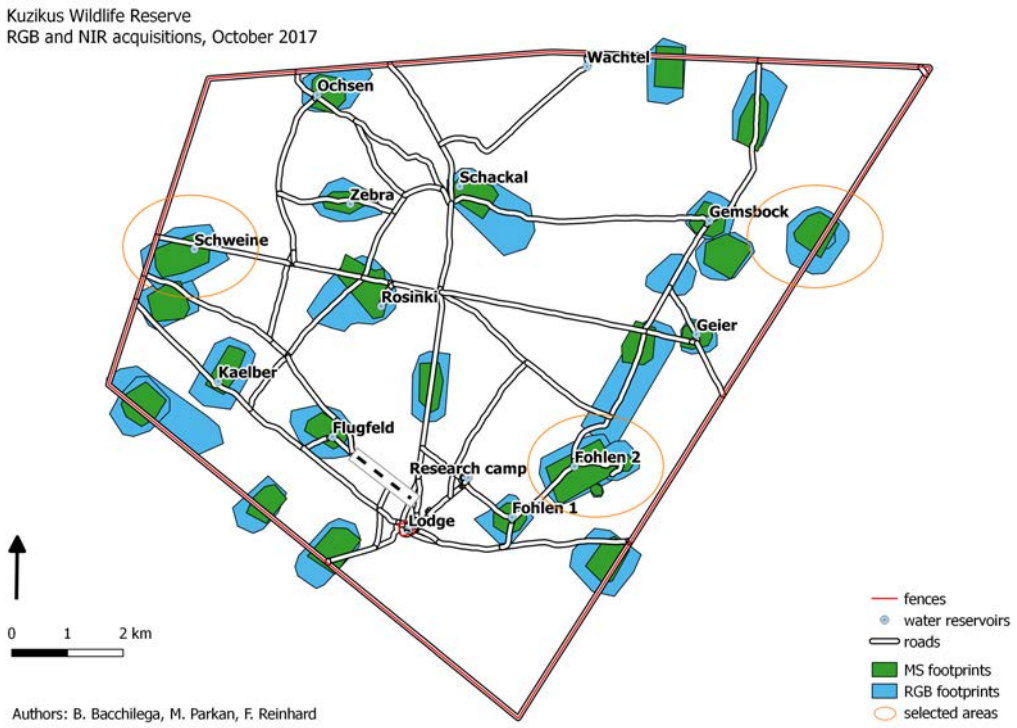

Figure 3.3: Mapped areas with MS and RGB sensors during the 2017 flight campaign [SAVMAP, 2017]

	RGB images	NIR images
Sensor	Sony Cyber-shot DSC-WX220	Canon PowerShot S110 NIR
Spectral resolution [nm]	470 (B), 570 (G), 660 (R)	550 (G), 625 (R), 850 (NIR)
Spatial resolution [cm]	2-4.5	2.5-4.5
Radiometric resolution [bits]	8	8
# of images	4838	1993
# of flights	26	16
Platform	eBee	eBee

Table 3.1: Details of the May 2015 campaign [SAVMAP, 2017]

	RGB images	MS images
Sensor	Sensefly S.O.D.A	Parrot Sequoia
Spectral resolution [nm]	450 (B), 520 (G), 660 (R)	550 (G), 660 (R), 735 (RE), 790 (NIR)
Spatial resolution [cm]	2.3-4.5	7-8.3
Radiometric resolution [bits]	8	16
# of images	7415	11125
# of flights	18	19
Hectars mapped	1889.27	851.53
Platform	eBee Plus	eBee SQ

Table 3.2: Details of the October 2017 campaign [SAVMAP, 2017]

3.2 Satellite data

For the purpose of this project, Sentinel-2 data are used. They are available on the United States Geological Survey (USGS) EarthExplorer [USGS, 2017].

Sentinel-2 is a mission developed by the European Space Agency (ESA) with the aim of performing terrestrial observations. It is composed by two identical satellites, Sentinel-2A and Sentinel-2B, launched in June 2015 and March 2017, respectively. They offer multispectral data in 13 bands with resolutions of 10, 20 or 60 meters in the visible, near infrared (NIR), and short wave infrared (SWIR) [ESA, 2017a]. Thanks to the simultaneous operation of the two satellites, one image every 5 days is available under the same viewing angle.

For the project, 10 m resolution bands of 81 images with less than 40% cloud cover are used. Details of the data and spectral resolutions of the bands used are given in table 3.3 and figure 3.4, respectively.

Location	Central Namibia
Field of view	290 km
Coordinate system	WGS84 / UTM zone 34S (EPSG:32734)
Period	August 6, 2015 (first image available) - November 21, 2017
Bands used	B2 (B), B3 (G), B4 (R) and B8 (NIR)
Spatial resolution	10 m

Table 3.3: Details of Sentinel-2 data [USGS, 2017]

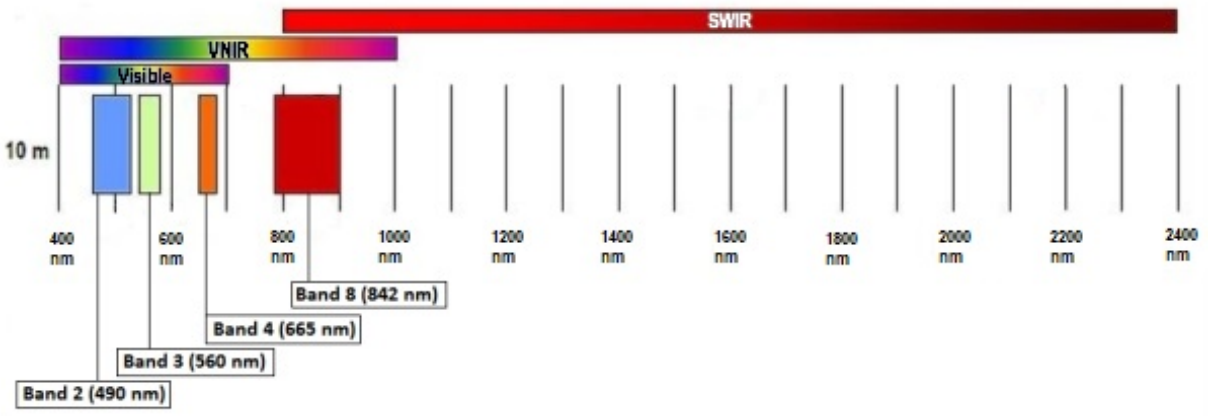

Figure 3.4: Sentinel-2, 10m resolution bands [ESA, 2017b].

CHAPTER 4

METHODS

4.1 Data selection and preparation

The first part of the project was dedicated to the selection and preparation of drone and satellite images used for the classifications.

Drone data selection

Drone data were selected based on the type of vegetation represented (as much differentiated as possible) and the overlap between orthomosaics acquired by different sensors in 2014 and 2015. As the main idea for the classification is to combine data in the visible and NIR parts of the spectrum, one area had to be covered by at least a NIR/MS and a RGB sensor: the images taken by both must overlap. Due to faulty NIR images acquired in 2014, some processings failed and too few diverse vegetation species in some images, only three areas were selected with overlapping NIR and RGB images from 2015. The same areas were selected from the 2017 flight campaign. The areas are shown in figure 4.2.

One orthomosaic per area, sensor and year was chosen: 3 NIR and 3 RGB images from 2015 and 3 MS and 3 RGB images from 2017 flight campaign. In order to retrieve information about vegetation height, digital terrain and surface models (DTM and DSM) from 2017 and point clouds from 2015 were used (DTM not available from 2015 data).

Drone data preparation

Parrot Sequoia, the camera used to acquire MS images during the 2017 campaign, outputs one image per band. Those images were combined into one multi band image to ease the calculations and the handling of data.

In order that the different images are correctly co-registered, NIR and RGB images from 2015 and MS and RGB images from 2017 were geo referenced using QGIS software [Sherman, 2002] by linking common tie points between the two images. The only reliable points were holes in the ground created by aardvarks (*Orycteropus afer*), which appeared as black holes in the sand and clearly visible in both images (figure 4.1). Unfortunately, aardvarks' holes are not visible in the point clouds, which were georeferenced with CloudCompare software [Girardeau-Montaut, 2003] using small shrubs as tie points.

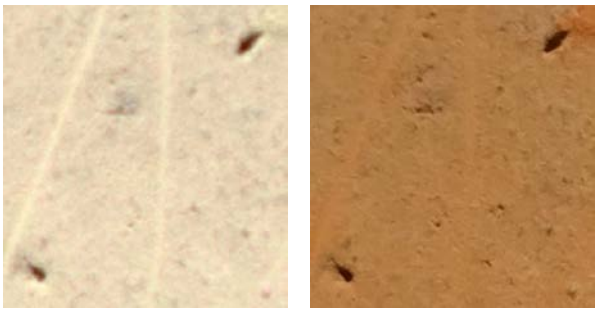

(a) NIR image **(b)** RGB image

Figure 4.1: Two aardvarks' holes in (a) a NIR image from 2015 and (b) in the corresponding RGB image

In order to reduce the processing time, only small sections of the images were used. Two squares of 150 by 150 meters per year and per sensor were extracted from the first area (*zone 1* and *zone 1bis*), 1 from the second (*zone 2*) and 1 from the third (*zone 3*) 4.2, for a total of 16 images (4 NIR and 4 RGB from 2015 and 4 MS 4 RGB from 2017), they are shown in figure 4.2. Two areas have been chosen in *zone 1* one in order to do some initial test of the classification algorithm on the same orthomosaic, before extending the classification to other images.

Within the same campaign, selected images were taken in different days, different times of the day, by different sensors and often with different radiometric and spatial resolutions. Therefore, raw orthomosaics are not comparable. To solve this problem, the histogram of all images from the same campaign and the same sensor were matched in MATLAB [MathWorks, 1984] with the *imhistmatchn* [MathWorks, 2017b] function and their resolution downgraded to 10 cm. After this procedure, all 16 images have $1500x1550$ pixels.

Satellite data selection

Satellite data already had the same resolution and format, the only limitation in the selection was cloud presence.

A first selection was done at the download time, when a filter was applied to download only images with less than 40% cloud cover. The cloud cover is computed over the entire image, but Kuzikus only occupies a minimal fraction of it. Therefore, the 40% arbitrary threshold was preferred to 0%. After the download, Sentinel-2 images where cut to the extent of the reserve and checked again one by one to make sure no clouds were present. This led to the selection of 81 images.

To perform the time series analysis, one image per month was considered enough to analyze the evolution of vegetation patterns. Therefore, the data set was further reduced to only one image per month (for the available months) leading to the final selection of 25 images from August 16, 2015 to November 20, 2017. All images have a 10 m spatial resolution and $1398x1677$ pixels. The dates corresponding to each image are presented in the appendix A.

To perform classification, only two images were used. The choice was dictated by the purposes of the project: quantify the vegetation at the end of the growing season and compare drone and satellite data. Only one image was available in May, dating May 24, 2017, and the satellite image closer to drone acquisitions was from October 21, 2017.

Satellite data preparation

The same procedure used for drone images was used to create multi-bands images for each date and to match the histogram of all images. Sentinel-2 images from different days were not coherently georeferenced between each other and were exploited with their original geolocations.

Figure 4.2: Selected working areas for drone images: zone 1, zone 1bis, zone 2 and zone 3

4.2 Ground truth and classes

Reference (ground truth) data is necessary to train the supervised classification models and assess their accuracy. Reference training/validation data are created by manually digitizing polygons on QGIS, each polygon corresponding to a specific class.

Three different ground truths were created: one for 2015 drone images, one for 2017 drone images and one for satellite images. The ground truth references for drone images were the drone images themselves: classes were defined visually by looking at the images. For satellite images, the digitization reference was a 2017 Bing map from DigitalGlobe [DigitalGlobe, 2018]. Polygons were refined according to distinguishable objects on the image from May 2017. Table 4.1 shows the classes present in the ground truths. Classes with the same name but different number represent different types of the same object and were distinguished on images according to their different color, texture or shape. Perennial class, in the ground truth from 2015 drone images, represents old perennial grasses [Reinhard, 2017].

Drone 2015	Drone 2017	Satellite
1. Road	1. Road	1. Grass 1
2. Tree	2. Tree 1	2. Grass 2
3. Shadow	3. Shadow	3. Sand 1
4. Soil	4. Soil	4. Sand 2
5. Bush 1	5. Bush 1	5. Limestone Soil
6. Grass 1	6. Grass 1	6. Tree
7. Grass 2	7. Grass 2	
8. Grass 3	8. Tree 2	
9. Perennial	9. Bush 2	
10. Bush 2		

Table 4.1: Classes for 2015 and 2017 drone images and satellite images. Classes with the same name but different number were distinguished on images according to their different color, texture or shape

Figures 4.3 and 4.4 show some classes examples for 2015 and 2017 drone images, respectively. All sub-figures represent an area of $14.4x13.1$ square meters.

(a) Grass 1 (green), Grass 2 (beige) and Soil

(b) Bush 1, Shadow, Grass 1 (green), Grass 2 (beige) and Soil

(c) Tree, Shadow, Road, Grass 2 (beige) and Perennial (bottom right)

(d) Perennial and Road

(e) Bush 2, Grass 3 and Soil

Figure 4.3: Examples of the classes used for 2017 drone images classification: (a) Grass 1 (green), Grass 2 (beige) and Soil , (b) Bush 1, Shadow, Grass 1 (green), Grass 2 (beige) and Soil, (c) Tree, Shadow, Road, Grass 2 (beige) and Perennial (bottom right), (d) Perennial and Road and (e) Bush 2, Grass 3 and Soil [SAVMAP, 2017].

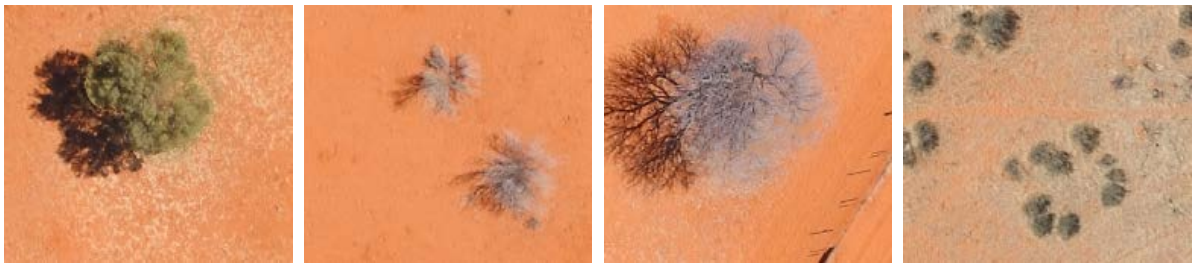

(a) Tree 1, Shadow, Grass 1 and Soil

(b) Bush 1 and Soil

(c) Tree 2, Shadow, Grass 1, Soil and Road (bottom right)

(d) Bush 2, Grass 2 and Soil

Figure 4.4: Examples of the classes used for 2017 drone images classification: (a) Tree 1, Shadow, Grass 1 and Soil, (b) Bush 1 and Soil, (c) Tree 2, Shadow, Grass 1, Soil and Road (bottom right) and (d) Bush 2, Grass 2 and Soil [SAVMAP, 2017].

Figures 4.5a, 4.5c, 4.5e, 4.5g, 4.5i and 4.5k show classes Grass 1, Grass 2, Sand 1, Sand 2, Tree and Limestone soil, respectively, on the Bing image used for digitizing the ground truth for satellite images. Figures 4.5b, 4.5d, 4.5f, 4.5h, 4.5j and 4.5l show the same patches on the false colors Sentinel-2 image from May 2017. One pixel measures $10x10$ meters.

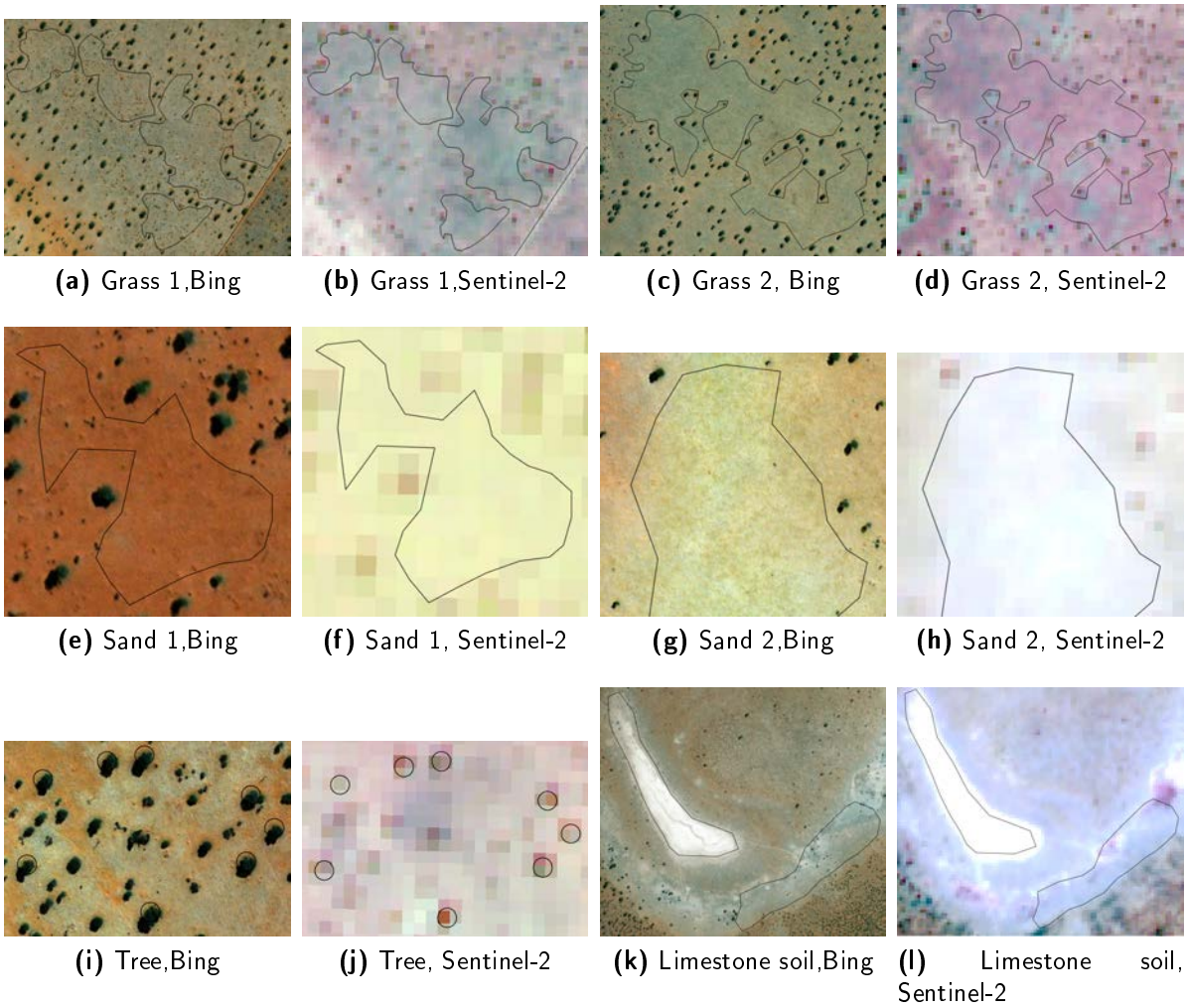

(a) Grass 1,Bing **(b)** Grass 1,Sentinel-2 **(c)** Grass 2, Bing **(d)** Grass 2, Sentinel-2

(e) Sand 1,Bing **(f)** Sand 1, Sentinel-2 **(g)** Sand 2,Bing **(h)** Sand 2, Sentinel-2

(i) Tree,Bing **(j)** Tree, Sentinel-2 **(k)** Limestone soil,Bing **(l)** Limestone soil, Sentinel-2

Figure 4.5: Examples of the classes used for satellite images classification: (a) Grass 1, (c) Grass 2, (e) Sand 1, (g) Sand 2, (i) Tree and (k) Limestone soil classes on the Bing image and (b),(d),(f),(h),(j),(l) corresponding polygons on the false color Sentinel-2 image from May 2017 [USGS, 2017]

.

As some classes are more abundant than others, the number of pixels per class in the ground truth are not equal. For drone images, grass classes have fewer pixels than other classes, mainly because of the difficulty of correctly delimiting polygons but also because patches of this type of vegetation are much smaller than those of other classes. In general, the smaller the patch, the more difficult to digitize it. This is particularly true for images from 2017, for which one type of grass is present in only a few and small patches. The same problem exists for satellite images, for which the least abundant class is Tree.

4.3 Features

For classification, not only the spectral information is useful, but also variables derived from them or ancillary data. Variables to be used in the classification are called features.

Five different types of features are used: spectral bands, vegetation indexes, principal components, textures and digital height models.

Spectral bands

Spectral bands include red, green, blue, near infrared and red edge.

Vegetation indexes

Vegetation indexes are useful to enhance vegetation. The Normalized Different Vegetation Index (NDVI), Difference Vegetation Index (DVI), Green Normalized Different Vegetation Index (GNDVI), Ratio Vegetation Index (RVI) and the Soil-Adjusted Vegetation Index (SAVI) are calculated from bands combination of NIR (for 2015), MS (for 2017) or satellite images. The formula used to calculate the vegetation indexes are the following [Jones and Vaughan, 2010]:

$$DVI = NIR - R \tag{4.1}$$

$$NDVI = \frac{NIR - R}{NIR + R} \tag{4.2}$$

$$GNDVI = \frac{NIR - G}{NIR + G} \tag{4.3}$$

$$RVI = \frac{NIR}{R} \tag{4.4}$$

$$SAVI = (1 + L) \cdot \frac{NIR - R}{NIR + R + L} \tag{4.5}$$

Where R is the red band, G the green band, NIR the NIR band and L is a coefficient equal to 0.5.

Specifically for satellite images classification, a new vegetation index is calculated from the temporal evolution of DVI. The index, called *stdev DVI*, represents the standard deviation of the DVI values of each pixel over one year (November 2016 - November 2017). More information about the choice of the period is given in chapter 4.7, page 34.

Principal component analysis

Principal component analysis is a statistical procedure that transforms a set of possibly correlated variables into a set of uncorrelated variables called principal components [Zey, 2017]. Here it is used with RGB, NIR, MS and satellite images to decorrelate the spectral bands.

Texture

Texture, which is the visual aspect of the image, allows to take into consideration the neighborhood of pixels. Those features are calculated from the co-occurrence matrix, using a window size of 7 pixel (70 cm) for drone images and 5 pixels (50 m) for satellite images. The window sizes were determined empirically based on the results. Contrast, correlation, energy, homogeneity and entropy co-occurrence indexes are extracted for each band.

Digital height models

Digital height models were calculated only for drone images, as no data were available at higher scale. DHM is given by the difference between DSM and DTM. For 2015 data, only DSM was available, thus DHM is calculated using the point cloud issued from NIR images and the digital forestry toolbox for MATLAB [Parkan, 2017].

Table 4.2 presents an exhaustive list of all calculated features and in which classification models they are used. The features to be used in each model are chosen based on the estimates of the variable importance got from the Random Forest's Out-Of-Bag error (see chapter 4.5) and

results of the classification. In general, only the positive variables are used. SVM model is more sensitive to the number of features used, many test were done to choose which variables to leave apart. According to the results and calculation times, textures were not used in those models. Models will be explained in chapter 4.4.

	Platform						
	Drone 2015			**Drone 2017**			**Satellite**
Features	**KM**	**SVM**	**RF**	**KM**	**SVM**	**RF**	**RF**
R, G, B, NIR	✓	✓	✓	✓	✓	✓	✓
RE				✓	✓	✓	
NDVI	✓	✓	✓	✓	✓	✓	✓
$NDVI_{RE}$						✓	
DVI		✓	✓		✓	✓	✓
DVI_{RE}						✓	
GNDVI		✓	✓		✓	✓	
RVI		✓	✓		✓	✓	✓
RVI_{RE}						✓	
SAVI		✓	✓		✓	✓	✓
$SAVI_{RE}$						✓	
Stdev DVI							✓
PCA R, G, B, NIR		✓	✓		✓	✓	✓
PCA RE					✓	✓	
Contrast R, G, B, NIR			✓			✓	
Contrast RE						✓	
Correlation R, G, B, NIR			✓			✓	
Correlation RE						✓	
Energy R, G, B, NIR			✓			✓	
Energy RE						✓	
Homogeneity R, G, B, NIR			✓			✓	
Homogeneity RE						✓	
Entropy R, G, B, NIR			✓			✓	
Entropy RE						✓	
DHM	✓	✓	✓	✓	✓	✓	

Table 4.2: Features used for each model. R is the red band, G is the green band, B is the blue band, NIR is the NIR band, RE is the red edge band, NDVI is the Normalized Difference Vegetation Index, DVI the Difference Vegetation Index, GNDVI the Green Normalized Difference Vegetation Index. RVI the Ratio Vegetation Index, SAVI the Soil-Adjusted Vegetation Index and DHM the Digital Height Model.

Finally, after the features calculation and prior to classification, images were normalized and only drone ones segmented. The normalization is performed in order to remove extreme values. Each feature is normalized as follow:

$$feature_i = \frac{(feature_i - q01_i)}{(q91_i - q01_i)} \tag{4.6}$$

$q01_i$ and $q99_i$ are the 0.01 and 0.99 quantiles of the i^{th} feature, respectively.

Segmentation is done using the MATLAB *superpixel* function [MathWorks, 2017c]. This function uses the simple linear iterative clustering (SLIC) algorithm [Achanta et al., 2012], which performs local K-means and groups pixels into regions with similar values based on color

and space. The number of segments is calculated as follows:

$$Nb_{superpixel} = \frac{(ImageWidth)^2}{(SizeSegment)^2} \tag{4.7}$$

The size of the segment is 0.5 m and the image width 150 m.

4.4 Classification

Classification aims at generalizing the information in an image by reducing the multidimensional information contained in a pixel. Pixels are grouped in coherent spatial units which correspond to thematic classes.

The process usually consists in three steps:

1. Selection of training examples, which teach data dependencies to the model.
2. Establishment of a model to decide the class membership of a pixel. A similarity measure is used to decide the class of belonging of each pixel.
3. Prediction on the image: the decision function of the model assigns a class to each pixel.

Two types of classification exist: supervised and unsupervised. The main difference is that in unsupervised methods class information is not available and the model learns data dependencies based on a given similarity criterion. In supervised methods, on the other hand, class information is available and the model learns from data examples, usually given by the user. Unsupervised methods (or clustering methods) return groups of similar pixels (clusters), which have to be assigned to a class by the user, while supervised methods directly return a thematic map [de Morsier, 2017].

For drone images, the K-means unsupervised method (chapter 4.4.1) is used with only spectral bands, NDVI and height data to see if these features are enough to approximately distinguish the different classes. Then, Support Vector Machine (chapter 4.4.2) and Random Forest (chapter 4.4.3) supervised methods are used to better classify the images using multiple features (table 4.2). All classifications were performed in MATLAB separately for 2015 and 2017 data.

For satellite images, Random Forest classification is used to predict the land cover (chapter 4.7).

In the description of methods that follows and the rest of the report, the pixels of images are called samples and the variables used for the classifications are called features.

4.4.1 K-means

K-means is an iterative unsupervised classification method that aims at partitioning the samples in the data set into k compact clusters. It builds the decision function based on features similarities between samples within the clusters. Each sample is assigned to the closest cluster [de Morsier, 2017].

The work flow of the classifier is the following:

1. Choice of the number k of clusters by the user.
2. Random selection of the clusters' centroids $c_1, ..., c_k$.
3. Calculation of the euclidean distance $D(c_i, x_i)$ between sample x_i and centroid c_i.
4. Assignment of each of the n samples $x_1, \ldots, x_n$ to the closest cluster's centroid.
5. Update of the centroids' positions as the mean of all points x_i assigned to the cluster c_i in step 4.

6. Steps 3-5 are repeated until the cluster assignments or the centroids' position do not change anymore.

Figure 4.6 explains the iterative process.

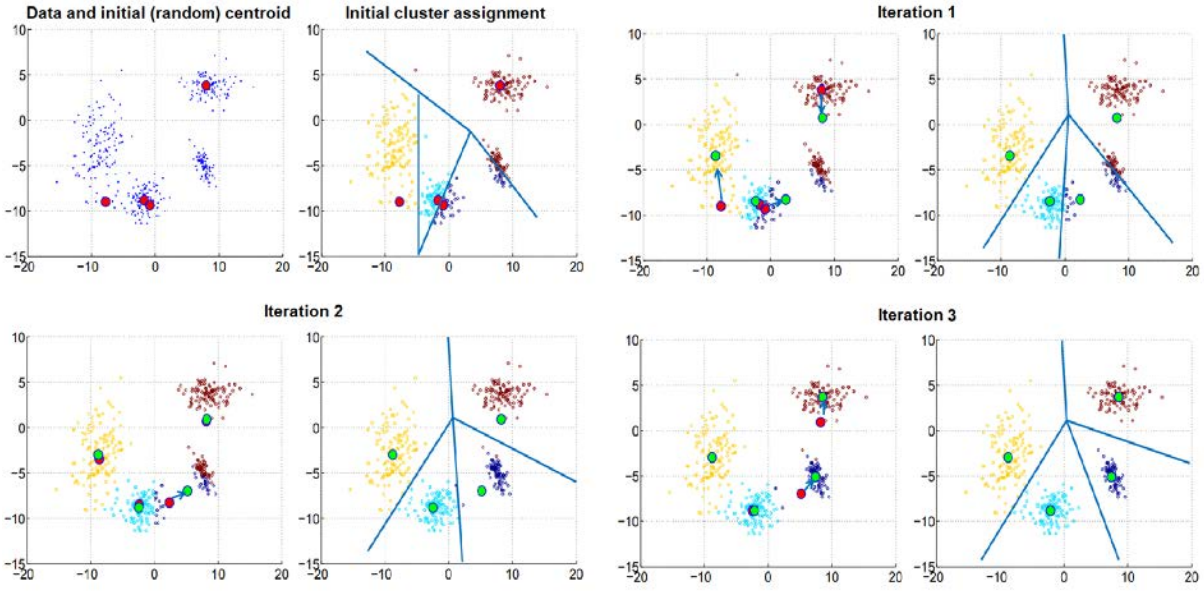

Figure 4.6: Iterative process of the K-means classifier, example with 4 clusters. Dots represent the samples and lines represent the boundary between the clusters according to the minimal euclidean distance [de Morsier, 2017].

How to choose the right value of k?

The choice of the number of clusters is never simple and there is no specific method to support the decision.

One of the most commonly used metrics is to compare the mean distance between samples and assigned centroid for different values of k. Increasing the number of clusters will decrease the mean sample - centroid distance. After a certain k, the rate of decrease will drop and the distance will continue to decrease slower until zero is reached when k is equal to n. By plotting the mean distance versus the number of clusters, the drop will appear as an "elbow" in the curve. The k at this "elbow" point should be the best number of clusters for the data set [Trevino, 2017].

This method helps in the choice, but it often over estimates the number of classes. Therefore, the user should always be critical about it. In order to better define the ideal number of clusters for each image, the results of the "elbow" method was compared to the number of classes estimated from the a priori knowledge of the environment.

Picking the initial centroids

The second step of the K-means classifier is critical for the performance of the classification. By picking centroids randomly, the algorithm might select points that are in the same cluster and the final clustering wont represent the real one [Leskovec et al., 2016]. Therefore, the K-means algorithm was run multiple times, to choose the best set of centroids.

4.4.2 Support Vector Machine (SVM)

SVM is a supervised machine learning algorithm that uses similarities between classes to build a linear or non-linear function to separate them [de Morsier, 2017]. It is a binary classifier that can be adapted to multiclass problems.

The samples are plotted in a n-dimensional space (where n is the number of features), then the classifier finds the hyper plane that better separates them into two classes. The classes are usually called +1 and -1 [Ray, 2017]. The equation of the hyper plane is of type:

$$y = \mathbf{w}'\mathbf{x} + b \tag{4.8}$$

Where $\mathbf{w}$ is a weight vector and $\mathbf{x}$ the features vector.

Within many possible hyper planes, the one that better separates the samples will be the one that has the smallest risk of making errors on new data. It will be at maximum distance from the closest samples of both classes. Those samples (marked in grey in the left of figure 4.7) are called the support vectors, and they alone define the hyper plane [de Morsier, 2017].

To predict the class of previously unseen samples, the decision function is based on the distance between the sample and the support vectors (equation 4.9). A cost matrix allows to consider the cost of a wrongly classified pixel.

$$\begin{cases} y \geq 0, \, class + 1 \\ y < 0, \, class - 1 \end{cases} \tag{4.9}$$

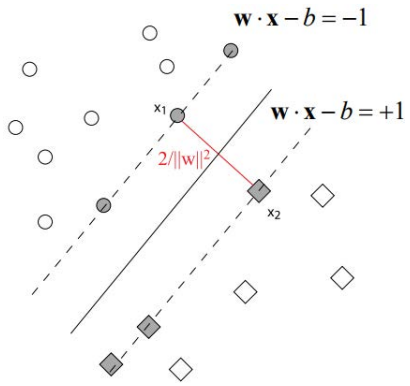

Figure 4.7: The best hyper plane and the support vectors (in grey) [de Morsier, 2017].

How to handle non linear responses?

When a linear classification is not possible in the feature space, SVM can also perform a non-linear classification using the so called kernel trick. The main idea is to add a new dimension, so that a linear separation of the classes is possible. The input data are projected into a new feature space where a linear problem is solved. They are then projected back in the input space to get a non linear model (figure 4.8). The SVM classification was performed using the MATLAB *fitcecoc* [MathWorks, 2017a] function with a gaussian kernel.

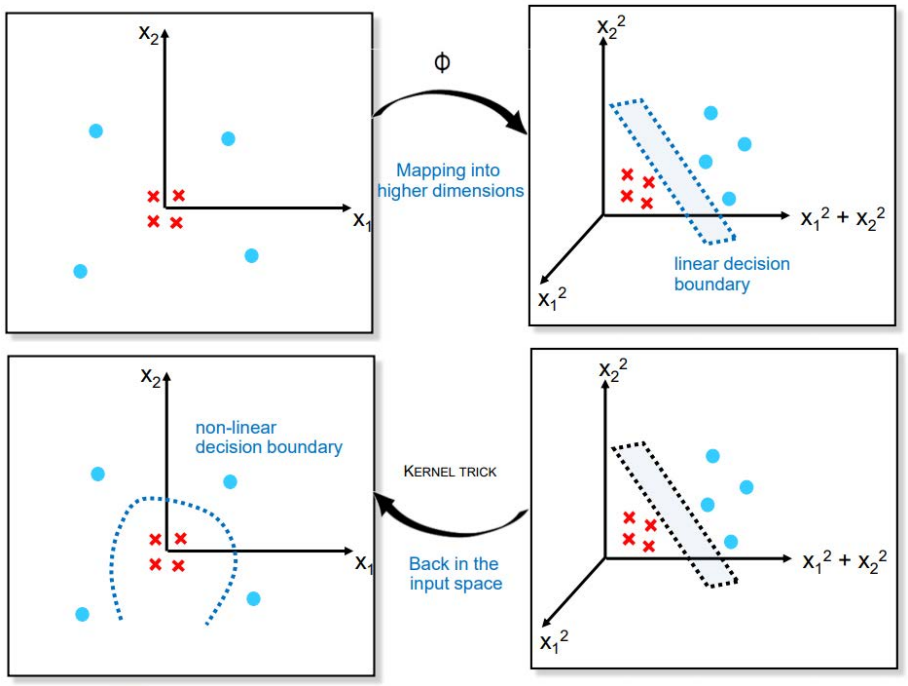

Figure 4.8: Kernel trick [de Morsier, 2017].

How to handle multiple classes?

fitcecoc takes into account more than two classes thanks to the coding design. This is translated as a matrix where each row corresponds to a distinct class and each column corresponds to a binary learner.

One of the most common coding designs is One Versus One (OVO). For each binary learner, OVO considers that one class is positive and another one is negative. The others are ignored. This design exhausts all combinations of class pair assignments [MathWorks, 2017a]. One hyper plane is created for each combination, then the information is combined.

4.4.3 Random Forest

Random Forest is a supervised ensemble learning algorithm based on classification trees. It grows decision trees using a bootstrap (random sampling with replacement) sample of the training data and selects a random subset of predictors to use at each decision split. The final choice for the class assignment is made by majority voting (figure 4.9).

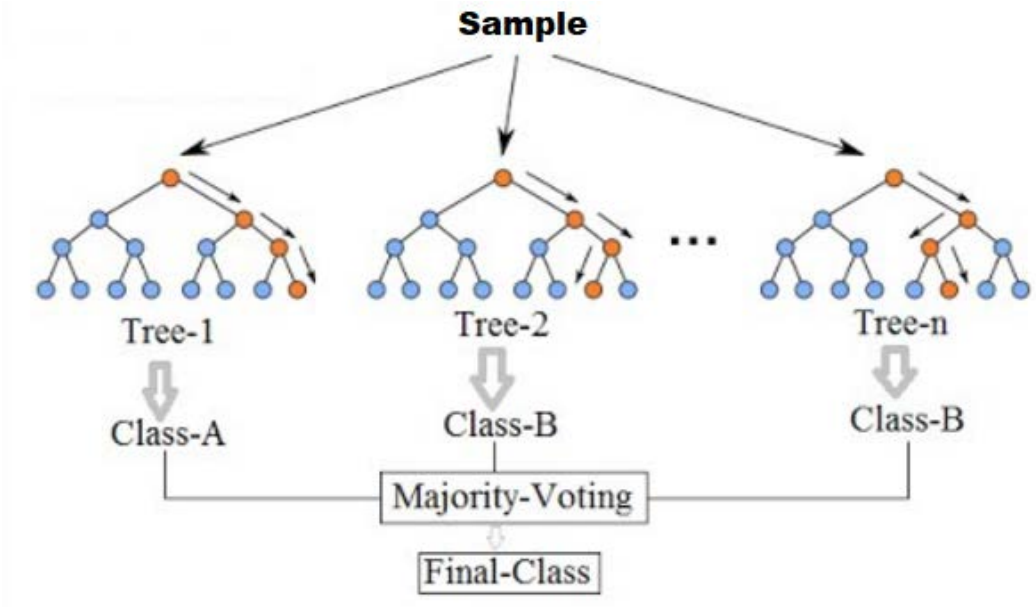

Figure 4.9: Random Forest algorith, simplified (Original image [Jagannath, 2017])

The forest is grown in the following way:

- Given the training set X, N subsets are created by selecting, with replacement, n samples from X. Because replacement is allowed, one sample can be in many subsets or not selected at all. One tree is trained for every subset (bootstrap technique).
- At each split of the tree, a subset of m features is randomly selected between the M available features. The feature and the value of this variable that give the best separation of classes is used to split the tree. In general, $m = sqrt(M)$, M being the total number of predictors. The best split is chosen according to the GINI coefficient (see Appendix B for further explanations about the coefficient).
- Each tree is grown to the largest extent possible. Branches are added until the trees predictions on the training subsets are 100% accurate, so that at the end of every branch the classes are pure.

Once the forest is grown, each sample goes through every tree which assigns it to a class. Finally, the sample is assigned to the class that was predicted by most of the trees [of California, 2017],[Yee and Chu, 2017].

Single classification trees tend to overfit data because they treat every detail in the subset of training data as important. In consequence, some boundaries between two classes are based on distinctions that don't really make a difference. The use of a multitude of trees and the final majority voting decrease this overfitting and give a greater accuracy [Yee and Chu, 2017]. The number of trees to use in the Random Forest classification depends on the size and nature of the training set. An optimal number can be found by observing the OOB error (chapter 4.5), which tends to stabilize as the number of trees increases. In general, the more trees in the forest, the higher accuracy in the results [of California, 2017]. Usually the error stabilizes before 500 classifications trees are achieved [Belgiu and Drăguţ, 2016].

The Random Forest classification is performed using the *TreeBagger* function in MATLAB [MathWorks, 2017d]. A cost matrix is added to consider the cost of a wrongly classified pixel .

4.5 Sampling and accuracy assessment

The first step of classification is the selection of training examples. While unsupervised methods calculate them internally based on similarities between samples, supervised methods need them as an input given by the user. For this reason, prior to perform supervised classification, the data set obtained from the ground truth is divided in training and test sets. The first will be used to train the models and the second to test their accuracy.

Every algorithm has a different sensitivity to the size and quality of the training set. Thus, the split fraction between train and test set differ from method to method. The ideal fraction for each one is found by testing different values and observing the classification results.

As K-means method does not need a training data set, all samples from the ground truth are used for testing.

To assess the accuracy of the classification, precision and recall [Joshi, 2016], overall accuracy [de Morsier, 2017], F1 scores [Joshi, 2016] and Cohen's Kappa [McHugh, 2012] statistics are calculated. Precision and recall are the percentage that a reference sample has been classified correctly and the percentage that a sample classified into a class belongs to this class, respectively. The overall accuracy is the percentage of correct classifications. F1 score is a measure of accuracy that harmonic mean precision and recall (formula 4.10):

$$F1 = 2 \cdot \frac{precision \cdot recall}{precision + recall} \tag{4.10}$$

Cohen's Kappa statistics takes into consideration the predictions by chance (formula 4.11):

$$K = \frac{p_0 - p_e}{1 - p_e} \tag{4.11}$$

Where p_0 is the overall accuracy and p_e the probability of prediction by chance.

For Random Forest, the Out-Of-Bag (OOB) error is also used as an unbiased estimate of the classification error as trees are added to the forest. Each time a tree is constructed, a different bootstrap sample of the original data is used. To calculate the OOB error, each observation that has never been used to build a tree (OOB observation) is run through all the trees to get a class. At the end of the run, suppose that c is the class that got the most of the votes every time the observation n was OOB. The OOB error estimate is the proportion of times that c is not the true class of n over all the observations [of California, 2017].

Finally, the spectral signature of each class obtained from SVM and RF is compared to the one of the ground truth classes. The spectral signature is calculated as the median value of each spectral band for each class.

4.6 Forage quantity estimation

Once the images are classified, the next step is to assess the quantity of forage. The estimation is calculated for both May (end of growing season) and October (dry season) images. Results are calculated by multiplying the the sum of pixels belonging to a certain class by the images' pixel area.

For drone images, as they cover only small and distinct areas of the reserve, results are calculated separately for the 8 images. The following values are calculated:

- Grass1, Grass2, Grass3 areas and the total grass area
- Bush1, Bush2 areas
- Tree1, Tree2 and the total tree area
- Total vegetation area

Calculated values can slightly vary from image to image as not all classes are preset in all images.

For satellite images, the following values are calculated:

- Grass1, Grass2 and the total grass area
- WoodyVegetation area
- Total vegetation area

Results are given in m^2 for drone images and in hectares for satellite images.

4.7 Land cover change analysis

To take advantage of the high temporal resolution given by Sentinel-2 data, the land cover change of some areas of Kuzikus is analyzed through the Difference Vegetation Index (DVI): the most relevant vegetation index in the classification according to the features importance calculated during Random Forest classification.

At first, the evolution of DVI per pixel is analyzed over one year, from November 2016 to November 2017. The choice of this particular period is due to the availability of images, the aim was to have the least missing months possible. Only January and March 2017 are missing, but one date at the beginning and one at the end of April 2017 are available. The standard deviation of the DVI per pixel over 1 year is then used as a feature for the Random Forest classification of the satellite images.

Then, DVI time series are calculated over 3 uniform patches of grass in Kuzikus and 1 in a neighbor farm and compared to rain data measured at water points in the wildlife reserve to detect trends (figure 4.10). The median of rain measurement of the water points in the reserve is used as a proxy to quantify rainfall.

Finally, a small area of Kuzikus is compared to 4 fields of a neighbor cattle and sheep farm to discover the different management strategies (figure 4.10).

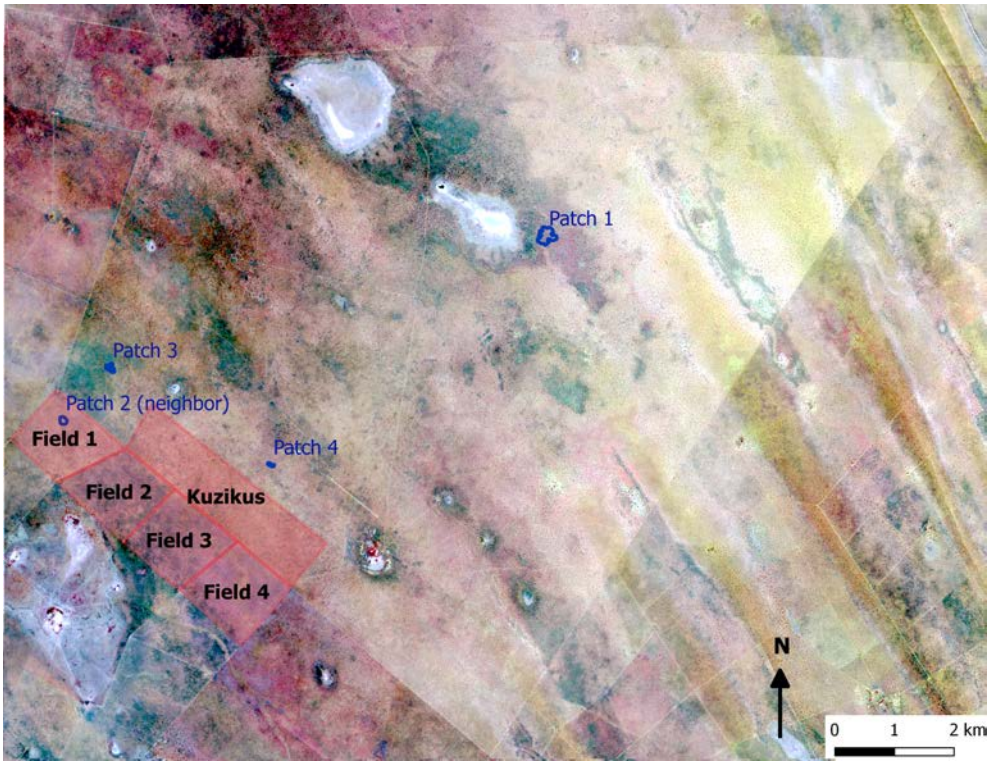

Figure 4.10: Location of fields and grass patches used for the temporal analysis. Background image: false color Sentinel-2 image from May 24, 2017

CHAPTER 5

RESULTS

5.1 Data selection and preparation

Selected drone data

The small areas to be classified on drone images were chosen based on the different plant species on them. Most of the classes are present in all of the four square images. Figures 5.1 and 5.2 show the four areas for 2015 and 2017, respectively. In May 2015, zones 1 (figure 5.1a) and 1bis (figure 5.1b) have a large cover of different grass species, while the same areas in October 2017 (figures 5.2a and 5.2b) only have a few small patches around trees. Zones 2 and 3 seem to have the same grass distribution in both years (figures 5.1c, 5.1d, 5.2c and 5.2d). In zone 1bis (figure 5.2b) and in particular in zone 2 (figure 5.2c) from 2017 it is possible to distinguish trees that are always green from trees that are just starting to get leaves. Finally, bushes from zones 1 and 1bis (figures 5.1a, 5.1b, 5.2a and 5.2b) are different from those in zone 3 (figures 5.1d and 5.2d) and roads are only present in the first three areas (figures 5.1a,5.1b, 5.1c, 5.2a, 5.2b and 5.2c).

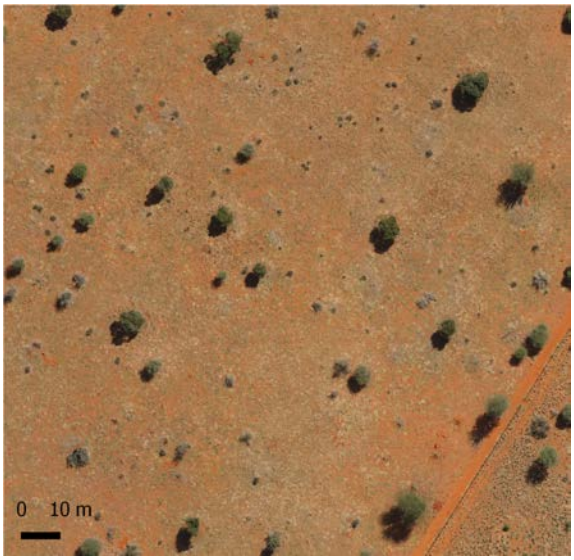

(a) *Zone 1*

(b) *Zone 1bis*

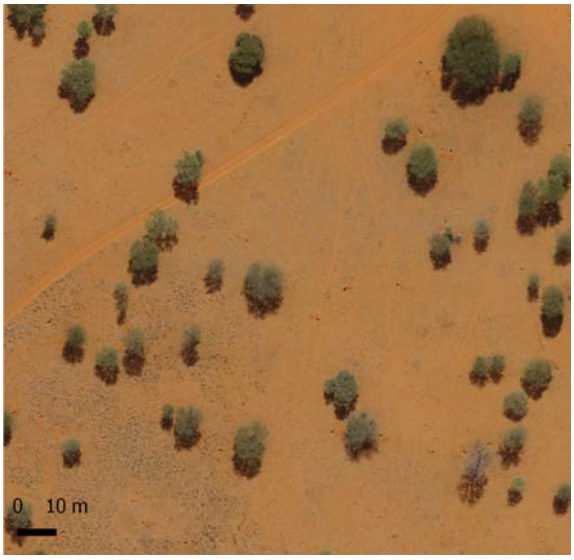

(c) *Zone 2*

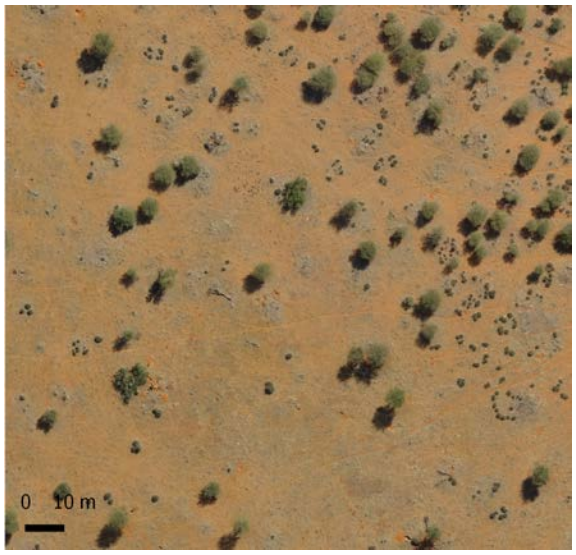

(d) *Zone 3*

Figure 5.1: Selected areas from 2015 drone images: (a) zone 1, (b) zone 1bis, (c) zone 2 and (d) zone 3

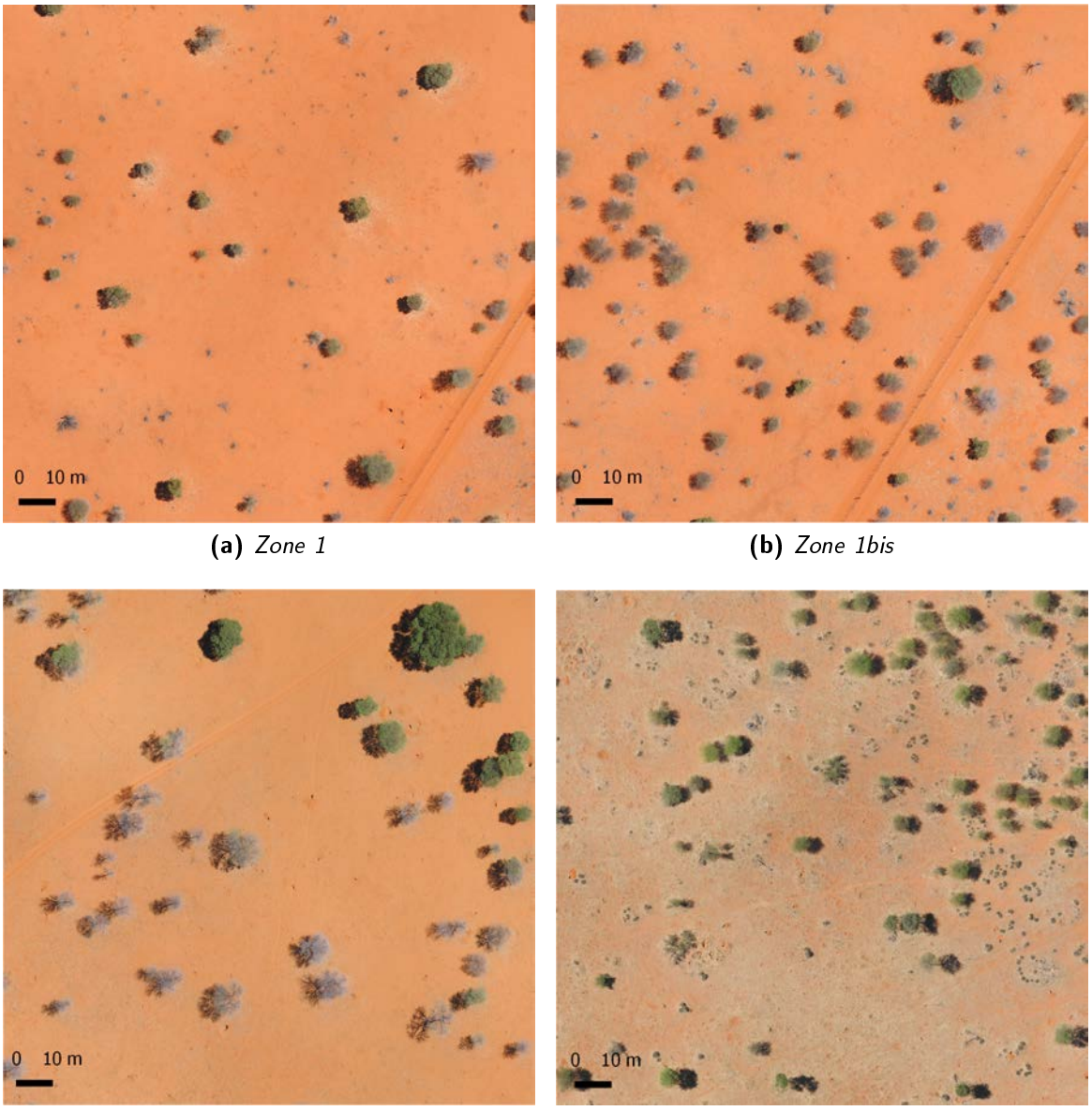

(a) *Zone 1* **(b)** *Zone 1bis*

(c) *Zone 2* **(d)** *Zone 3*

Figure 5.2: Selected areas from 2017 drone images: (a) zone 1, (b) zone 1bis, (c) zone 2 and (d) zone 3

Selected satellite data

About satellite images, cloud free data between August 16, 2015 and November 20, 2017 are available at least once in a month with the exception of 4 months: May and June 2016 and January and March 2017. Figure 5.3 represents the false color composition of the two Sentinel-2 images chosen for classification. Kuzikus reserve's contour and some soil cover patterns stand out in the images. The eastern part of the reserve is mostly characterized by red sand soil with some sand's dunes, while the western part has more vegetation and is more bush encroached. Limestone soil characterizes the two grey and white areas in the north, while the small grey spots all around the reserve are mostly water points. Because of the false color composition, vegetation appears in shades of red and blue/green, while sand and soil in shades of yellow/white and grey. Green vegetation (dark red in the images) is clearly visible around water points and in particular around the lodge, in the south of Kuzikus.

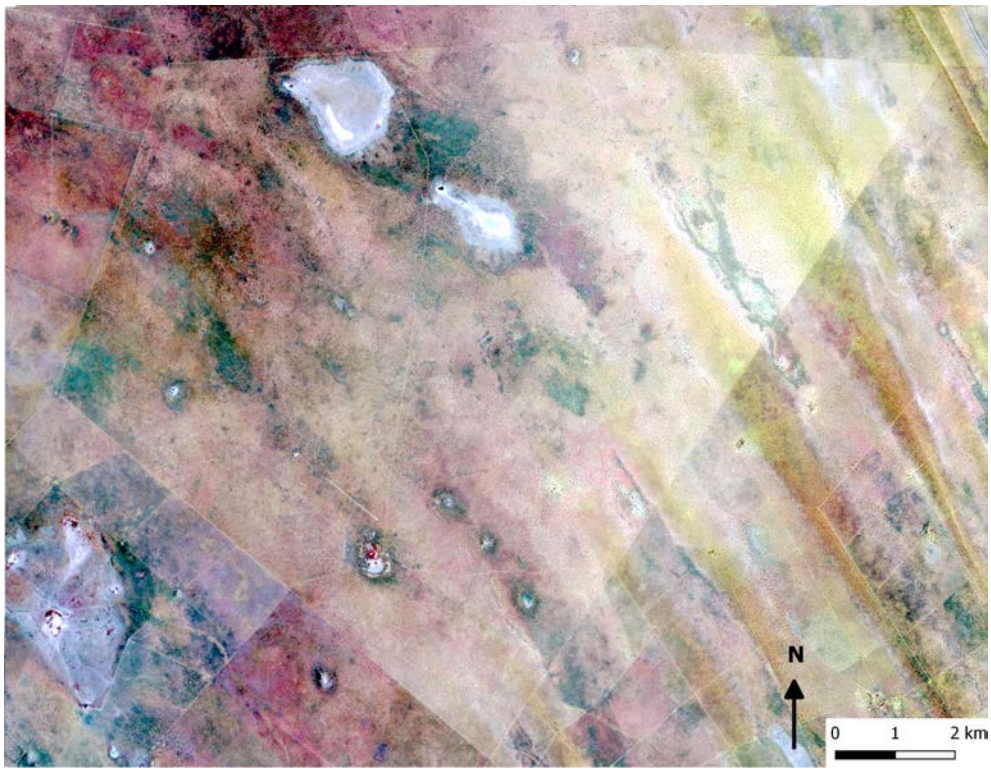

(a) Sentinel-2, May 24, 2017

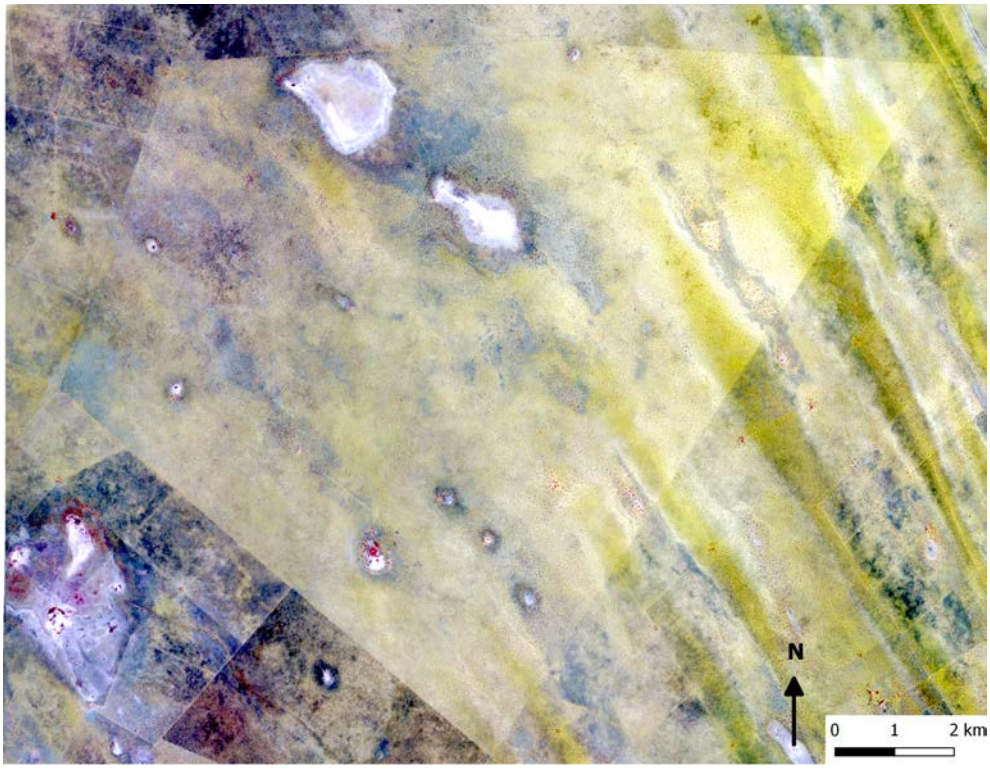

(b) Sentinel-2, October 21, 2017

Figure 5.3: Selected satellite images in false colors: (a) May 24, 2017 and (b) October 21, 2017

5.2 Ground truth and classes

Table 5.1 shows the percentage of ground truth samples for each class used for drone images' classification. Some of them, like Tree, Road and Soil, are abundant, while others, in particular bushes and some types of grasses, are scarce. In 2017 some classes count for less than 2% of the ground truth. In 2015, the ground truth pixels represent the 2% of the total number of samples of the 4 images, while in 2017 they represent the 3.7%.

Drone 2015			**Drone 2017**		
Class	**# of samples**	**% of ground truth samples**	**Class**	**# of samples**	**% of ground truth samples**
Road	28544	15.5	**Road**	53232	15.8
Tree 1	60061	32.6	**Tree 1**	116933	34.8
Shadow	13364	7.3	**Shadow**	30734	9.1
Soil	26121	14.2	**Soil**	61797	18.4
Bush 1	9001	4.9	**Bush 1**	6381	1.9
Grass 1	9536	5.2	**Grass 1**	3788	1.1
Grass 2	7032	3.9	**Grass 2**	23381	7.0
Grass 3	18753	10.2	**Tree 2**	34414	10.2
Perennial	7541	4.1	**Bush 2**	5832	1.7
Bush 2	3829	2.1			

Table 5.1: Number of ground truth samples per class for 2015 and 2017 drone images

For Sentinel-2 images, Limestone soil class is the most abundant, representing 24% of the ground truth, while the class Tree is the scarcest with only 8.8%. Table 5.2 shows the percentage of ground truth samples for each class. The number of ground truth samples per class is more homogeneous for satellite than for drone data.

Satellite		
Class	**# of samples**	**% of ground truth samples**
Grass 1	4064	18.4
Grass 2	3330	15.1
Sand 1	4441	20.1
Sand 2	2939	13.3
Limestone soil	5358	24.3
Tree	1951	8.8

Table 5.2: Number of ground truth samples per class for satellite images

5.3 Features

Figure 5.4 shows the features' ranking for the classification of drone images from the least important (on top) to the most important (at the bottom). All features were positive for both 2015 and 2017. Contrast, correlation and PCA of green, red and NIR bands were the most important features in 2015, while height is largely the most important feature in 2017. Despite all features being positive for both years, SVM models resulted more sensitive than RF to the number of features used in the classification and after some tests, it was decided not to use textures with this classifier.

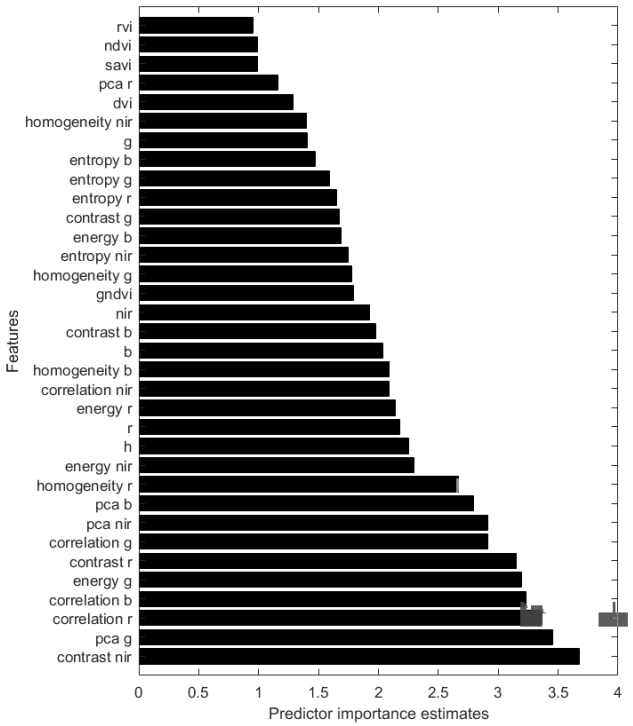

(a) Drone May 2015

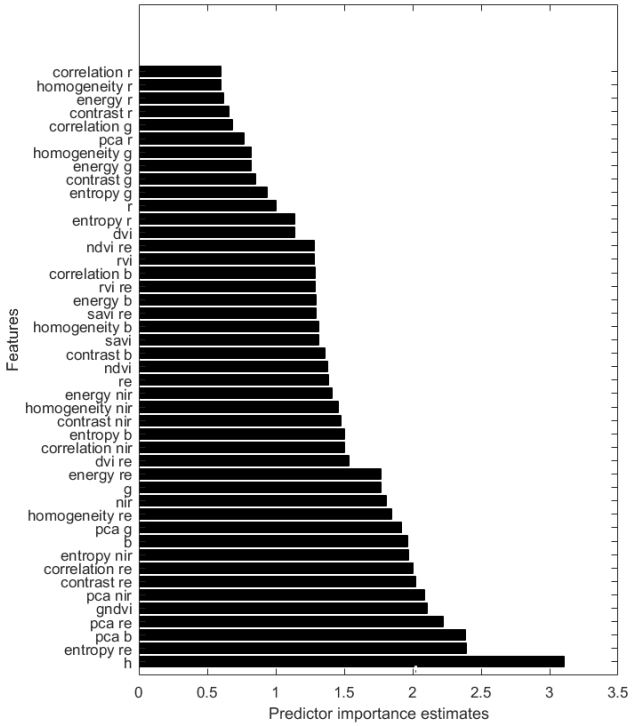

(b) Drone October 2017

Figure 5.4: Features importance for (a) 2015 and (b) 2017 drone images

As far as satellite images are concerned, textures were all negatively ranked and therefore not used in the classification. Figure 5.5 represents the ranking of the features used. For both images, the standard deviation over the 1 year DVI time series is largely the most discriminant feature for classification. It is followed by principal components and spectral bands.

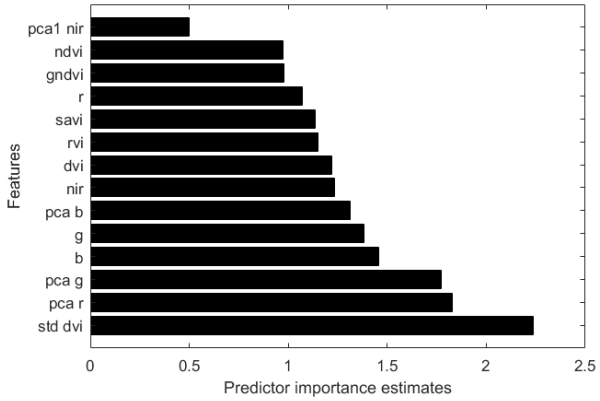

(a) Sentinel-2 May 2017

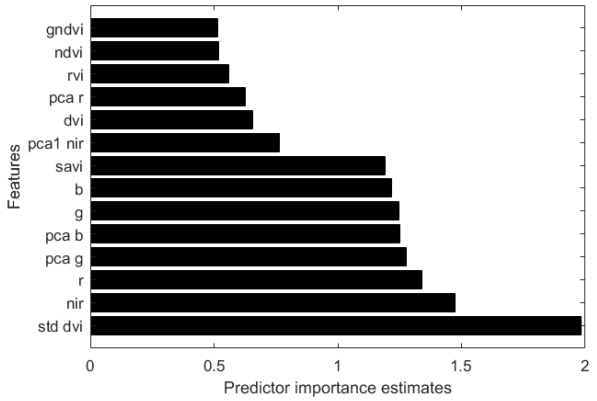

(b) Sentinel-2 October 2017

Figure 5.5: Features importance for (a) May and (b) October 2017 satellite images

5.4 Classification

The three following sections show the results of the classification of drone and satellite images obtained with K-Means, Support Vector Machine and Random Forest methods.

5.4.1 K-Means

K-Means classification algorithm was only used with drone images. The elbow method used to decide the best number of clusters k resulted inconclusive for both 2015 and 2017 images. Therefore, k was chosen visually, based on the best results between many classifications tests. The 4 images for each year were classified independently and later every cluster was assigned to a class. Because of the complexity of assigning clusters to classes, some of the classes presented in chapter 4.2 were grouped. Here, there is no distinction between grass species, which are all in the same class called Grass. Bushes and trees are merged into the class WoodyVegetation, with the exception of the class Tree 2 for 2017 images, which is called TreeNoLeaves and represents trees without green leaves.

Figure 5.6 shows the 2015 classified images and their legend of colors. For images in zones 1

(figure 5.6a) and 1bis (figure 5.6b) k was equal to 5 and for zones 2 (figure 5.6c) and 3 (figure 5.6d) it was equal to 4. The algorithm roughly distinguishes all trees and shadows, sometimes over-predicting shadows and the expense of trees (zones 2 and 3, figures 5.6c and 5.6d, respectively). Its performance is low in the distinction between grass and soil, which are often confused. Soil is over-predicted at the expenses of grass, in particular in zones 1 and 2 (figures 5.6a and 5.6c). Soil and road are also often confused and small bushes in zone 3 (figure 5.6d) are classified as shadow instead of vegetation.

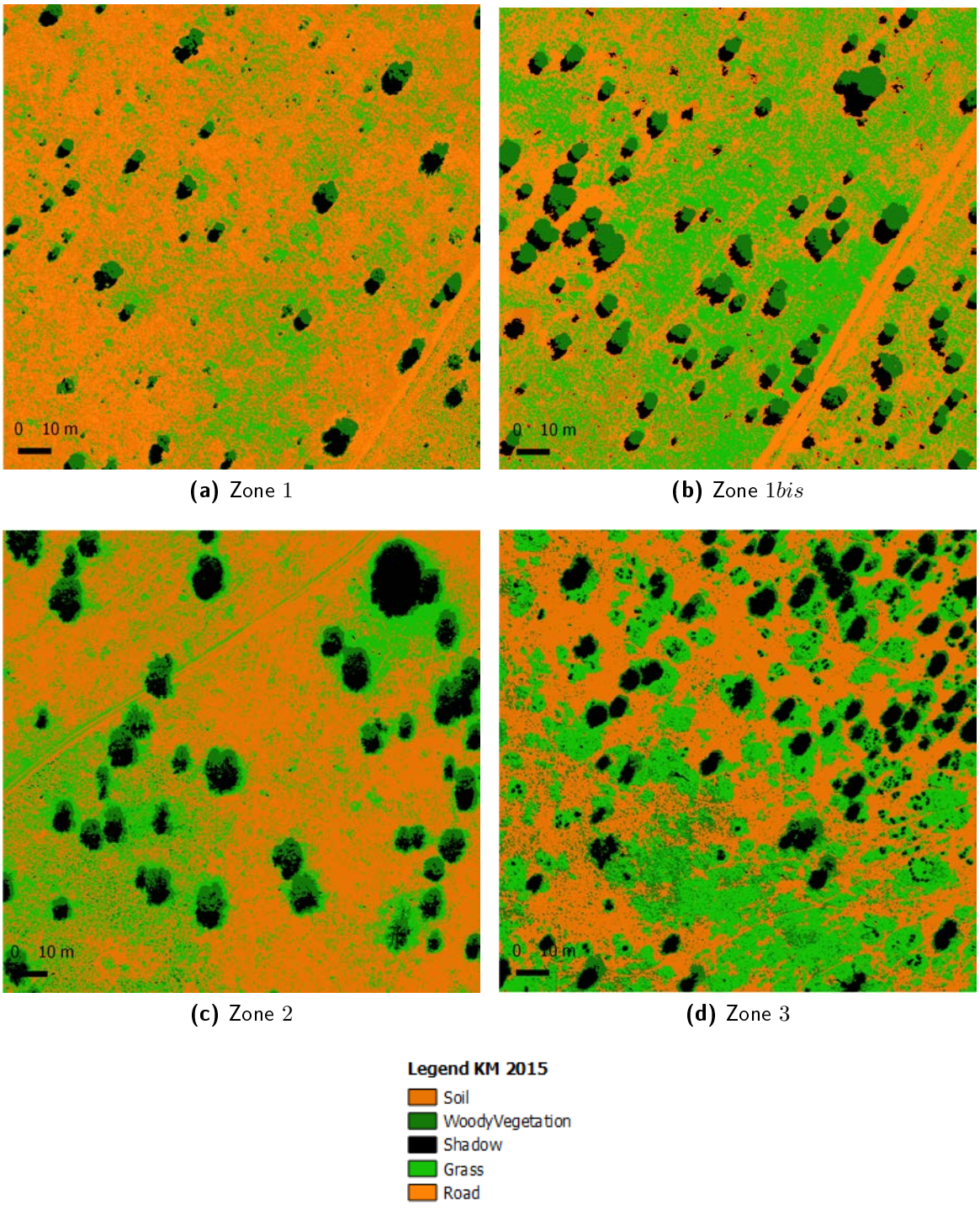

(a) Zone 1

(b) Zone 1*bis*

(c) Zone 2

(d) Zone 3

(e) Legend

Figure 5.6: K-Means classification of drone images from May 2015 over (a) zone 1, (b) zone 1bis, (c) zone 2 and (d) zone 3. (e) is the legend of the colors

Figure 5.7 shows the results for 2017 images. The number of clusters k was equal to 5 for all images. The same comments for the results obtained for 2015 images hold. In addition to that, trees without leaves are well spotted in zone 3 (figure 5.7c) but not in zone 1bis (figure 5.7b).

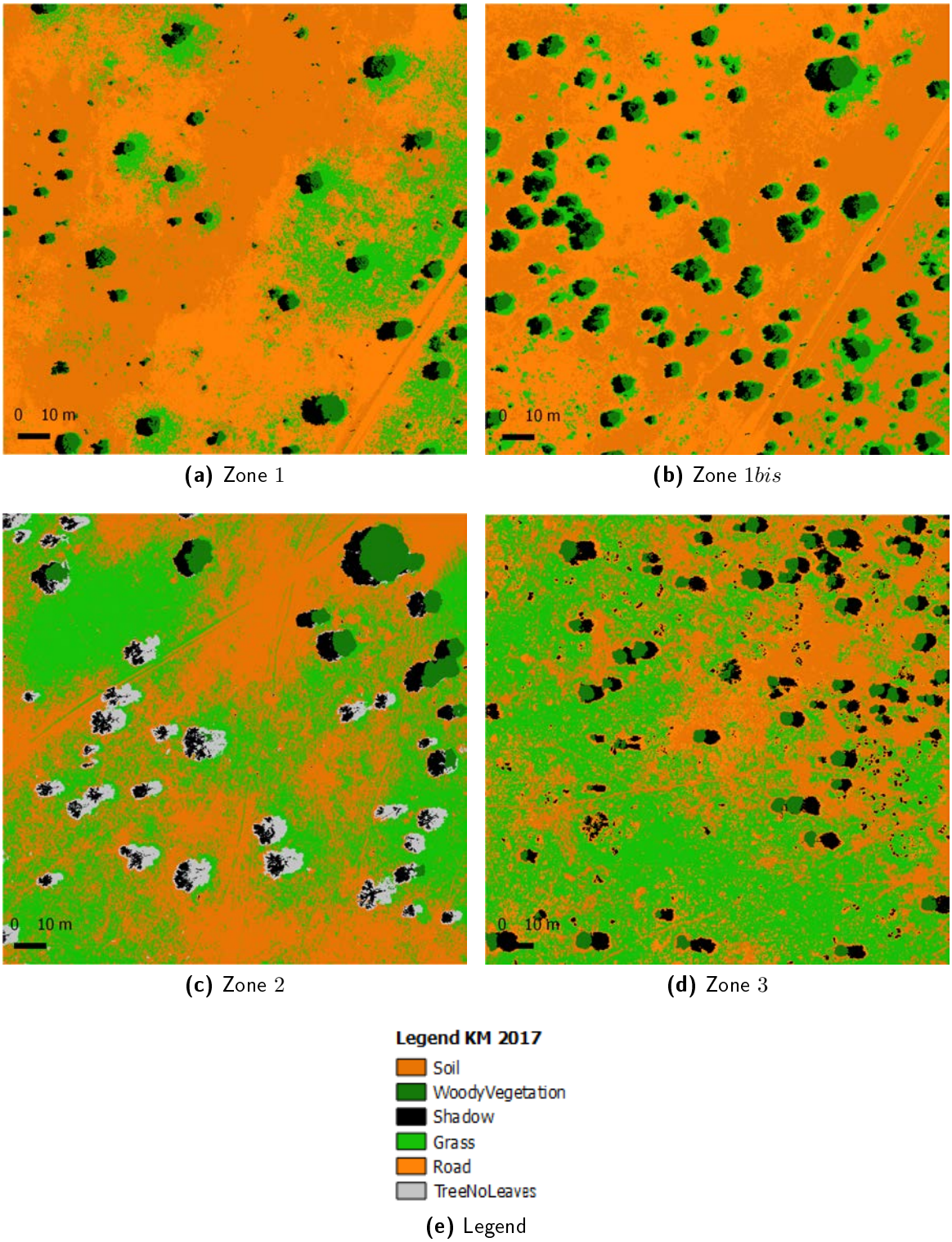

(a) Zone 1

(b) Zone $1bis$

(c) Zone 2

(d) Zone 3

(e) Legend

Figure 5.7: K-Means classification of drone images from October 2017 over (a) zone 1, (b) zone 1bis, (c) zone 2 and (d) zone 3. (e) is the legend of the colors

Accuracies for the K-Means classifications over drone images are low. For 2015 images (table 5.3), the overall accuracy and Cohen's Kappa are 42% and 26%, respectively. The statistics

confirm that samples belonging to Shadow and Woody Vegetation classes are the best classified, their precision is 96% and 47%, respectively and F statistics are above 50%. Those classes also have the higher recall: 34% and 83%, respectively. Soil, Grass and Road classes are often interchanged and have a F statistic below 35%. More details about misclassifications are available in the confusion matrix (Appendix C, table 2).

	Precision	**Recall**	**F**
Soil	0.320	0.384	0.349
Woody Vegetation	0.468	0.832	0.599
Shadow	0.955	0.341	0.503
Grass	0.312	0.246	0.275
Road	0.315	0.274	0.293

Table 5.3: Precision, recall and F statistics for K-Means classification over drone images from May 2015

For 2017 images (table 5.4), overall accuracy and Cohen's Kappa are 55% and 40%, respectively. Soil and Woody Vegetation classes have the best accuracies, with F statistics of 62% and 72%, respectively. Shadow and TreeNoLeaves, on the other hand, have the worst statistics (F is equal to 19% and 0.1%, respectively). More details about misclassifications are given in the appendix (Appendix C, table 3).

	Precision	**Recall**	**F**
Soil	0.672	0.566	0.615
WoodyVegetation	0.649	0.814	0.722
Shadow	0.288	0.147	0.194
Grass	0.367	0.367	0.367
Road	0.522	0.630	0.571
TreeNoLeafs	0.001	0.001	0.001

Table 5.4: Precision, recall and F statistics for K-Means classification over drone images from October 2017

5.4.2 Support Vector Machine (SVM)

Like K-Means, SVM was also only used with drone data. For 2015 images, results and legend are shown in figure 5.8.

Trees and shadows are generally well spotted, but shadows are often under-predicted and classified as trees, in particular in zones 2 and 3 (figures 5.8c and 5.8d). Roads are well differentiated from soil in all images and Bush 1 class is correctly classified the most of the times. Sometimes bushes of type one are classified as both Bush 1 and Tree. Bush 2 class (only present in zone 3) is well classified and rarely object of misclassifications. The majority of classification errors appear at the transition between trees and shadows, where shadows are often classified as Bush 1 or Tree. Perennial class, in yellow, is correctly classified at the bottom right of zone 1 (figure 5.8a) and at the bottom left of zones 1bis (figure 5.8b) and 2 (figure 5.8c). It is generally over-predicted elsewhere, in particular around trees and bushes.

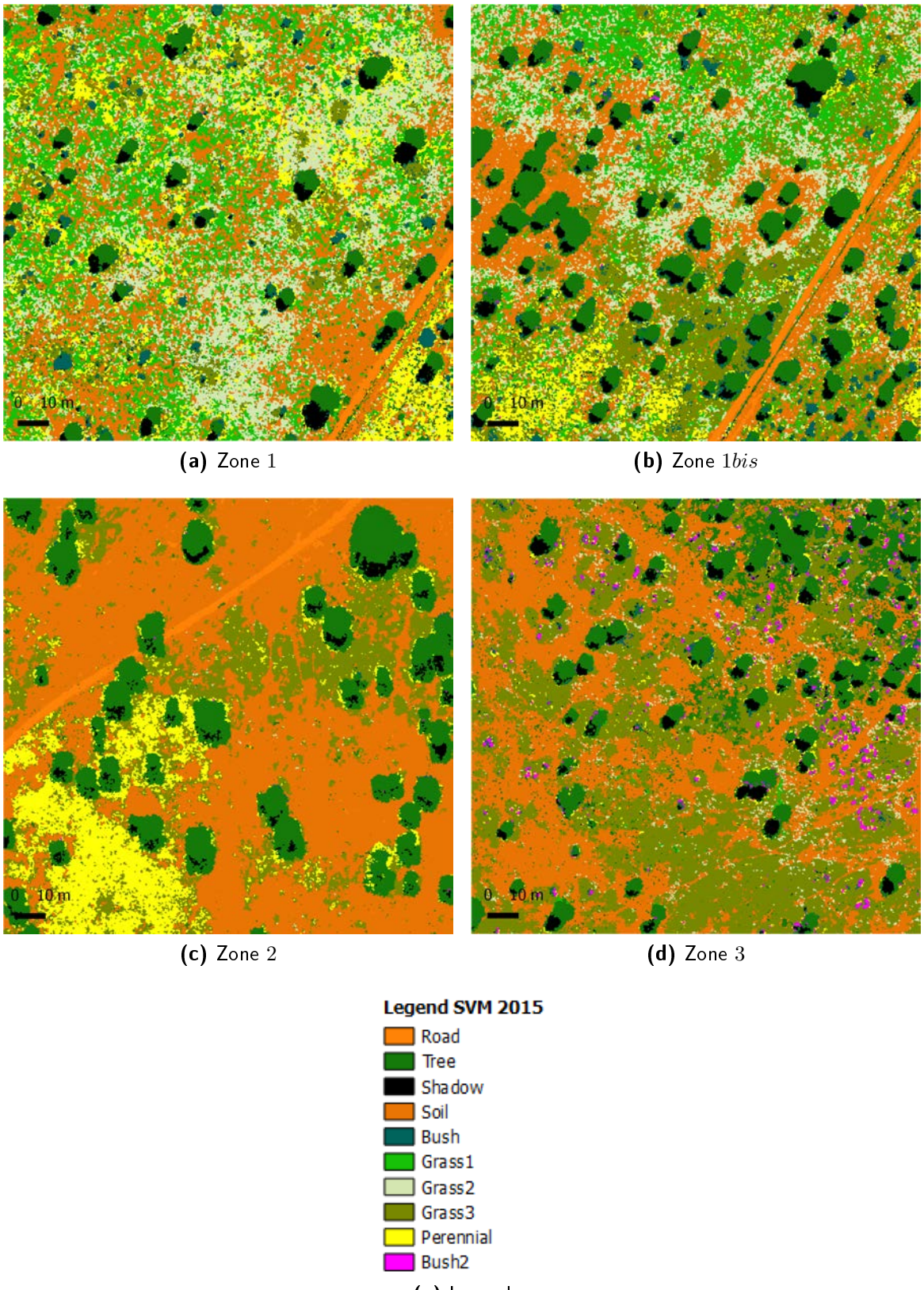

(a) Zone 1

(b) Zone $1bis$

(c) Zone 2

(d) Zone 3

(e) Legend

Figure 5.8: SVM classification of drone images from May 2015 over (a) zone 1, (b) zone 1bis, (c) zone 2 and (d) zone 3. (e) is the legend of the colors

Figure 5.9 shows a detail from zone 3 (figure 5.8d) representing the correct classification of Bush 2 (in pink) and some patches of Grass 3 (dark green) and the over-prediction of perennial

grasses (in yellow).

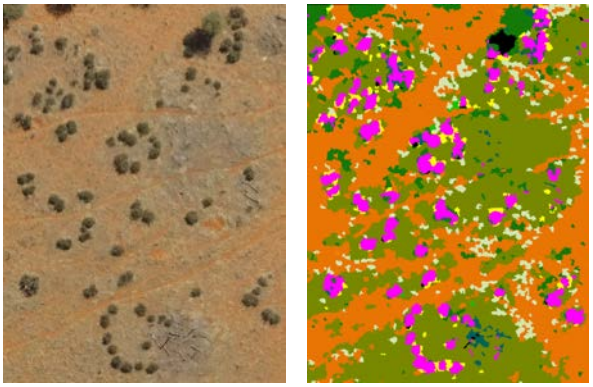

(a) Detail of the original RGB image over zone 3 from 2015

(b) Corresponding classified image

Figure 5.9: Detail of (a) the original RGB image over zone 3 from 2015 data representing Bush 2, Soil and Grass 3 classes and (b) the corresponding classified image

Figure 5.10 shows a small area of zone 1 with Grass 1 (in green), Grass 2 (in beige) and Soil (in orange) classes (figure 5.10a) and the corresponding classification results (figure 5.10b). Objects are almost all correctly classified.

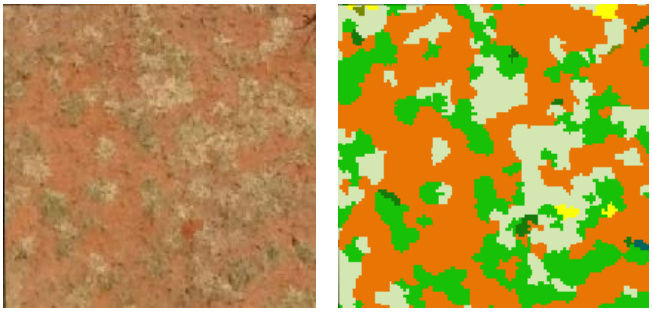

(a) Detail of the original RGB image over zone 1 from 2015

(b) Corresponding classified image

Figure 5.10: Detail of (a) the original RGB image over zone 1 from 2015 data representing Grass 1, Grass 2 and Grass 3 classes and (b) the corresponding classified image

Although in the most of the images grasses are well classified, they are sometimes wrongly classified as trees, in particular in zone 3 (figure 5.8d). The classification allows to also spot small details like narrow roads created by animals, which are visible in zone 1 (figure 5.8a).

Figure 5.11 shows the results for 2017 images. Although some classes like Bush 2 and Road are well classified, the class Tree 1 is largely over-predicted at the expenses of all other classes, in particular soil. This is particularly visible in zones 1 and 1bis (figures 5.11a and 5.11b). Bushes of type 1 are small in this season. They are correctly spotted but their contours wrongly classified as Tree 1. Tree 2 is well distinguished from Tree 1 (figures 5.11b and 5.11c).

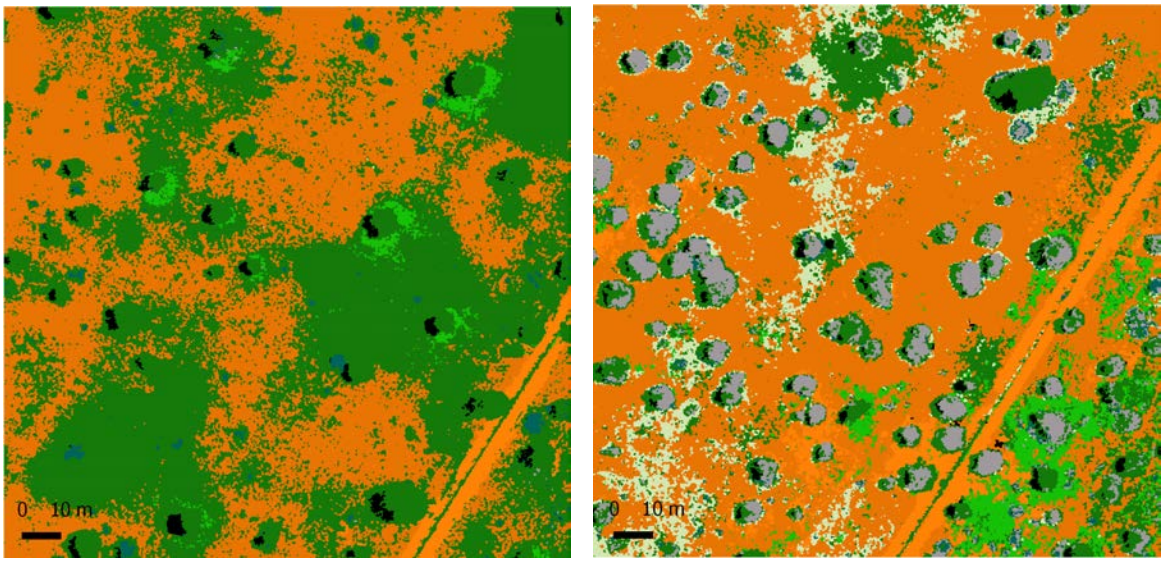

(a) Zone 1 **(b)** Zone 1*bis*

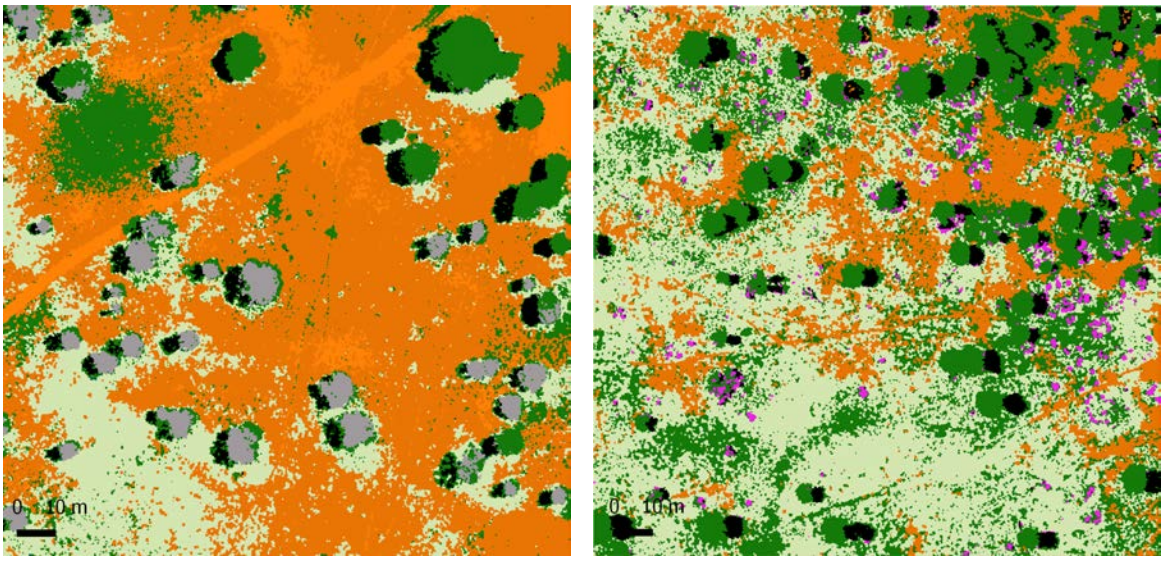

(c) Zone 2 **(d)** Zone 3

(e) Legend

Figure 5.11: SVM classification of drone images from October 2017 over (a) zone 1, (b) zone 1bis, (c) zone 2 and (d) zone 3. (e) is the legend of the colors

Table 5.5 shows the calculated statistics for 2015 images, which are all very high. Overall accuracy and Cohen's Kappa are both 98% and precision, recall and F1 statistics are above 93% for all classes. The worst accuracies are for Bush 1 and Perennial classes, which have F statistics of 95% and 94%, respectively. The confusion table is in the appendix (Appendix C, table 4).

	N Tain	N test	Precision	Recall	F
Road	11417	17127	0.979	0.991	0.985
Tree	24024	36037	1.000	0.993	0.996
Shadow	5345	8019	0.986	0.985	0.985
Soil	10449	15672	0.986	0.976	0.981
Bush1	3600	5401	0.952	0.944	0.948
Grass1	3815	5721	0.978	0.984	0.981
Grass2	2921	4381	0.975	0.990	0.982
Grass3	7501	11252	0.974	0.984	0.979
Perennial	3017	4524	0.945	0.935	0.940
Bush2	1532	2297	0.955	0.995	0.974

Table 5.5: Number of training and test samples and precision, recall and F statistics for SVM classification over drone images from May 2015

Table 5.6 reports the statistics for 2017 images. All statistics are above 96%, overall accuracy and Cohen's Kappa are both 99%. Those results contrast with the classified image, where many samples where clearly wrongly classified. The confusion table in the appendix (Appendix C, table 5) gives an overview of the misclassifications, Tree 1 class is the one with most samples actually belonging to other classes.

	N Tain	N test	Precision	Recall	F
Road	21292	31940	0.999	1.000	0.999
Tree	46773	70160	0.998	0.992	0.995
Shadow	12293	18441	0.991	0.987	0.989
Soil	24719	37078	0.994	0.999	0.996
Bush1	2552	3829	0.965	0.997	0.981
Grass1	1516	2272	0.971	1.000	0.985
Grass2	9353	14028	0.997	0.999	0.998
Tree2	13766	20648	0.995	0.996	0.995
Bush2	2333	3499	0.961	0.965	0.963

Table 5.6: Number of training and test samples and precision, recall and F statistics for SVM classification over drone images from October 2017

5.4.3 Random Forest

Random Forest classifier was used for both drone and satellite images.

Drone images

Results for 2015 drone images classification are shown in figure 5.12.

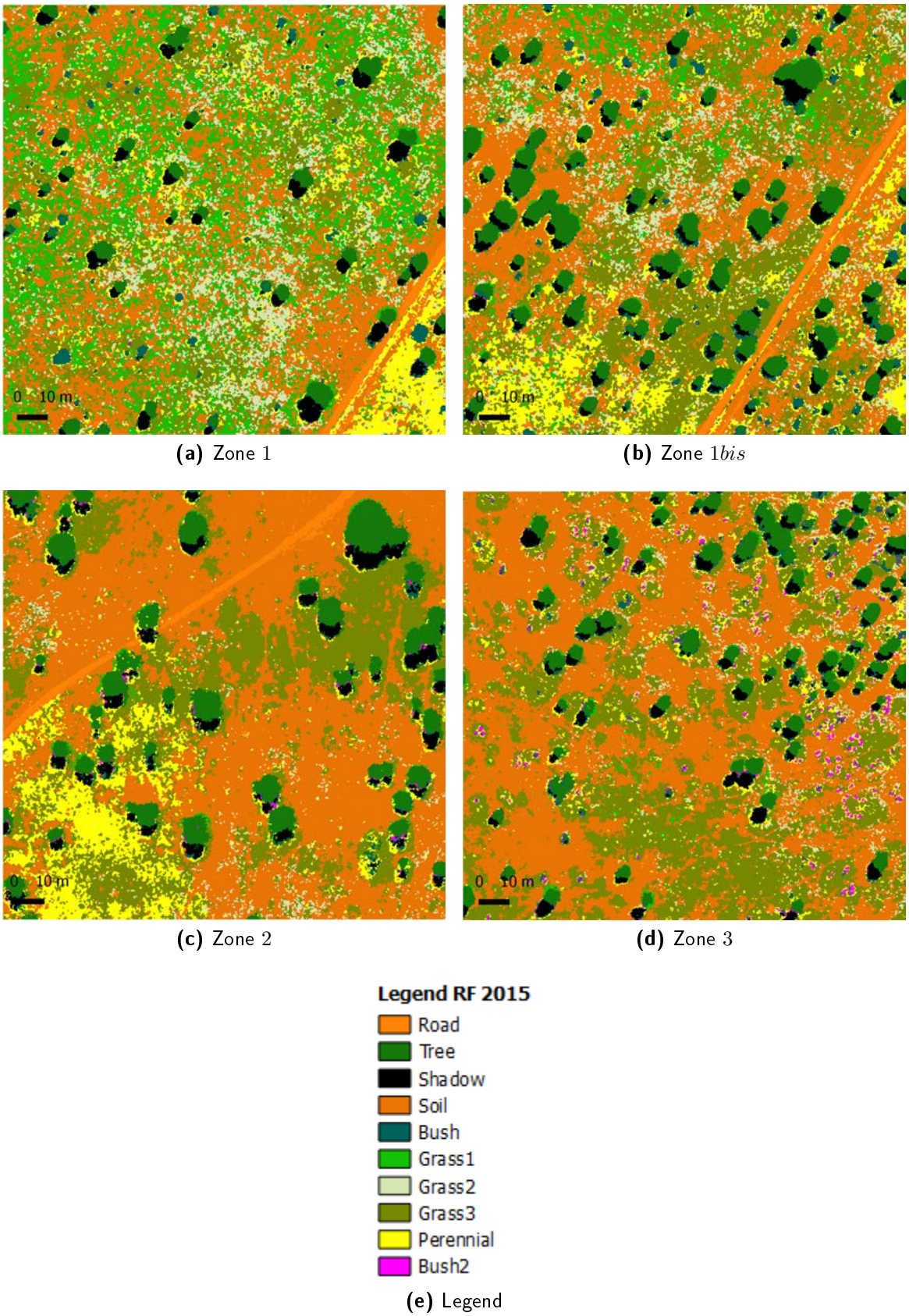

(a) Zone 1

(b) Zone $1bis$

(c) Zone 2

(d) Zone 3

(e) Legend

Figure 5.12: RF classification of drone images from May 2015 over (a) zone 1, (b) zone 1bis, (c) zone 2 and (d) zone 3. (e) is the legend of the colors

Objects belonging to classes Bush 1, Bush 2, Tree, Road and Shadow are generally correctly

classified and perennial grasses are less over-predicted than with SVM classifier. On the other hand, Grass 1, 2 and 3 classes are under-predicted, samples belonging to this class are often classified as soil. Like with SVM, but in a larger extent, many misclassifications exist at the transitions between objects. Pixels between shadows and soil are often wrongly classified as Bush 1, Bush 2 or Perennial. Figure 5.13 shows an example of this phenomenon: shadows, (black) are contoured by pixels classified as Bush 1 (blue) or Perennial (yellow).

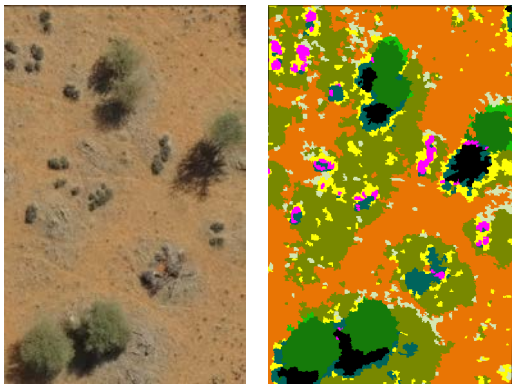

(a) Detail of the original RGB image over zone 3 from 2015

(b) Corresponding classified image

Figure 5.13: Detail of (a) the original RGB image over zone 1 from 2015 data and (b) the corresponding classified image showing the misclassifications at the transitions between objects

Classified images from 2017 drone data are given in figure 5.15. All classes are well classified and there is fewer noise around objects than in 2015. The bigger mistakes are in zone 3 (figure 5.15d), where parts of shadows are often classified as Bush 2. Tree 2 is also over-predicted in some areas, in particular in zone 1 (figure 5.19a), where some pixels belonging to Grass 1 or Grass 2 are classified as Tree 2. In the same zone, some pixels belonging to Bush 1 are wrongly classified as Tree 2. In general Tree 1 and Tree 2 are well distinguished and it is possible to see which trees already have green leaves, which one do not have them yet and which one are starting to get them. Figure 5.14 shows a detail of zone 2 where it is possible to see these three types of trees.

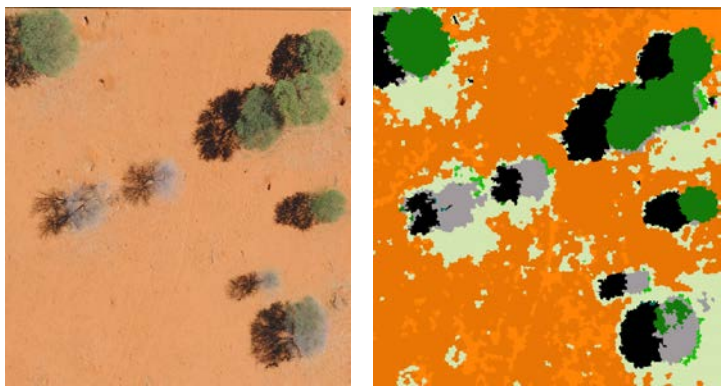

(a) Detail of the original RGB image over zone 2 from 2015

(b) Corresponding classified image

Figure 5.14: Detail of (a) the original RGB image over zone 2 from 2015 data showing trees that already have green leaves, that do not have them yet and that are starting to get them and (b) the corresponding classified image

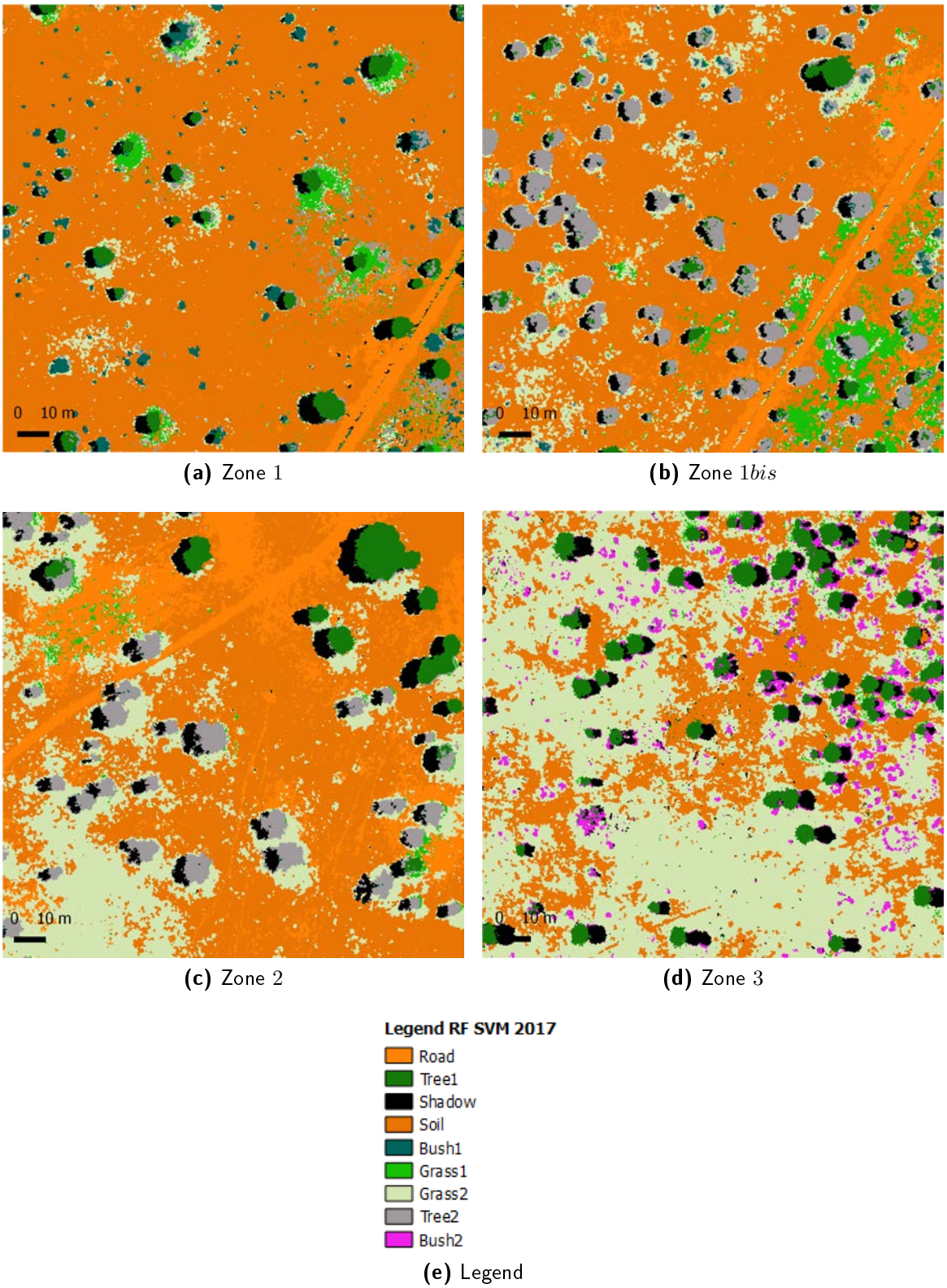

(a) Zone 1

(b) Zone $1bis$

(c) Zone 2

(d) Zone 3

(e) Legend

Figure 5.15: RF classification of drone images from October 2017 over (a) zone 1, (b) zone 1bis, (c) zone 2 and (d) zone 3. (e) is the legend of the colors

Statistics on 2015 images are shown in table 5.7. Overall accuracy and Cohen's Kappa are both 97%. Precision, recall and F1 statistics range between 67% and 99%. Road and Shadow classes have excellent statistics and are the most pure classes (confusion matrix in Appendix C, table 6). Some misclassifications appear between Road and Soil classes. Tree and Soil have also

excellent statistics, but samples belonging to other classes are often assigned to those classes. Bushes and grasses have the lowest statistics and highest impurities, in particular perennial grasses (F statistic equal to 80%). Indeed, bushes and Grass 3 are often classified as Perennial.

	N Tain	N test	Precision	Recall	F
Road	2855	25689	0.977	0.992	0.984
Tree	6006	54055	0.998	0.994	0.996
Shadow	1337	12027	0.967	0.992	0.979
Soil	2612	23509	0.985	0.968	0.976
Bush1	901	8100	0.917	0.873	0.894
Grass1	953	8583	0.977	0.974	0.975
Grass2	730	6572	0.951	0.978	0.965
Grass3	1875	16878	0.972	0.959	0.966
Perennial	754	6787	0.946	0.854	0.898
Bush2	383	3446	0.676	0.991	0.803

Table 5.7: Number of training and test samples and precision, recall and F statistics for RF classification over drone images from May 2015

Statistics for 2017 images, shown in table 5.8, are all above 90%. Overall accuracy and Cohen's Kappa are both 98%. The classifiers led to only a few misclassifications, which mainly concern confusion between the two types of tree (confusion table in the Appendix C, table 7).

	N Tain	N test	Precision	Recall	F
Road	5324	47908	0.997	0.998	0.998
Tree	13543	121896	0.972	0.995	0.983
Shadow	2970	26721	0.996	0.980	0.988
Soil	6180	55617	0.991	0.998	0.994
Bush1	638	5743	0.952	0.973	0.962
Grass1	378	3410	0.994	0.992	0.993
Grass2	2338	21043	0.999	0.997	0.998
Tree2	3441	30973	0.983	0.901	0.940
Bush2	584	5248	0.971	0.953	0.962

Table 5.8: Number of training and test samples and precision, recall and F statistics for RF classification over drone images from October 2017

Figure 5.16 show the OOB error estimate for 2015 and 2017 classifications. For 2015 images it decreases and stabilizes below 0.1 while for 2017 it continues to slowly decrease. After 500 trees it is below 0.2.

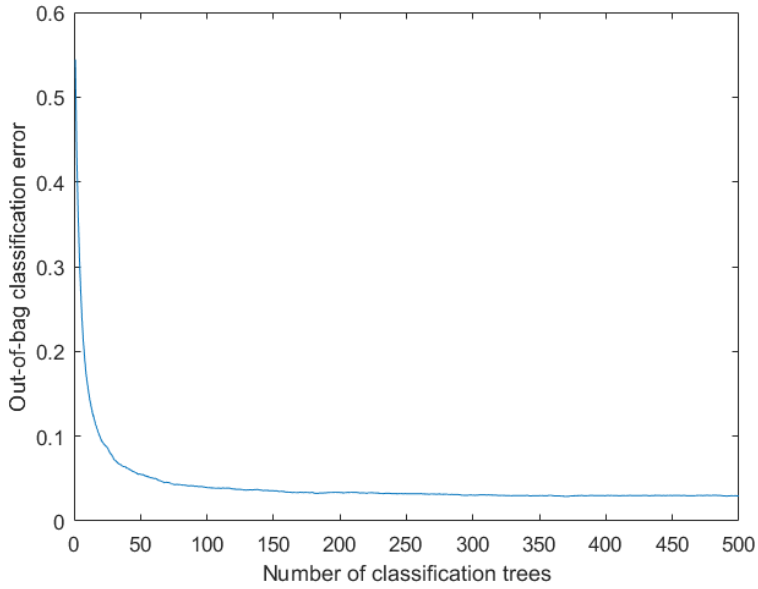

(a) 2015

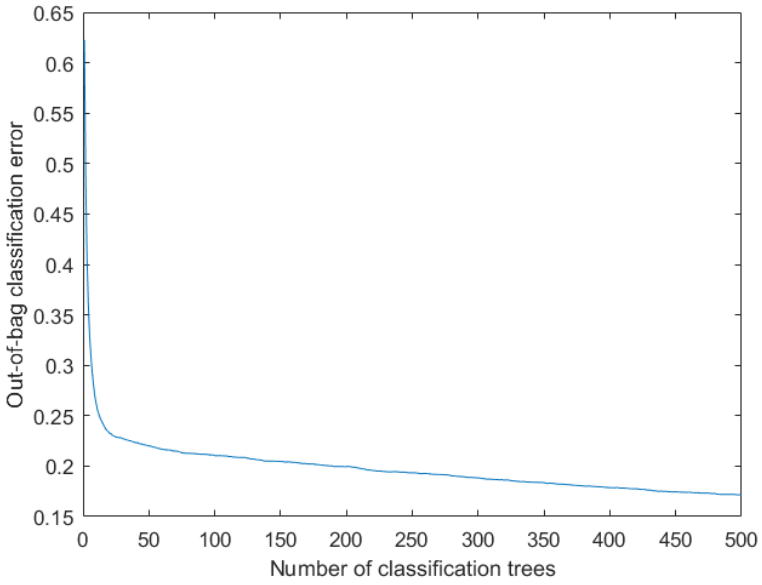

(b) 2017

Figure 5.16: OOB error estimate for RF classification over (a) 2015 and (b) 2017 drone images

Satellite images

Results given by RF classifier with Sentinel-2 images from May and October 2017 are shown in figures 5.17 and 5.18, respectively. The general patterns of the classified images well represent those of the original ones, in particular in the distinction between soil and vegetation. Limestone soil is correctly classified in the northern part of the reserve and allows to recognize the location of water points. Almost no pixels are classified as sand in the western part of the reserve, while this class dominates the north eastern part of Kuzikus. Classifications from May and October images are similar, the biggest differences are in the vegetation classes. The class representing trees is more abundant in May than in October, while for grasses it is the opposite.

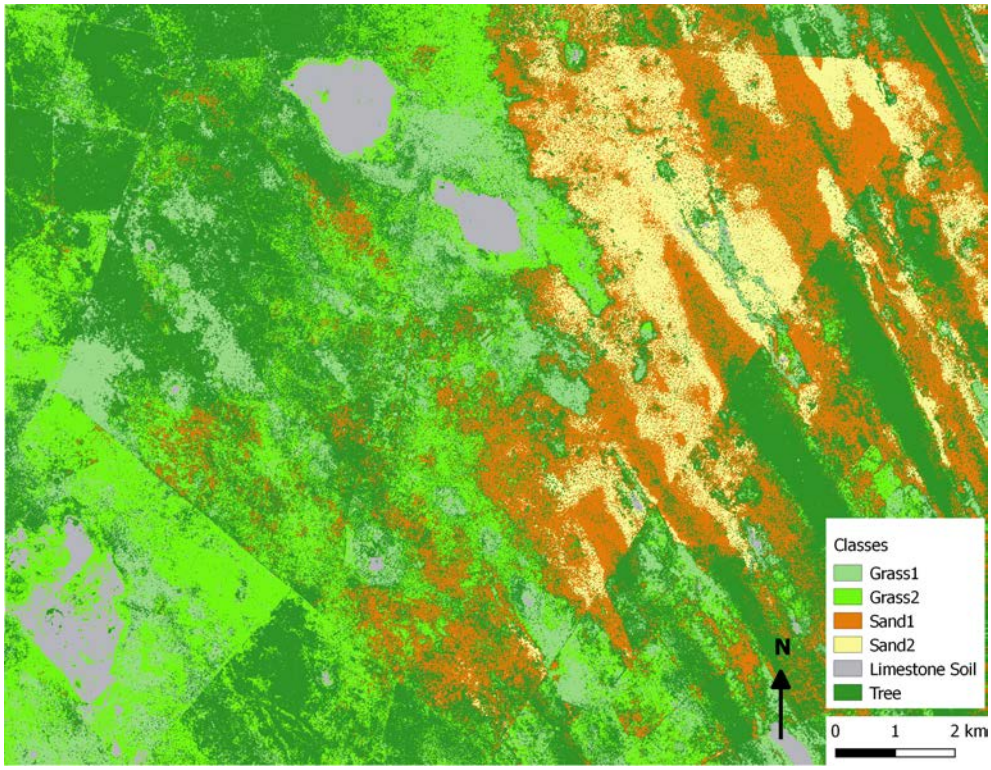

Figure 5.17: Random Forest classification, Sentinel-2 May 2017

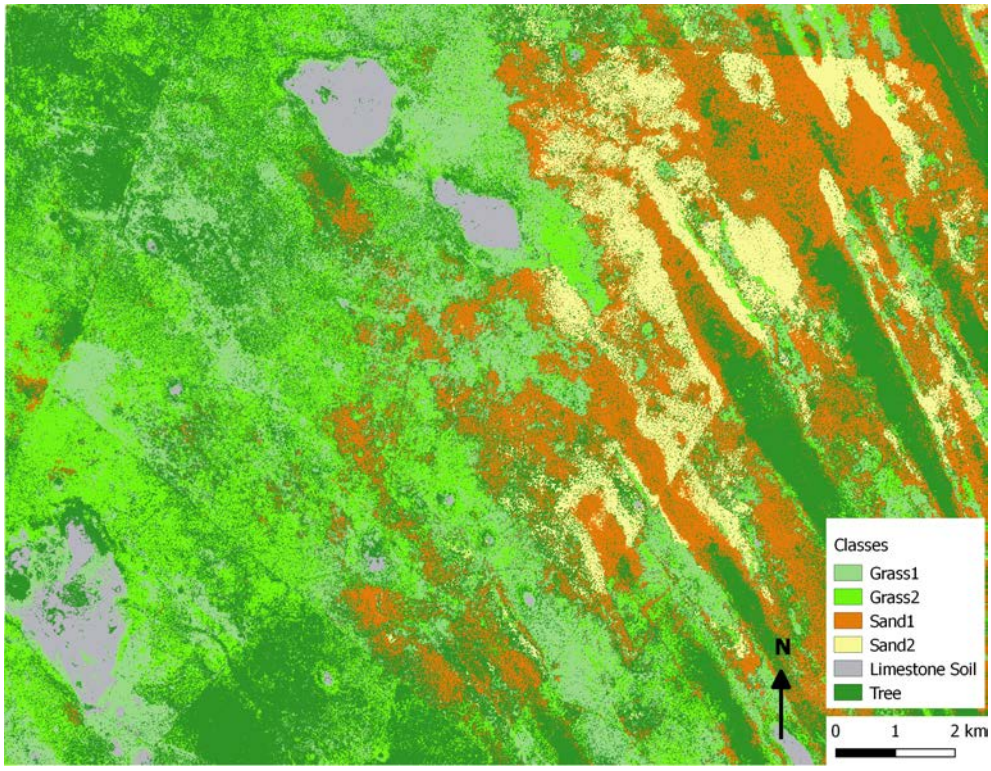

Figure 5.18: Random Forest classification, Sentinel-2 October 2017

For the image dating May 2017, statistics are given in table 5.9. An overall accuracy of 94%

and a Cohen's Kappa of 93% are reached. Precision, recall and F statistics for Limestone soil, Sand 1 and Sand 2 classes are all above 96%. Grass 1 and Grass 2 come after and Tree is the least precisely classified class (F1 score is 79%). The Limestone soil class is hardly ever misclassified, while samples belonging to the Tree class are often classified as grasses. Some misclassifications between the two grass species also exist. More information is given in the confusion matrix in the appendix (Appendix C, table 8).

	N Tain	N test	Precision	Recall	F
Grass1	1355	2709	0.895	0.928	0.911
Grass2	1109	2221	0.906	0.881	0.893
Sand1	1481	2960	0.967	0.969	0.968
Sand2	980	1959	0.989	0.994	0.992
Limestone soil	1785	3573	0.999	0.998	0.999
Tree	651	1300	0.798	0.772	0.785

Table 5.9: Number of training and test samples and precision, recall and F statistics for RF classification over Sentinel-2 image from May 2017

Sentinel-2 images from October 2017 gave similar results (table 5.10). The overall accuracy of the classification is 93% and Cohen's Kappa 91%. The confusion matrix is available in the appendix C, table 9.

	N Tain	N test	Precision	Recall	F
Grass1	1354	2710	0.867	0.898	0.882
Grass2	1110	2220	0.877	0.845	0.861
Sand1	1480	2961	0.965	0.967	0.966
Sand2	980	1959	0.984	0.996	0.990
Limestone soil	1786	3572	0.999	0.998	0.999
Tree	651	1300	0.801	0.779	0.790

Table 5.10: Number of training and test samples and precision, recall and F statistics for RF classification over Sentinel-2 image from October 2017

The OOB error estimate (figure 5.19) rapidly stabilizes around 0.1 for both classifications.

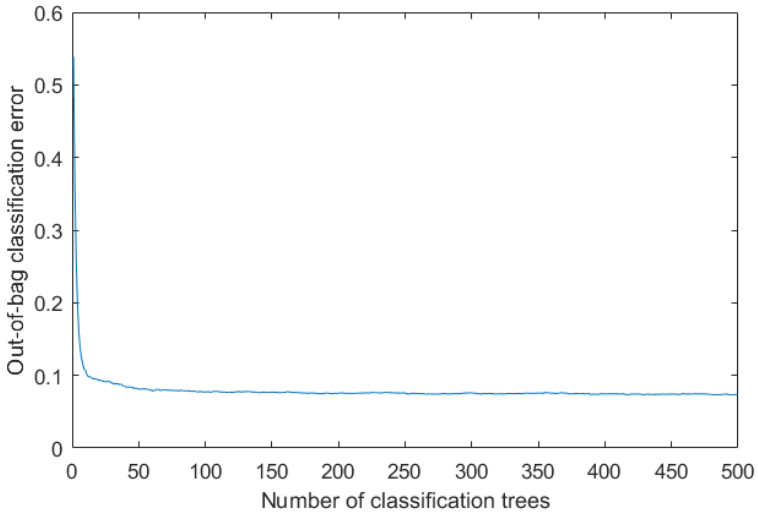

(a) 2015

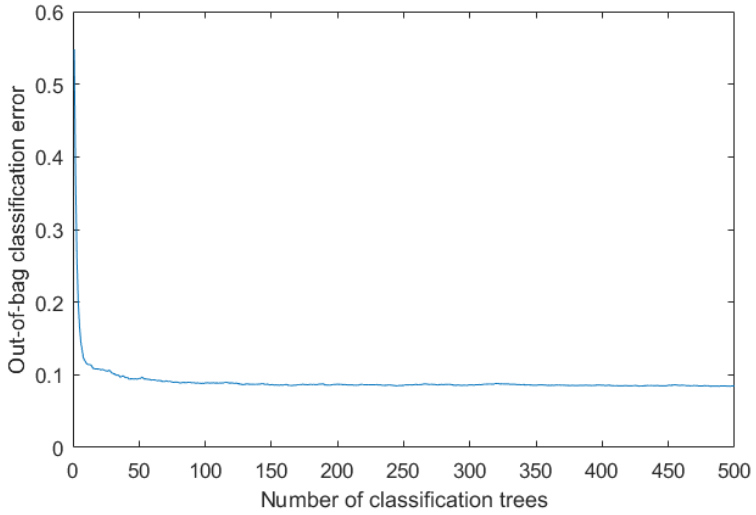

(b) 2017

Figure 5.19: OOB error estimate for RF classification over (a) May and (b) October satellite images

The following three figures show a comparison between Sentinel-2 classification results and drone orthophotos from October 2017 over zones 1 and 1bis (figure 5.20), zone 2 (figure 5.21) and zone 3 (figure 5.22). Drone images are superposed to satellite classification results with 40% transparency. In figure 5.20, Random Forest classification over the Sentinel-2 image correctly identified the majority of trees, in particular the big ones or trees close to each other. In the bottom right part of the figure, all is classified as tree, while in reality it is mostly grasses. In the rest of the image, grass patches, which are smaller than the pixel size of $10x10$ meters, are not identified. In figure 5.21 the situation is similar. In figure 5.22 the grass cover on the ground is more abundant than sand and Sand 1 and Sand 2 classes are not present. In the middle of the image there is a water point with bare soil around (grey), in turn contoured by big trees. Again, trees are almost always correctly identified.

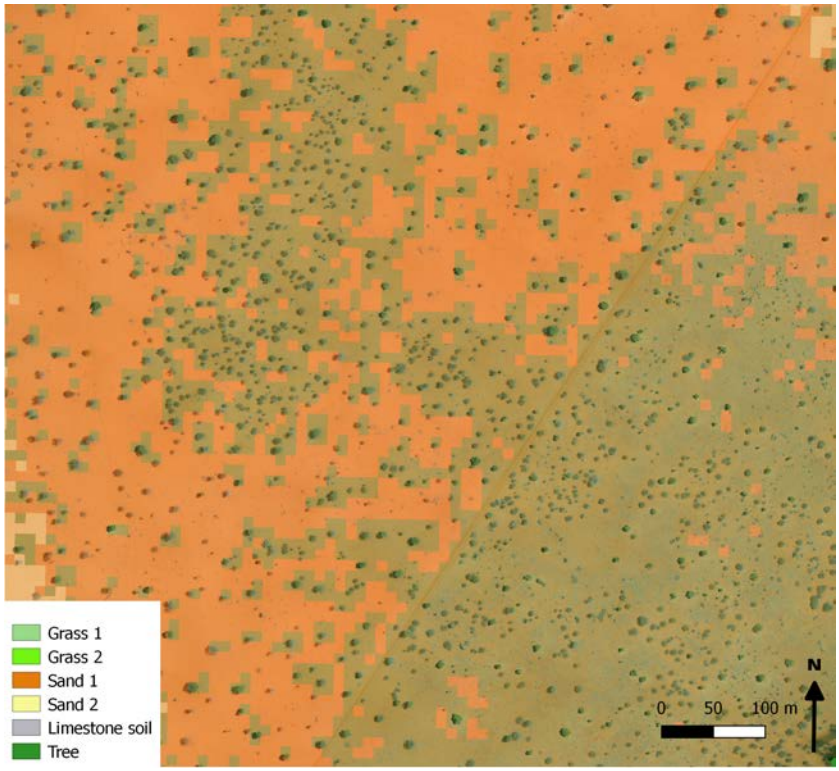

Figure 5.20: Comparison between RF classificatin results over the Sentinel-2 image from October 21, 2017 and an eBee Plus Orthophoto from October 17, 2017 over zone 1

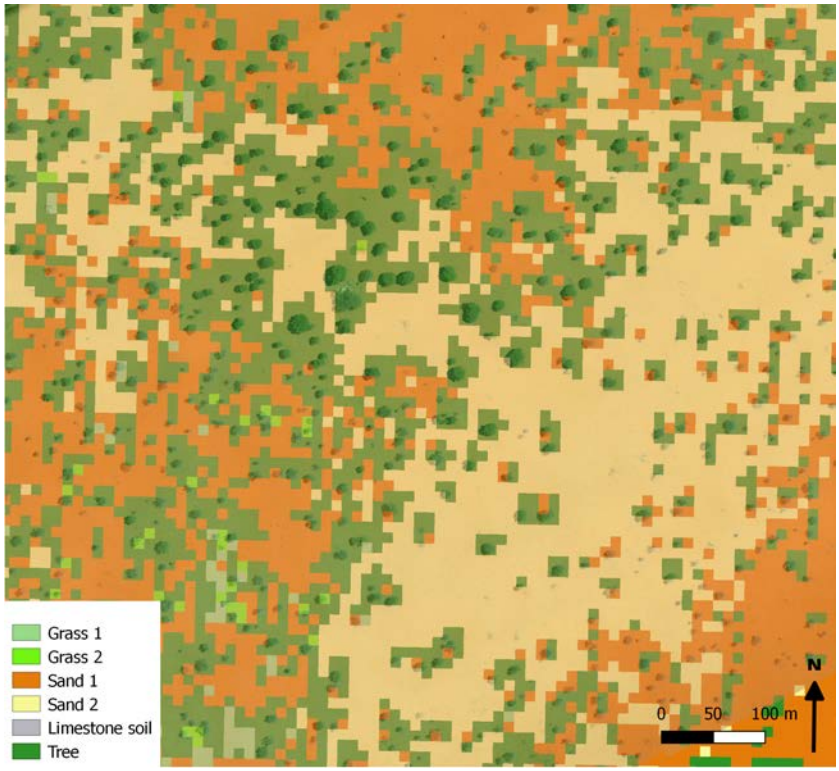

Figure 5.21: Comparison between RF classificatin results over the Sentinel-2 image from October 21, 2017 and an eBee Plus Orthophoto from October 16, 2017 over zone 2

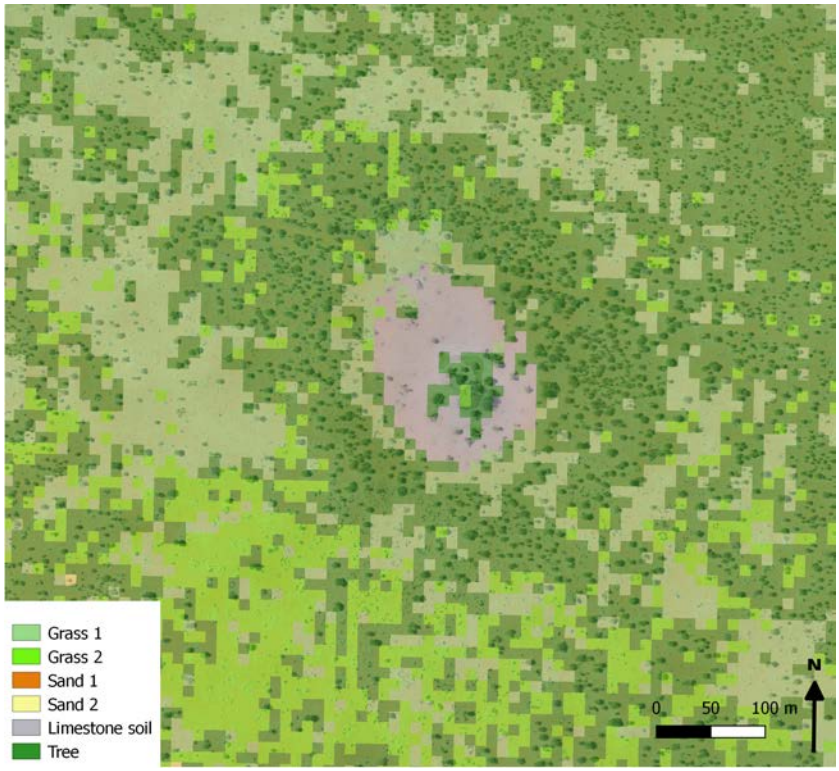

Figure 5.22: Comparison between RF classificatin results over the Sentinel-2 image from October 21, 2017 and an eBee Plus orthophoto from October 17, 2017 over zone 3

5.5 Sampling and accuracy assessment

Table 5.11 summarizes the overall accuracies and Cohen's Kappa statistics for all classifications. Considering drone images, SVM classification gave slightly better statistics than RF for both years. However, from the 2017 classified images with this algorithm, many mistakes were visible.

Platform	Classification	Overall accuracy	Cohen's Kappa
Drone	K-Means 2015	42%	26%
	K-Means 2017	55%	40%
	SVM 2015	98%	98%
	SVM 2017	99%	99%
	RF 2015	97%	97%
	RF 2017	98%	98%
Sentinel-2	RF May	94%	93%
	RF October	93%	91%

Table 5.11: Comparison of overall accuracy and Cohen's Kappa for all classifications

The following of this chapter gives the sampling fractions and accuracy assessments through spectral signature comparison for RF and SVM classifications. K-Means was not taken into account as classification results led to the distinction of only a minimal part of the original classes. The spectral signature comparison compares the median values of the spectral bands for each class before and after classification. The spectral signature before classification is calculated using the ground truth samples, while the one after classification using all samples of

the images.

Drone images

The split fraction of the train and test sample for both 2015 and 2017 SVM classifications was 0.6 for testing and 0.4 for training the model. For Random Forest, the split fraction was 0.9 for testing and 0.1 for training the model for both 2015 and 2017 images.

For drone images, medians of green, red and NIR bands are calculated from the same camera (NIR for 2015 and MS for 2017) while the blue bands come from the RGB cameras. Graphs obtained from 2015 images (figures 5.23, 5.24 and 5.25) show similar curves before and after classifications, with the exception of Bush 1 class (figure 5.24). RF classifier gave lower values for Bush 1 compared to the curves obtained from SVM and ground truth data. Medians over vegetation classes and Shadow class have higher values compared to ground truth data. Standard deviations of the median values are given in the appendix D, figure 1.

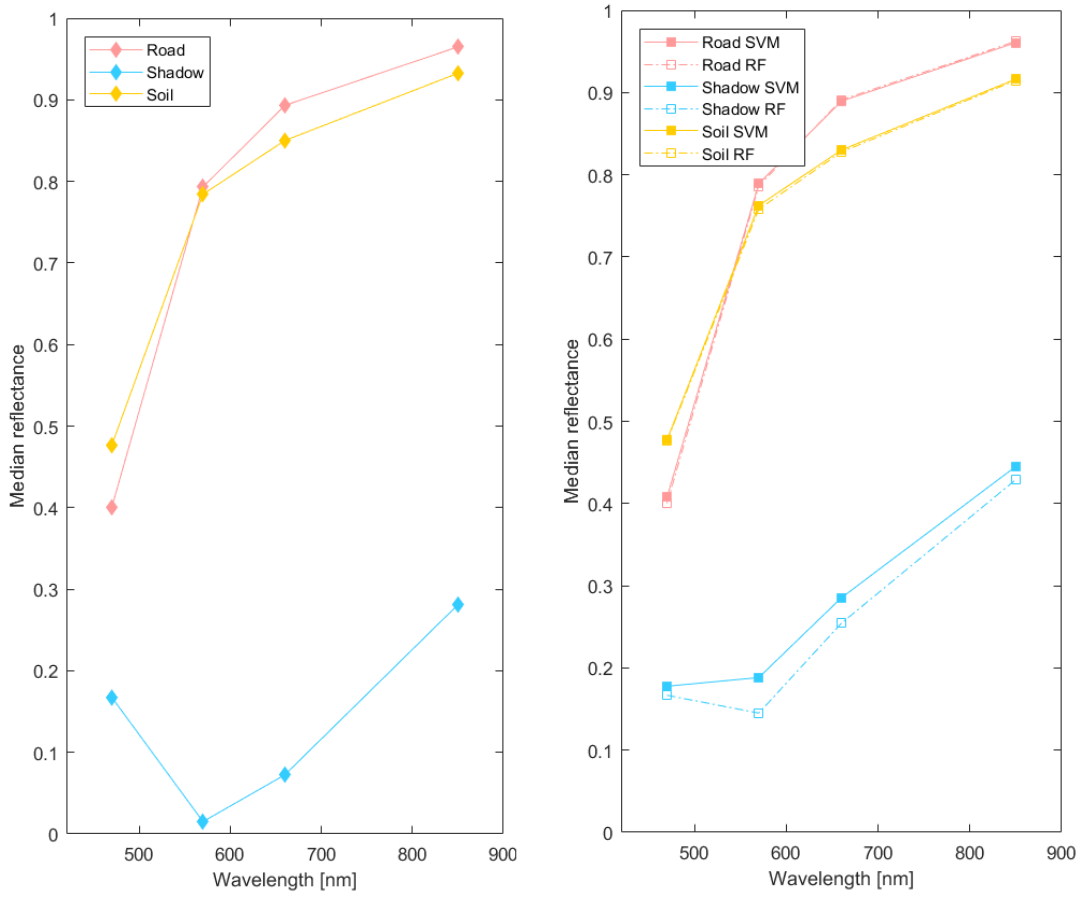

(a) Before classification **(b)** After classification

Figure 5.23: Spectral signatures of Soil, Road and Shadow classes (a) before classification and (b) after SVM and RF classifications of 2015 drone images

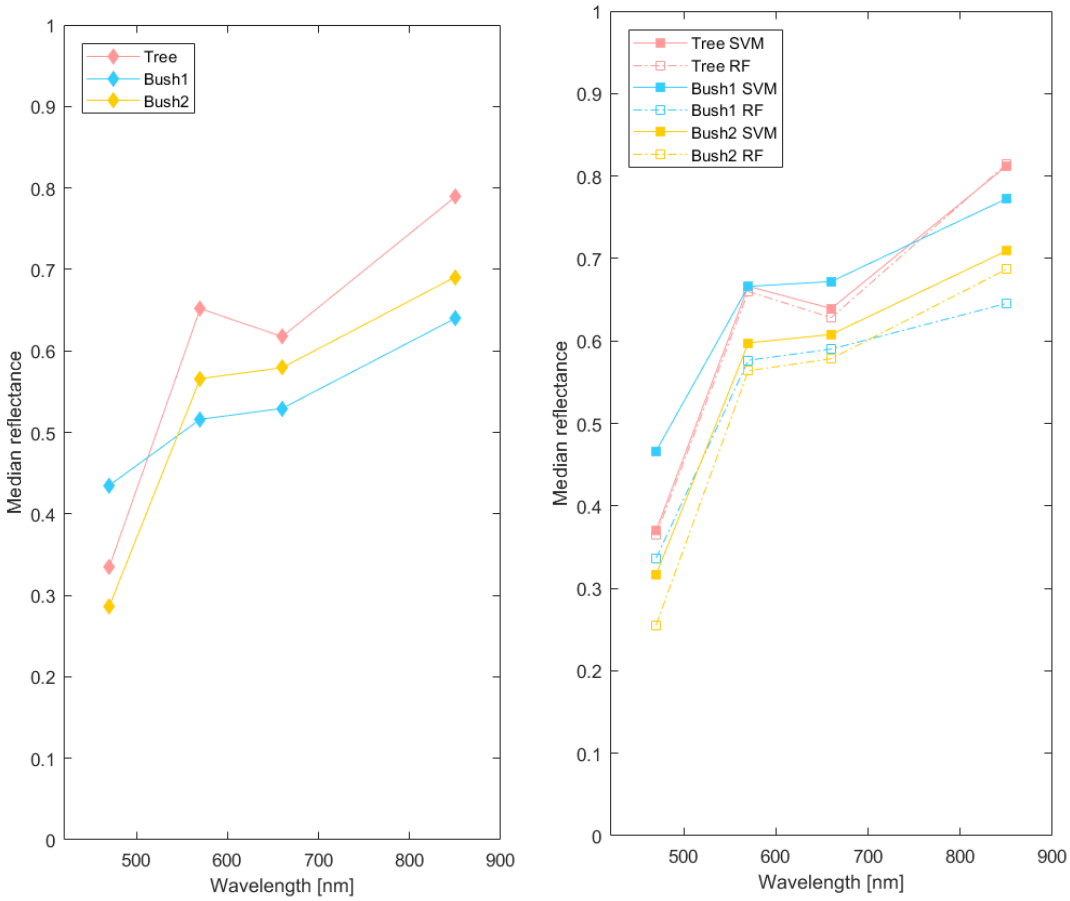

(a) Before classification **(b)** After classification

Figure 5.24: Spectral signatures of Tree, Bush 1 and Bush 2 classes (a) before classification and (b) after SVM and RF classifications of 2015 drone images

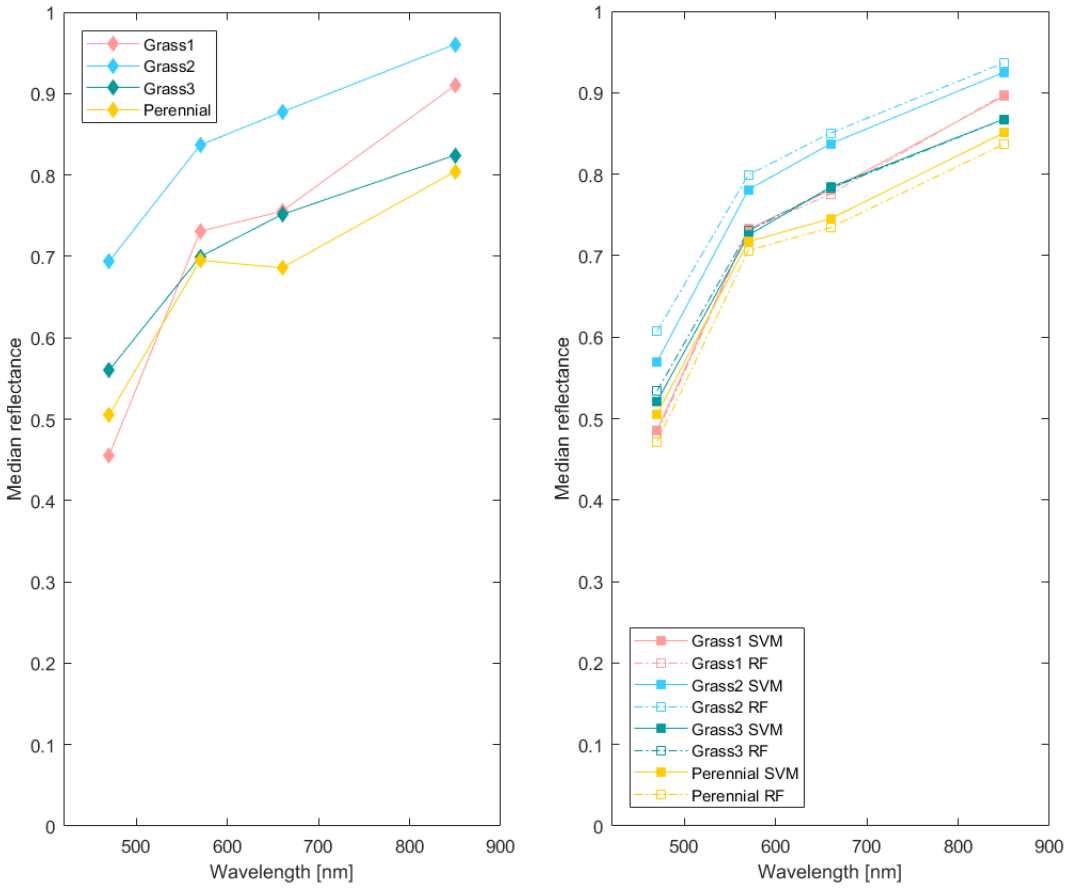

(a) Before classification **(b)** After classification

Figure 5.25: Spectral signatures of Grass 1, Grass 2, Grass 3 and Perennial classes (a) before classification and (b) after SVM and RF classifications of 2015 drone images

Graphs from 2017 images (figures 5.26, 5.27 and 5.28) show that RF and SVM had almost the same results and that they are consistent with the spectral signature obtained from ground truth data for all classes except Tree 1 with SVM classifier (figure 5.27b). Here is very well visible the wrong classification of Tree 1 class with this classification method. Indeed, this class has median values completely different from those obtained from ground truth data and RF. Values for Bush 1 and Shadow slightly differ between SVM and RF and are higher than those from the ground truth (figures 5.26 and 5.27). Standard deviations of the median values are given in the appendix D, figure 2.

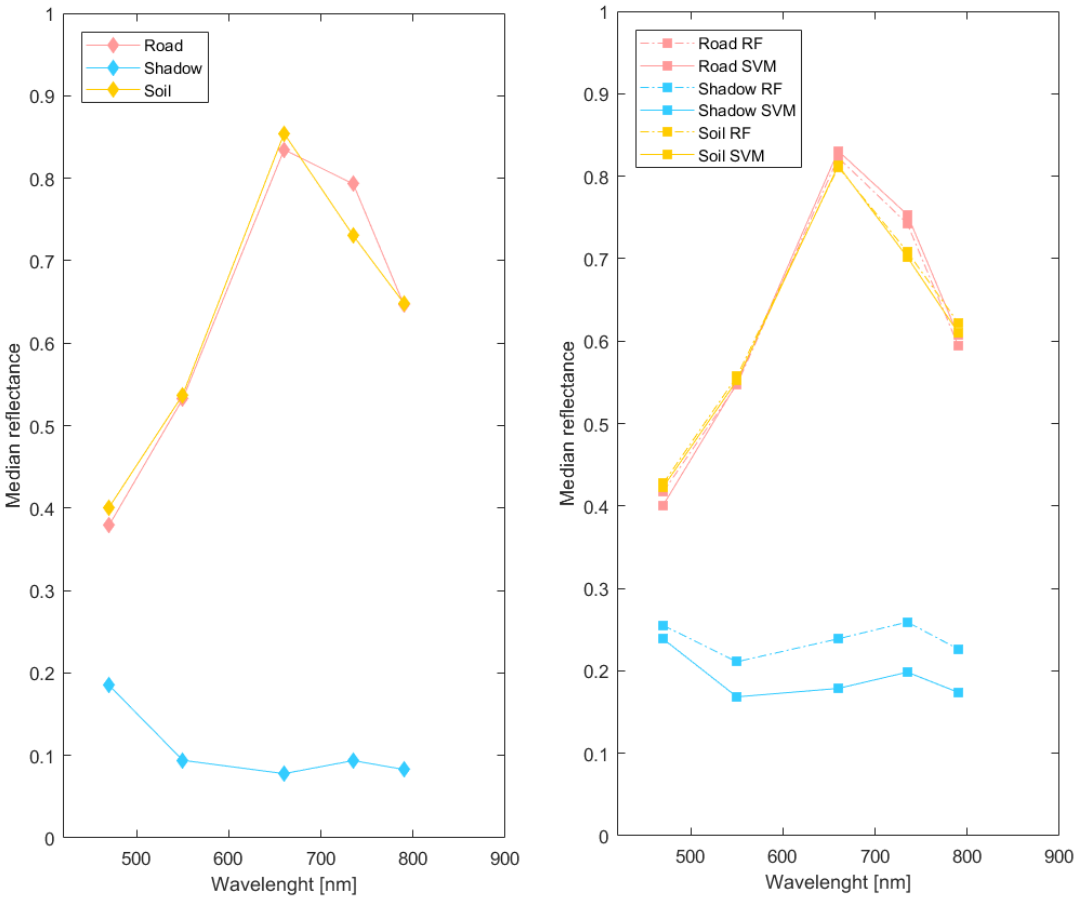

(a) Before classification **(b)** After classification

Figure 5.26: Spectral signatures of Soil, Road and Shadow classes (a) before classification and (b) after SVM and RF classifications of 2017 drone images

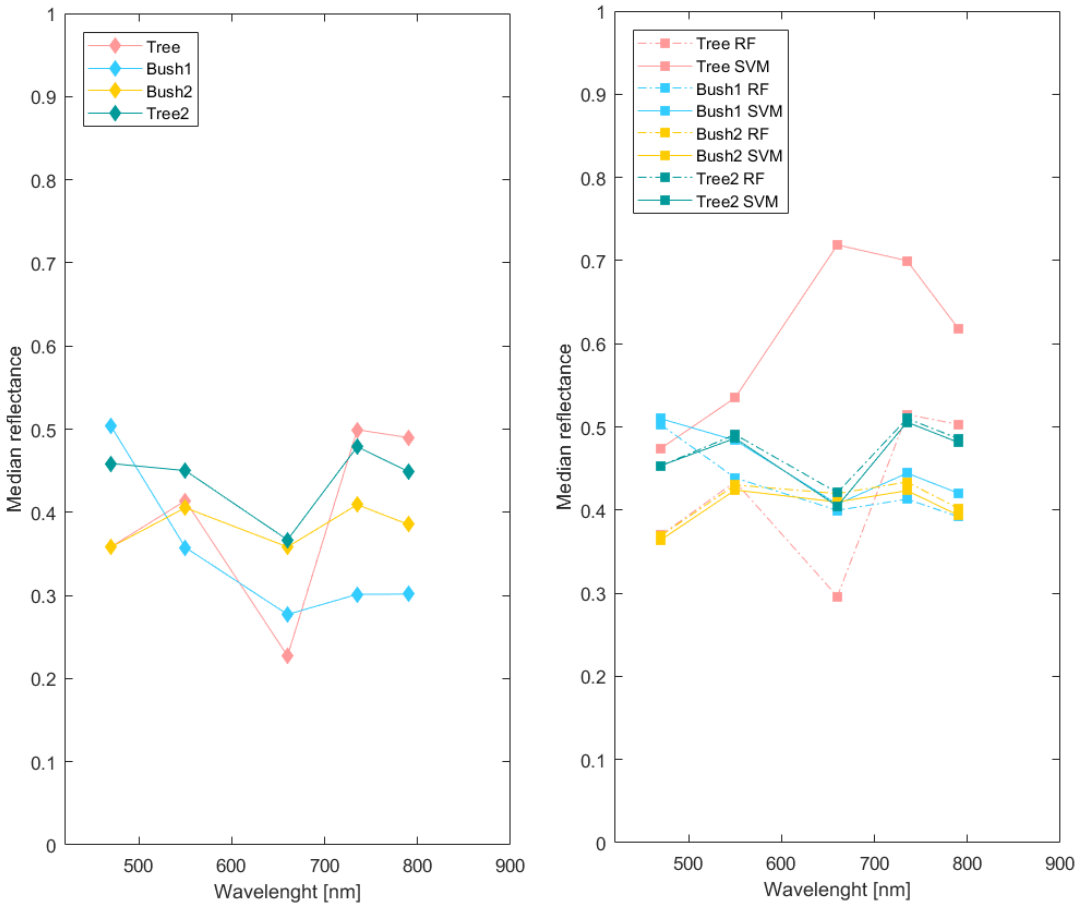

(a) Before classification **(b)** After classification

Figure 5.27: Spectral signatures of Tree 1, Tree 2, Bush 1 and Bush 2 classes (a) before classification and (b) after SVM and RF classifications of 2017 drone images

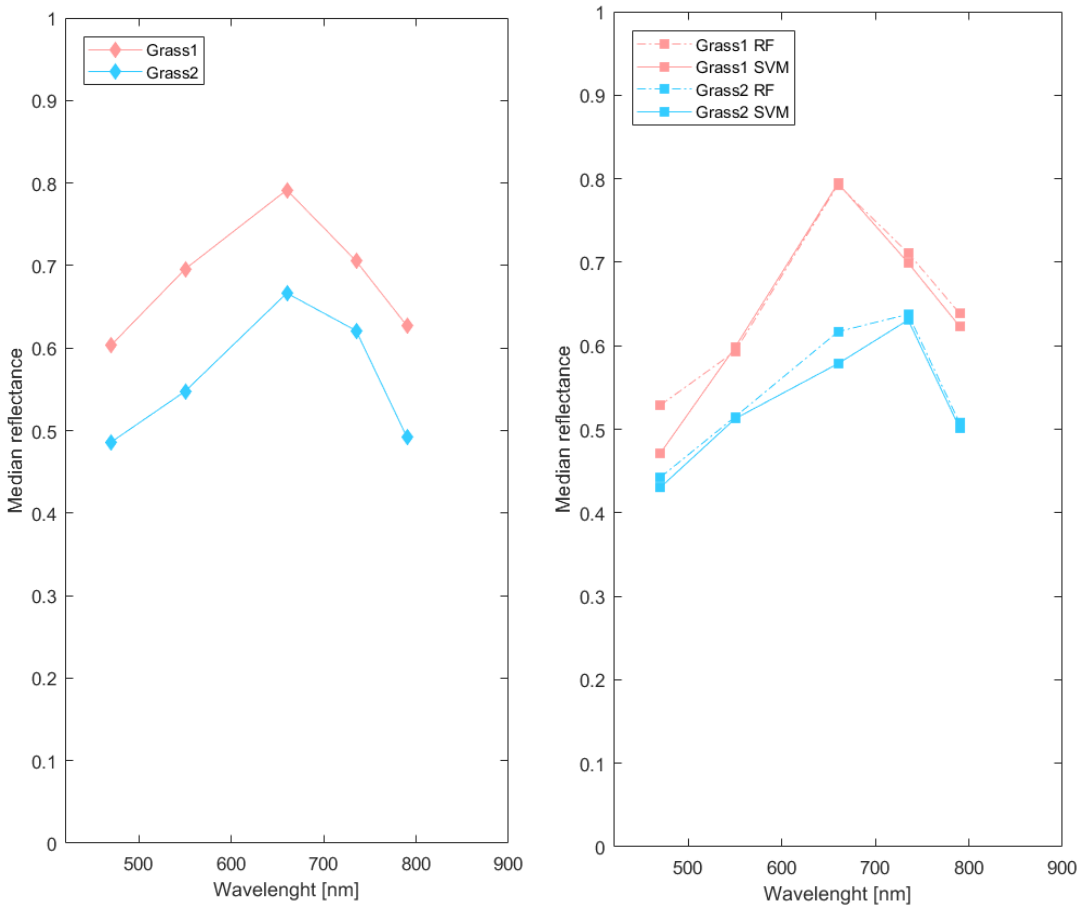

(a) Before classification **(b)** After classification

Figure 5.28: Spectral signatures of Grass 1 and Grass 2 classes (a) before classification and (b) after SVM and RF classifications of 2017 drone images

Satellite images

Sentinel-2 images were only classified with RF classifier. The best split fraction for test and train was 0.66 of ground truth samples used for testing and 0.33 for training the model.

Figures 5.29 and 5.30 show the spectral signature of each class before and after classification for May and October satellite images, respectively. The two figures show that the shift between the spectral signatures before and after classification vary according to the class and season, results are less precise than those obtained with drone images. Median values for spectral bands obtained from samples classified as tree are similar to those obtained from the ground truth for both classifications. Limestone soil class varies considerably. Standard deviations of the median values are given in the appendix D, figures 3 and 4.

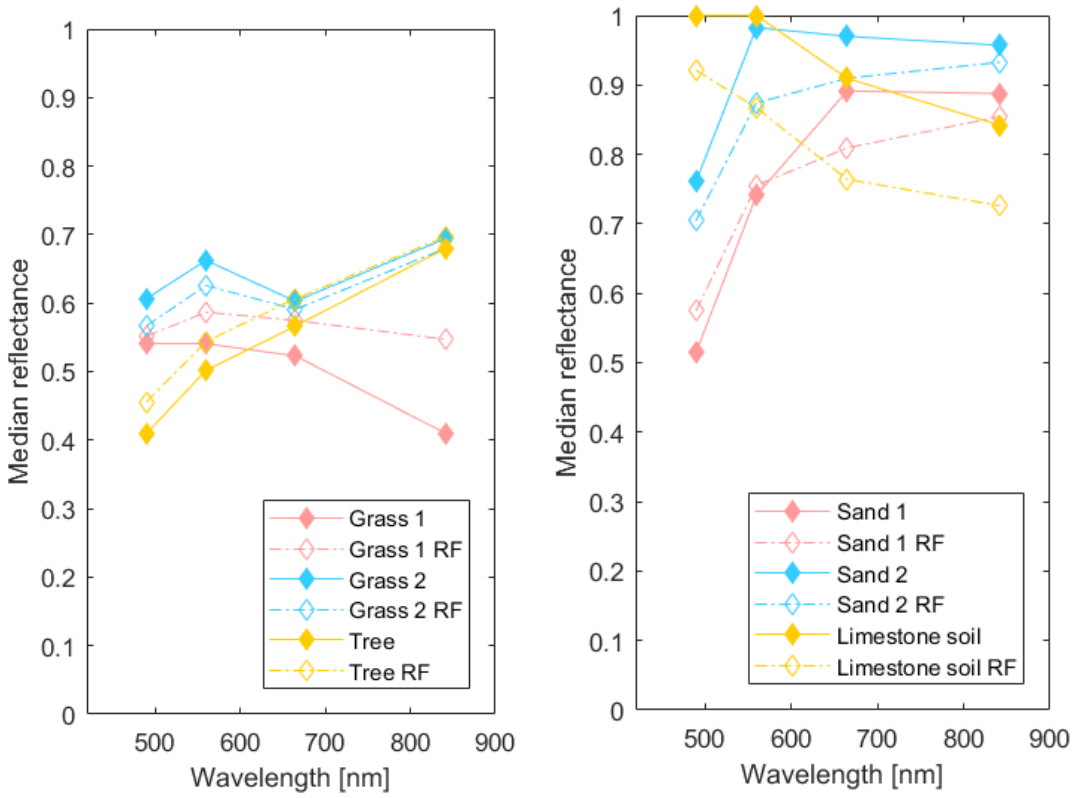

(a) Grass 1, Grass 2 and Tree classes **(b)** Sand 1, Sand 2 and Limestone soil classes

Figure 5.29: Spectral signatures of (a) Grass 1, Grass 2 and Tree and (b) Sand 1, Sand 2 and Limestone soil classes before classification and after RF classifications of the Sentinel-2 May image

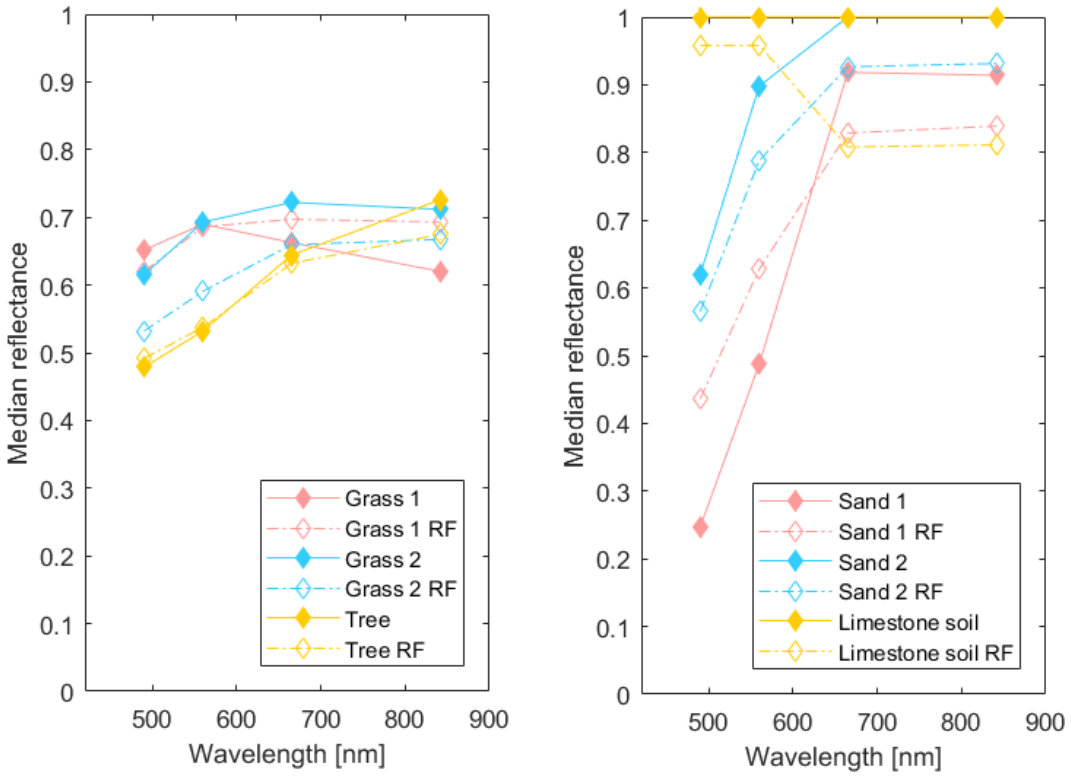

(a) Grass 1, Grass 2 and Tree classes **(b)** Sand 1, Sand 2 and Limestone soil classes

Figure 5.30: Spectral signatures of (a) Grass 1, Grass 2 and Tree and (b) Sand 1, Sand 2 and Limestone soil classes before classification and after RF classifications of the Sentinel-2 October image

5.6 Forage quantity estimation

Estimation from drone images

Table 5.12 shows the vegetation estimation for 2015 drone images and compares the results obtained from SVM and RF models. Estimations are not calculated from K-Means results because of the low performance of the classification algorithm. Results are given in m^2. The area of one pixel is $0.01m^2$ and there are 2250000 pixels per image. The total grass and vegetation areas for all zones differ for both models. Differences in total grass cover range from $162.4\,\mathrm{m}^2$ for zone 1 to to $1608.5\,\mathrm{m}^2$ for zone 2 and differences in total vegetation cover range from $197.2\,\mathrm{m}^2$ in zone 2 to $2478.8\,\mathrm{m}^2$ in zone 3.

Drone 2015								
Area [m^2]	**Zone 1 (RF)**	**Zone 1 (SVM)**	**Zone 1bis (RF)**	**Zone 1bis (SVM)**	**Zone 2 (RF)**	**Zone 2 (SVM)**	**Zone 3 (RF)**	**Zone 3 (SVM)**
Grass 1	5428.7	5394.1	1490.3	3562.6	144.0	9.7	219.1	61.0
Grass 2	2688.8	4367.7	1919.7	3162.7	467.3	26.5	752.2	542.7
Grass 3	3888.2	1334.8	5885.9	4400.7	5492.2	4097.6	7181.1	8763.5
Perennial	1852.6	2599.2	2156.8	1416.3	2243.2	2604.5	1029.3	318.9
Total grass	13858.3	13695.9	11452.6	12542.3	8346.8	6738.3	9181.7	9686.1
Bush 1	481.2	706.4	755.2	888.7	195.4	31.9	467.4	290.3
Bush 2	19.4	0.9	27.7	21.7	65.6	3.9	278.1	396.4
Total bush	500.7	707.3	782.9	910.4	261.1	35.8	745.5	686.7
Tree	672.6	1394.9	2019.1	2870.2	1989.8	3626.3	1383.4	3416.5
Total vegetation	15031.6	15798.0	14254.5	16322.9	10597.6	10400.4	11310.5	13789.3

Table 5.12: Vegetation estimation from RF and SVM classifications results per zones, drone May 2015

Results for 2017 classification are given in table 5.13. As noticed with previous results, SVM largely over-predicts the Tree 1 class, leading to faulty results of vegetation estimation. Therefore, SVM and RF results are not compared and only RF results are shown. The total grass and total vegetation estimations are significantly lower than in May 2015, except for zone 3.

Drone 2017				
Area [m^2]	**Zone 1 (RF)**	**Zone 1bis (RF)**	**Zone 2 (RF)**	**Zone 3 (RF)**
Grass 1	637.7	1176.0	200.6	159.4
Grass 2	898.1	2094.1	5195.5	12397.5
Total grass	1535.7	3270.1	5396.1	12556.9
Bush 1	644.7	156.9	10.2	8.7
Bush 2	0.0	1.8	0.3	1071.5
Total bush	644.7	158.7	10.5	1080.2
Tree 1	526.4	370.7	671.6	1518.0
Tree 2	538.2	2149.4	1269.1	30.5
Total tree	1064.5	2520.1	1940.7	1548.5
Total vegetation	3244.9	5948.9	7347.2	15185.6

Table 5.13: Vegetation estimation from RF and SVM classifications results per zones, drone October 2017

Estimation from satellite images

Table 5.14 gives the results, in hectares, of the vegetation estimation for satellite images from May and October 2017. The surface occupied by one pixels is $100\,\mathrm{m}^2$. The total grass surface is higher in October than in May, while the Tree and bushes cover is higher in May. The total vegetation cover is higher in October.

Satellite		
	May [ha]	**October [ha]**
Grass 1	1236.1	1840.9
Grass 2	1536.1	1765.2
Total grass	2772.9	3606.1
Trees and bushes	3705.8	3159.3
Total vegetation	6478.7	6765.4

Table 5.14: Vegetation estimation from RF classification results, Sentinel-2 May and October 2017

5.7 Land cover change analysis

Figure 5.31 shows the standard deviation of the DVI between November 2016 and November 2017. Dark colors represent areas that slightly change over the year or that do not change at all. In blue, we can see limestone soils and some roads and fences. The sandy north-east corner of Kuzikus is characterized by low standard deviations. Small yellow dots could represent trees or vegetation that stands out in the surrounding sand. The standard deviation increases around water points, where more vegetation is present. The standard deviation is high in the more vegetated western part of the reserve.

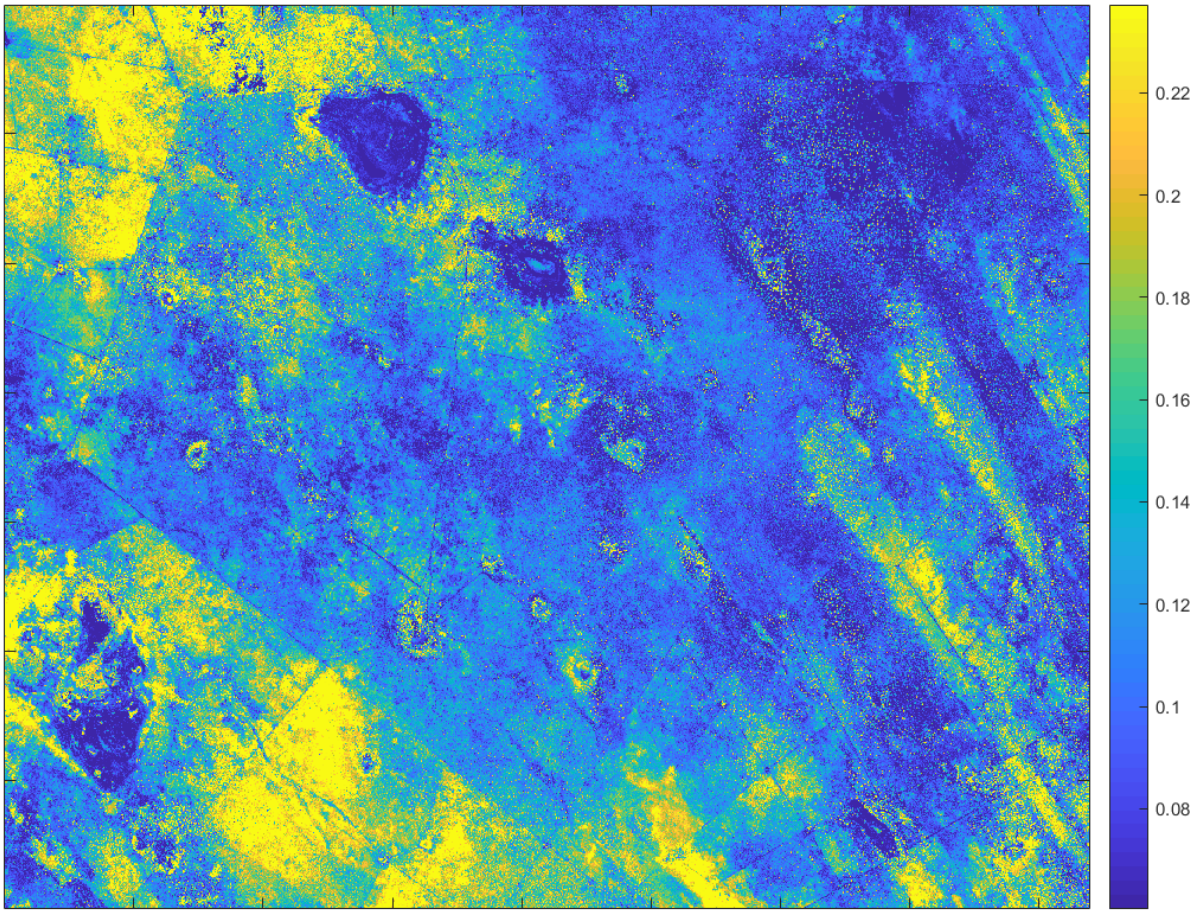

Figure 5.31: Standard deviation of the Difference Vegetation Index over 1 year, from November 2016 to November 2017

Figure 5.32 shows the temporal series of the median DVI over three uniform patches of grass in Kuzikus and one in a neighbor farm (figure 4.10). According to the rain data, rainfall was

more abundant between 2016 and 2017 than 2015 and 2016, but in 2015 it started raining earlier than in 2016. All patches of grass follow the same trend: they peak after the rain comes. For 2017, all patches peak in April, while for 2016 Patches 1 and 4 peak in February and Patches 2 and 3 in April.

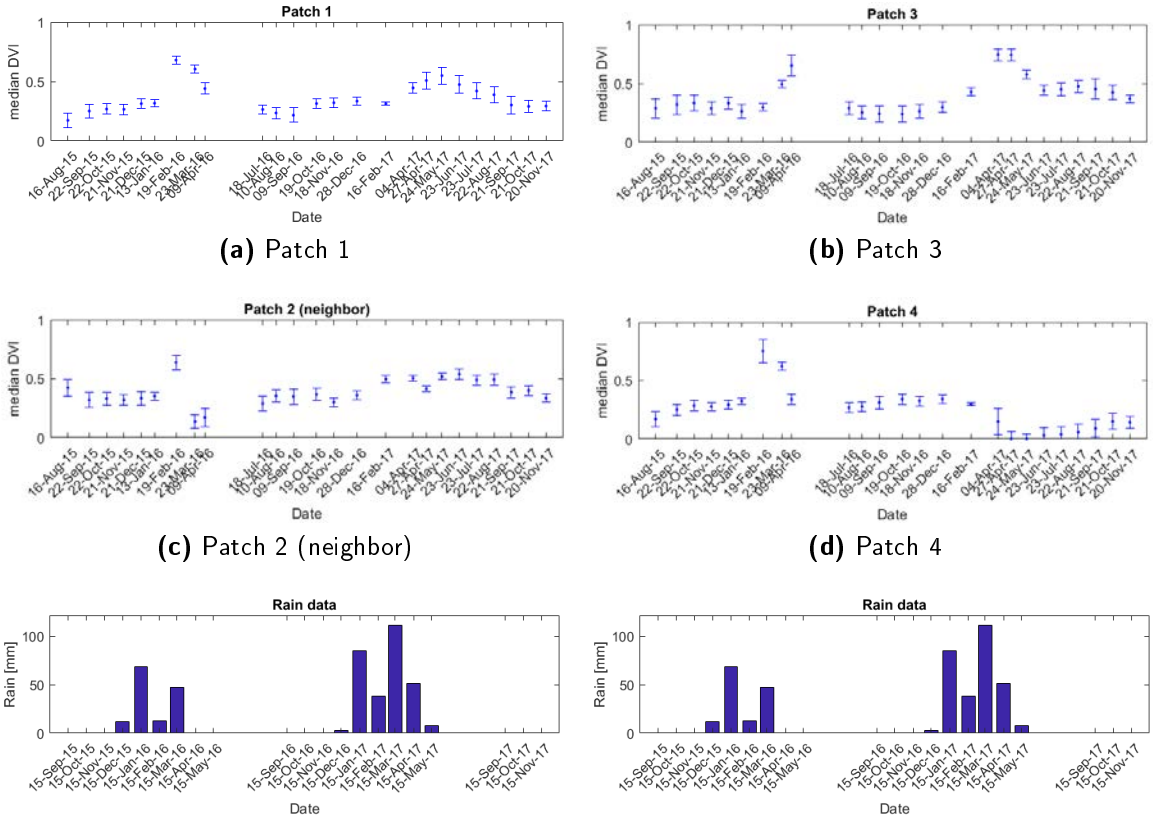

(a) Patch 1 **(b)** Patch 3

(c) Patch 2 (neighbor) **(d)** Patch 4

(e) Rain data **(f)** Rain data

Figure 5.32: Median DVI of grass patches (a) 1, (b) 3, (c) 2 and (d) 4 and (e) (f) rain data

Figures 5.33 and 5.34 show the evolution of the DVI in 4 fields in a neighbor farm and in an area in the south west of Kuzikus. The fields' partition is given in figure 4.10. It is easy to see the difference between a wildlife farm and a cattle and sheep farm. In the neighbor farm, small fields are fenced and are all treated in a different way. Plots from 2016 show that on Kuzikus there is low vegetation cover in October and November (figure 5.33), and that it starts growing in December and continues until April (figure 5.33, left). On the other hand, in the neighbor farm, vegetation cover is low in October and November (figure 5.33), but in field 1 there is more. Vegetation grows until February. In March the vegetation cover is low for fields 1 and 2 but it still increased in fields 3 and 4 (figure 5.34). In April it decreases also in fields 3 and 4. A similar strategy is applied in 2017, but about a month later (figure 5.34). In May 2017 the vegetation cover slightly increased.

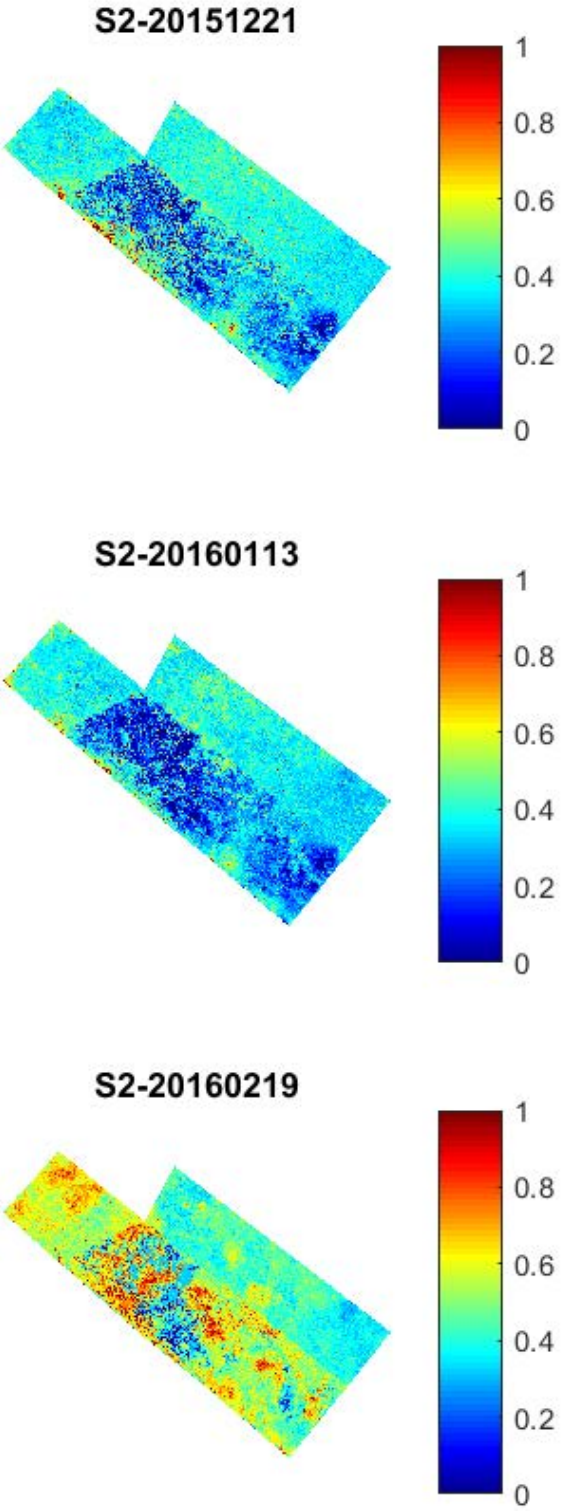

Figure 5.33: Median DVI over 4 neighbor fields and a Kuzikus area in December 2015, January and February 2016

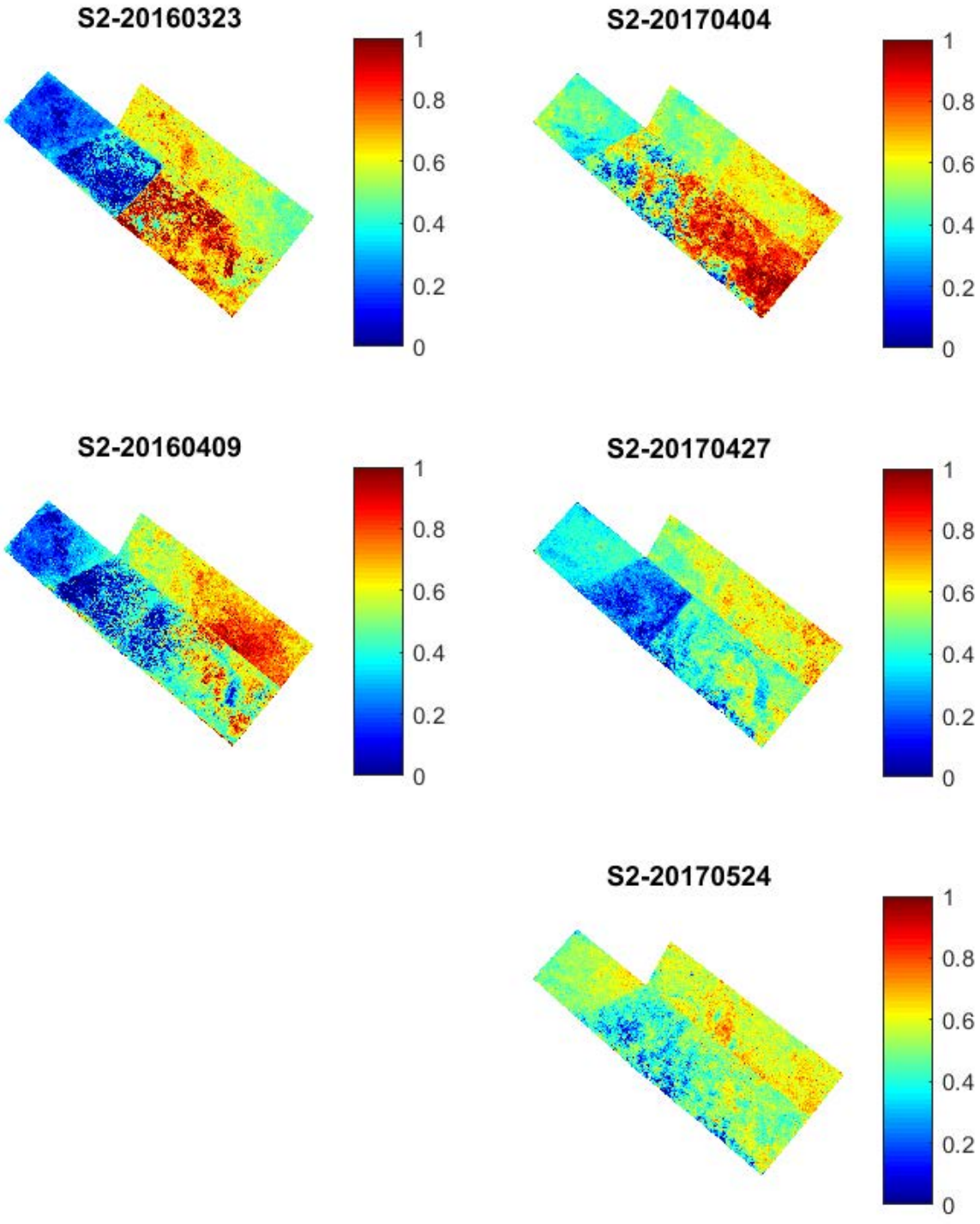

Figure 5.34: Median DVI over 4 neighbor fields and a Kuzikus area in March and April 2016, beginning and end of April 2017 and May 2017

CHAPTER 6

DISCUSSION

Classification of remotely sensed images is a challenging problem and the performance of the algorithms highly depends on the input data, which require to be accurately selected and prepared. Data selection and preparation was a long process because of the huge and varied amount of data available. Satellite data, despite being all acquired with the same sensor, were highly influenced by the meteorological conditions, in particular the cloud cover. Drone data, on the other hand, were less influenced by the weather but were acquired with different sensors and resolutions, which made their comparison complicated.

Image superposition

One of the biggest challenges in this research was the combination of drone images acquired by RGB sensors with those taken by NIR ad MS ones. Without ground control points (GCPs) on the ground or instruments that correctly calculate the geotags of the images while the drone is flying, their absolute positioning accuracy varies between 1 to 5 meters [senseFly, 2017b]. Before being combined, images need to be manually georeferenced between each other. In vegetated landscapes this procedure is complicated because vegetation does not have a precise and sharp shape, making it difficult to find the exact same point in two different images. This task was accomplished using holes on the ground dug by aardvarks, because they were the smallest and more precise shape recognizable in both images. Drones were flying at different heights, taking pictures with different angles and overlaps. All these factors influenced the reconstruction of the orthomosaics, hence the matching of objects on the ground can not be perfect. For example, the same tree or bush can have slightly different shapes in two different images. The main problem in the superposition of images was caused by shadows. If NIR or MS and RGB pictures are not taken at the same time or at a very short time distance, shadows in the orthomosaics will be different and will not correctly superpose. While during the flight campaign in October 2017 attention was payed to fly the two sensors at the same time over the same area, this was not the case in 2015. Figure 6.1 shows an example of shadow mismatch between a RGB and a NIR image from 2015 drone campaign.

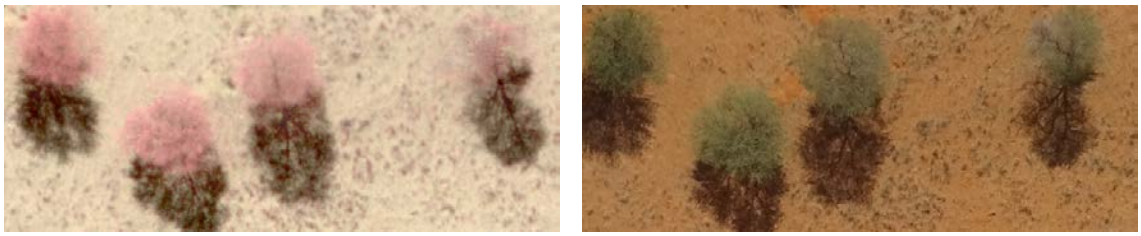

(a) RGB image **(b)** NIR image

Figure 6.1: Shadow mismatch between NIR (a) and RGB (b) images acquired in 2015 over zone 2

For satellite images this problems did not exist because images from all bands were taken at the same time and, anyway, the size of the pixel do not allow to recognize such small details. On the other hand, satellite images taken on different days were not georeferenced between each other and the resolution of the images did not allow to do it manually like with drone images. Indeed, the resolution of Sentinel-2 images was too low to correctly identify the same features on different images. Therefore, land cover change analysis were performed on non-matched images.

Ground truth

The imperfect superposition of images strongly influenced the ground truths, which in turn influenced the classification. The ground truthing process was the most challenging part of the research. As no data about the soil cover in Kuzikus were available, it was only based on the visual differences between objects on the images.

For drone images, classes were distinguished based on the different colors, shapes and textures of the objects visible on the images representing the selected areas for classification. Some objects like trees, roads, shadows and bushes were easy to distinguish. Bushes, for example, have no shadow, while trees do, and the two types of bushes have different shapes and are then easy to distinguish. Roads have a different texture and slightly different color compared to soil. On 2015 images, soil was easy to distinguish from grasses, while in 2017 images their distinction was more challenging. Indeed, in those images grass patches were small and did not stand out on the sandy soil, except when they were located around trees. Grasses were the most complicated objects to ground truth in both years. Despite the fact that different grass species were distinguished, there is no proof that they are actually different grasses and not the same, but at different growing stages. The distinction was only based on colors. In addition to this, they are represented by small patches, with diameters ranging between 20 cm and 1 m, hence delimited by small polygons. Polygons of the smallest patches have more or less 6 pixels and those of the biggest ones around 100, while the entire image has more than 2 millions pixels. Digitizing a polygon that matches between the RGB and NIR or MS images further reduces its dimensions. That is why in general there are less grass samples in the ground truth compared to other classes: one tree polygon corresponds to more or less ten of the biggest grass polygons. The inequality between classes is bigger for 2017 images because there is only a few grass and it is more difficult to separate it from sand.

For satellite images, the ground truthing process was more complicated because the resolution of the image do not allow to well recognize objects on the ground. Polygons were digitized using both the band combinations of Sentinel-2 images and a Bing image composed by multiple images stuck together, probably taken at different times of the year. The fact that the base image used to build polygons was composed by different images made it more difficult to distinguish objects, in particular grass species, which change appearance during the year. Trees were particularly challenging to recognize because their size is smaller than the pixel size. Therefore, only the bigger ones or trees close together were correctly spotted on Sentinel-2 images.

As for both drone and satellite images ground truth polygons were difficult to define, mostly

because of the wrong matching between images and ambiguous objects on the ground, the more polygons were added, the more the chances to be mistaken. This is the main reason why ground truth samples represent a small fraction of the total number of pixel of the images. In particular for drone images, even if some classes like Tree or Road were easy to distinguish, the more polygons of those classes were added, the bigger the disproportion with the number of samples of scarce classes, like grasses. This disproportion can influence the classification at the point when the data set is divided between train and test sets. Despite the algorithm trying to roughly take the same number of samples from all classes, if one class in the ground truth is over represented it will still be over represented in the training data set. This can have big influences in the classification. Usually a bigger fraction of ground truth data is used for testing than for training, but in this case the risk was to have not enough samples of some classes. While RF classifier managed to perform correct classifications even with just a few training samples (10% of the ground truth samples), SVM classifier revealed to be more sensible to the train fraction, which had to be increased to 40%.

Classification results

Despite the small number of ground truth samples, the results of the classifications are satisfying.

For drone images, the most of the misclassifications appear at the transitions between objects, where there are mismatches in the superposition of the NIR or MS images with the RGB ones. This phenomenon is particularly present around shadows in 2015 (figure 5.13). The situation improves in 2017, because more attention was paid to fly the different sensors at the same time over the same areas. Perennial and Bush 2 classes are less over-predicted by SVM than RF. On the other hand, SVM is more sensible to the training data set, which needs to be larger than for RF. The bigger number of samples of Tree 1 class in 2017 drone images compared to other classes caused the failure of the classification. Grass cover is under-predicted in zone 3 for both years and classified as soil instead. Different bushes and trees species are well distinguished. When trained using training data sets with relative abundance of absence of a certain species, models like RF and SVM are known to be not well adapted at predicting those species in areas of high vegetation diversity [Savage et al., 2015]. They usually under-predict the target species where it is absent or rare and over-predict it when it is abundant [Savage et al., 2015]. This is what happened with trees and grasses classes. The first is over-predicted and the second under-predicted.

Classification over drone images was only performed on small parts of a few images as a proof of concept for bigger classifications. With more and, above all, more precise ground truth it would be possible to perform satisfying classifications over the entire reserve using the same models.

As far as satellite images are concerned, it is quite difficult to interpret the results. While with drone images it was easy to visually check if the classification performed well, here the small resolution only allows to check general patterns and it is complicated to say which objects are actually represented by each class. Indeed, classes are never pure, even in the ground truth polygons. For example, the Tree class not only comprehends trees, but also groups bushes; and isolated bushes are also present in Grass 1 and Grass 2 polygons. In general, in dense vegetated areas, with many woody vegetation like big trees or bushes close together, everything is classified as tree. Therefore, in those areas, which are mostly in the west side of the reserve, sand is under-predicted. On the other hand, when the vegetation is scarce, like on the north-east part of Kuzikus, sand is over-predicted and vegetation in under-predicted. Everything depends on what is captured by each pixel, which covers $10x10$ meters. If one pixel mostly represents vegetation it will be classified as vegetation and if it mostly represents sand with some scarce vegetation it will be classified as sand. The classification allows nevertheless to well define the different soil covers in the Namibian reserve: on the eastern side there are a few trees and

mostly red sand while the western part is more vegetated, with more trees, grasses and some bush encroachment.

Despite the classifications were visually satisfying, the lack of ground truth performed on the field did not allow to validate the results.

Statistics for all models, except K-Means, are very high and do not well represent the real quality of the classification. The main reason is the small amount of ground truth, which allows to check results only on a minimal part of the images. As a result, K-Means statistics under-predict the performance of the algorithm and SVM and RF statistics over-predict them. A better control is given by the graphs showing the median values of the spectra of each class, which compare the median R, G, B and NIR values of the ground truth classes to all the pixels of the classified images. From there it is possible to see the mistake in SVM classification for 2017 drone images, which was not visible in the statistics. The graphs show that classification results only slightly differ from the original spectral signatures of most of the classes, confirming that results are satisfying. It was noticed that the spectral signature of the Shadow class issued from drone images classification is significantly higher than for ground truth data (figures 5.23 and 5.26). This can be explained by the fact that many pixels, belonging to other classes, and thus with higher reflectances, are classified as shadow. The same phenomenon appears with Limestone soil class in RF classification of satellite images, where the spectral signature decreases (figures 5.29b and 5.30b). This time, samples with lower reflectances than this class are classified as limestone soil. Moreover, the spectral signatures of non-vegetation classes differ between 2015 and 2017 drone images, while the objects represented by those classes did not change between the two years. This could be due to the different sensors used in the two campaigns.

The models used are different and all have positive and negative aspects. K-Means is not well adapted for this type of classification. It returns only clusters and not classes, which require a post interpretation of results. The choice of the classes is subjective and the results change according to the initial randomly picked centroids. On the other hand, supervised classification methods like SVM and RF directly output a thematic map, without needing post interpretation, but they strongly rely on the quality of the training data (e.g number of discriminative examples). The two classifiers both work well with large data sets and high dimensionality. SVM has longer processing times and some parameters to tune, but can handle non-linear separation and only uses a subset of the data: the support vectors [de Morsier, 2017]. In the project it was noticed that this classifier is more sensible to the input training set. RF has shorter processing times, gives an estimate of the variable importance, do not over fit and generates an internal unbiased estimate of the generalization error as the forest is built. Moreover, trees are not correlated because they are all built with different training sets.

Forage quantity estimation

After classification, biomass was only estimated by pixel counting because of the lack of a model to predict the volume or weight per surface $[t/ha]$.

For satellite images, results gave higher biomass estimates in October than in May, which is counter intuitive. Grass estimates were higher in October and woody vegetation cover was higher in May. One explanation can be that in May all trees and bushes have bloomed and occupy a bigger surface on the image, probably hiding some grass under their canopy. In October many of them do not have leaves at leave grasses uncovered. Therefore, more pixels are classified as tree in May and more are classified as grasses in October, but this still does not justify why there is more total vegetation in October. Another explanation can be that the same ground truth based on the May image was used for both May and October classifications. The fact that the two images were not perfectly georeferenced between each other and that it was complicated to do a correct ground truth could have caused misclassifications in the October image, leading to an over estimation of the amount of vegetation.

Considering drone images, biomass is probably under estimated due to the misclassification of grasses. Moreover, many grass patches were not detected because they were hidden by the shadows of trees. An option to improve their estimation would be interpreting what is under shadows. According to Yu et al. [2006], shadow, in association with terrain effects, is one of the significant barriers to vegetation classification with airborne high resolution multi-spectral images.

Perennial and annual grasses

The absence of a ground truth on the field makes it impossible to say if Grass 1, Grass 2 and Grass 3 classes for 2015 images and Grass 1 and Grass 2 classes for 2017 images are annual or perennial grasses. Perennial grasses are easy to distinguish when they are 2 or 3 years old because they are higher than other grasses and form small patches on their own, but when they are young they can be easily confused with annual grasses [Reinhard, 2017]. Perennial class for 2015 classification was called like this because of assumptions made by the director of Kuzikus [Reinhard, 2017] while looking at the images.

A few small areas of Kuzikus are fenced out for vegetation studies and mainly contain perennial grasses [Reinhard, 2017]. One of these study plot was used to understand whether grass classes used for classification are perennial or annual. Figure 6.2 shows two small areas of the study plot in May 2015 (figure 6.2a) and in October 2017 (figure 6.2b) to give an example of how perennial grasses should look like in these periods.

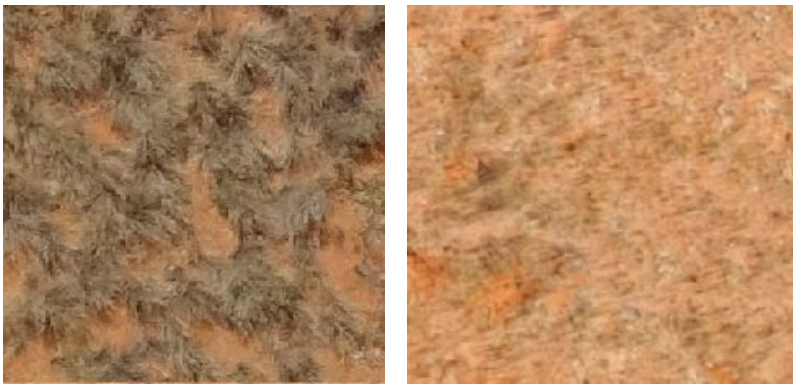

(a) Example of perennial grass appearence in May 2015

(b) Example of perennial grass appearence in October 2015

Figure 6.2: Appearence of perennial grass in (a) May 2015 and (b) October 2017

In 2015 drone images, the same type of grass as in figure 6.2a was visible at the bottom right of figure 5.1a and at the bottom left of figures 5.1b and 5.1c. The spectral signature of these patches was compared to the one of the grasses in the study plot to confirm that they are perennial grasses with a positive response. Therefore, the class Perennial in 2015 classification really represents perennial grasses. The other grass classes can be both young perennials or annuals.

While in 2015 it was quite easy to visually distinguish old perennial grasses from annual plants just by looking at the images, in 2017 this was not possible because all grasses looked the same. Nevertheless, the same spectral signature analysis was performed comparing both Grass 1 and Grass 2 classes with the grasses in the study plot, leading to positive results for Grass 2.

According to the season it is possible to distinguish more or less objects and more or less easily. The second campaign aimed at mapping the vegetation in the dry season to better distinguish perennial from annual plants, in particular grasses. At that moment, a few perennial grasses were starting to get green (figure 1.5), but they were not green enough to be well spotted

on the images. They were already green at the bottom but still yellow on the top and as the images are taken from above, the green was hidden by the yellow on top and was not visible. More knowledge about the phenology of grasses would be useful to better decide the period for a drone flight campaign and correctly spot perennial grasses. Moreover, as grasses are a small detail on the images, in order to correctly classify them it would be necessary to have precisely georeferenced images and perfect superposition of R, G, B and NIR bands. This could be achieved with a sensor able to capture all of them together. Nevertheless, the campaign in October eased the distinction between perennial and annual trees (Tree 1 and Tree 2 classes in 2017 classification).

Comparison between UAV and satellite data

Different type of information can be retrieved from satellite and drone images. With the first, it is possible to have a general overview of big areas in just one image, but this image do not have many details. Moreover, the main problem of freely available satellite imagery, like Sentinel-2, is their coarse spatial resolution. The second type of images can have high levels of detail but images are smaller and the general overview of the area is missing. One of the principal limitations of using UAVs is the relative small spatial extent of the mappings.

Vegetation appears differently according to the scale of observation. At large scale a tree consist of leaves, branches, litter and soil, all having different reflectance spectra. At the small scale of coarse satellite images all these components are not spatially resolved and the pixels that capture them represent the composite spectral response of these components [Smith et al., 1990]. Those mixed pixels often result in either overestimation or underestimation of land cover [Giri et al., 2013]. This phenomenon is particularly important in semi arid regions, where the low density of the vegetation causes the spectral dominance of the background soil [Moleele et al., 2001]. This problem can be solved by separating the spectral contributions of the scene components and transforming radiance data into fractions of a few dominant spectra [Smith et al., 1990]. The technique of estimating the proportion of different type of vegetation in a pixel is called unmixing [Keshava, 2003] and requires to have a “pure” pixel to know the signature of a specific type of soil cover (e.g. tree, bush, sand, ...). Unfortunately, in semi arid landscape and with Sentinel-2 data, which has 10 m resolution this is quite difficult because one pixel rarely represent only one type of soil cover. Figure 6.3 shows an example of the footprint of a Sentinel-2 pixel in this kind of landscape, the background image is figure 5.1a. In one pixel there are one tree with its shadow, one bush, some soil and different types of grass.

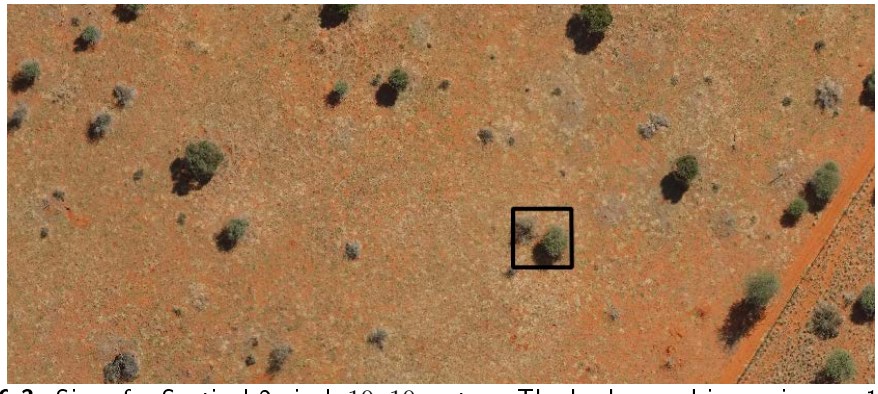

Figure 6.3: Size of a Sentinel-2 pixel, $10x10$ meters. The background image is zone 1 in 2015

Despite the disadvantage of the coarse resolution, satellite imagery offers a high temporal resolution, which can allow to study the vegetation evolution. Landsat, for example, offers the "world’s most extensive collection of continuously acquired satellite data” [Giri et al., 2013].

For detailed vegetation studies, though, high spatial resolution UAV imagery provides more

information than coarse spatial resolution satellite data, which have often proven ”insufficient or inadequate for differentiating species-level vegetation” [Zhang et al., 2015]. Ultra-high resolution images allow to see small details and even to distinguish single plants, but this cause high computational times for the algorithms and salt and pepper effects in the classification results. In these images, one single pixel “is not closely related to vegetation physiognomy as a whole", but "vegetation always shows heterogeneity as a result of irregular shadow or shade”, for example in tree crowns [Yu et al., 2006]. This problem, together with the salt and pepper effect, can be partially solved by grouping contiguous pixels and using this objects instead of single pixels during classification.

Drone and satellite data can be used together to take advantage of the best quality of both. The lower resolution of satellite data compared to drone ones only allows to distinguish small objects, but permits to have a general idea of the patterns on the ground. Drone images, on the other hand, allow to distinguish small objects and can be used as a ground truth for satellite images, without needing to do it on the field. Using drone images as a ground truth could help the unmixing procedure by giving relevant predictions of the proportion of different soil cover represented by a pixel of a satellite image.

CHAPTER 7

CONCLUSION & PERSPECTIVES

In this research, the land cover of Kuzikus Wildlife Reserve, in the south-eastern Kalahari region of Namibia, was classified using ultra-high resolution UAV images and coarse resolution Sentinel-2 satellite images. The main goal was to provide a rough estimation of the quantity of food for wildlife at the end of the growing season.

Drone images acquired during two different campaigns - May 2015 and October 2017 - were classified using K-means, Support Vector Machine and Random Forest algorithms. The last two classifiers gave the best results and allowed to distinguish between 10 soil cover classes in 2015 images and 9 in 2017 images. The classes mainly represented vegetation species: different tree, bush and grass species. Perennial grasses were of particular interest and were spotted on multiple images from both years.

Sentinel-2 images were classified with Random Forest classifier, which allowed to distinguish the principal land cover patterns: low and high vegetation, sand and bare soil. Results were compared to drone orthophotos over a few areas to observe the performance of the algorithm in more detail. Despite the low resolution (10 m) of Sentinel-2 images, Random Forest succeeded in correctly differentiating vegetation from non-vegetation soil cover the most of the time.

The main difficulties of this research concerned the preparation of data for the classification, in particular the ground truthing process. For drone images, features were calculated combining spectral bands of images acquired by different sensors. The incorrect superposition of those images negatively influenced the quality and quantity of the ground truth samples and in consequence the performance of the classification algorithms, often leading to unrealistic statistics. For satellite images, the ground truthing process was even more complicated because of the difficulty of correctly delimiting polygons on coarse resolution images. Despite classification results for both drone and satellite images are visually satisfying, the lack of a valuable ground truth does not allow to validate the results.

Ultra-high resolution drone data and coarse resolution satellite data offer different and complementary information about soil cover. The first gives high level of details, but only covers small areas and does not allow to have a bigger overview of the study area and its surrounding. The second type of data can cover larger areas but gives less details on specific zones. Thanks to their high resolution, drone images could be used to help extracting useful information from satellite data. For example, they could be used as a ground truth to quantify the contribution of different vegetation species to the spectral signature of single pixels on satellite images. This information would facilitate the long term exploitation of satellite data to estimate the fodder quantity.

In conclusion, this research proved that plant recognition from ultra-high resolution UAV images is possible and that these data can be combined to satellite imagery to help farmers in

the resource management of their properties. More accurate ground truths and a better understanding of plants' phenology would significantly improve the biomass estimation. Moreover, the collection of field data would help building models to provide not only estimates about fodder quantity, but also its quality.

CHAPTER 8

APPENDIX

A Selected satellite dates

	2015	2016	2017
January	-	13	-
February	-	19	16
March	-	10, 23	-
April	-	9	4, 27
May	-	-	**24**
June	-	-	23
July	-	18	23
August	16	10	22
September	22	9	21
October	22	19	**21**
November	21	18	20
December	21	28	-

Table 1: Dates of selected satellite images for the temporal analysis. In bald the images chosen for classification

B Gini index

The Gini index is a measure of purity of the classes.

Its general formula of the Gini index at node t with k classes is:

$$Gini(t) = 1 - \sum_{c=0}^{c=k} P_c^2 \tag{1}$$

P_c is the proportion of observations with target variable value c.

The Gini of a split is given by:

$$Gini(s,t) = Gini(t) - P_L Gini(t_L) - P_R Gini(t_R) \tag{2}$$

and is calculated for every variable and split value.

s: split

t: node

$Gini(t)$: Gini index of node t
P_L: proportion of observation in left node after split s
$Gini(t_L)$: Gini of left node after split s
P_R: proportion of observation in right node after split s
$Gini(t_R)$: Gini of right node after split s
The best split is given by the highest Gini [Institute, 2015b], [Institute, 2015a], [Lösch, 2017].

C Confusion matrices

	Soil	**Woody Vegetation**	**Shadow**	**Grass**	**Road**
Soil	12103	677	0	22965	2048
Woody Vegetation	1312	34141	24594	8481	4363
Shadow	0	584	12758	0	22
Grass	16385	5611	31	13462	7643
Road	1724	0	0	9828	5320

Table 2: Confusion matrix for K-Means classification on drone images from May 2015

	Soil	**Woody Vegeta-tion**	**Shadow**	**Grass**	**Road**	**Tree No Leafs**
Soil	48978	939	3	1	11359	11584
Woody Vegeta-tion	12642	106350	38659	6129	10	28
Shadow	0	21131	8558	2	0	0
Grass	4735	0	6118	9975	1551	4790
Road	20154	0	1	3	22007	0
Tree No Leafs	0	2162	5002	11069	0	15

Table 3: Confusion matrix for K-Means classification on drone images from October 2017

	Road	Tree	Shadow	Soil	Bush 1	Grass 1	Grass 2	Grass 3	Perennial	Bush 2
Road	16773	29	0	325	0	0	0	0	0	0
Tree	0	36019	0	0	5	9	0	0	1	3
Shadow	0	7	7907	0	102	0	0	0	3	0
Soil	149	39	0	15451	4	12	6	8	3	0
Bush 1	0	20	97	0	5142	0	0	54	88	0
Grass 1	0	57	0	23	0	5593	12	18	18	0
Grass 2	0	1	0	18	4	42	4270	37	9	0
Grass 3	0	13	0	13	76	3	22	10960	162	3
Perennial	0	54	19	0	85	26	5	56	4274	5
Bush 2	0	47	8	0	29	0	0	5	15	2193

Table 4: Confusion matrix for SVM classification on drone images from May 2015

	Road	Tree	Shadow	Soil	Bush 1	Grass 1	Grass 2	Tree 2	Bush 2
Road	31896	19	0	25	0	0	0	0	0
Tree	0	70054	1	0	0	0	0	39	66
Shadow	0	103	18269	11	3	0	0	0	55
Soil	7	39	174	36850	0	0	8	0	0
Bush 1	0	91	2	0	3694	0	0	42	0
Grass 1	0	65	0	2	0	2205	0	0	0
Grass 2	0	40	0	6	0	0	13980	0	2
Tree 2	0	101	4	0	7	0	1	20535	0
Bush 2	0	85	51	0	0	0	1	0	3362

Table 5: Confusion matrix for SVM classification on drone images from October 2017

	Road	Tree	Shadow	Soil	Bush 1	Grass 1	Grass 2	Grass 3	Perennial	Bush 2
Road	25094	0	0	585	0	1	5	0	4	0
Tree	0	53945	8	2	17	59	0	0	24	0
Shadow	0	11	11627	0	351	0	0	0	26	12
Soil	204	33	0	23149	0	34	30	53	6	0
Bush 1	0	63	81	0	7424	0	16	233	282	1
Grass 1	0	16	0	41	0	8382	19	67	58	0
Grass 2	0	2	0	25	0	83	6253	136	73	0
Grass 3	0	0	0	119	22	14	51	16400	272	0
Perennial	0	43	0	0	66	30	17	203	6419	9
Bush 2	0	137	1	0	626	1	0	2	351	2328

Table 6: Confusion matrix for RF classification on drone images from May 2015

	Road	Tree	Shadow	Soil	Bush 1	Grass 1	Grass 2	Tree 2	Bush 2
Road	47774	2	0	122	0	7	3	0	0
Tree	1	118442	23	6	50	0	7	3184	183
Shadow	0	18	26626	0	12	0	0	1	64
Soil	85	0	392	55101	0	5	34	0	0
Bush 1	0	94	32	0	5465	0	1	151	0
Grass 1	0	0	0	5	4	3390	8	3	0
Grass 2	0	0	0	5	0	10	21026	0	2
Tree 2	0	402	21	0	87	4	1	30458	0
Bush 2	0	82	66	0	0	0	5	0	5095

Table 7: Confusion matrix for RF classification on drone images from October 2017

	Grass 1	Grass 2	Sand 1	Sand 2	Soil	Tree
Grass 1	2424	182	0	0	0	103
Grass 2	100	2013	3	0	0	105
Sand 1	1	5	2862	6	0	86
Sand 2	0	0	10	1937	0	12
Soil	0	2	0	0	3571	0
Tree	88	84	78	5	7	1038

Table 8: Confusion matrix for RF classification on the Sentinel-2 image from May 2017

	Grass 1	Grass 2	Sand 1	Sand 2	Soil	Tree
Grass 1	2349	257	0	1	0	103
Grass 2	195	1947	5	0	0	73
Sand 1	1	7	2858	2	0	93
Sand 2	0	5	3	1928	0	23
Soil	0	0	0	0	3569	3
Tree	71	87	90	5	6	1041

Table 9: Confusion matrix for RF classification on the Sentinel-2 image from October 2017

D Standard deviation of spectral signatures

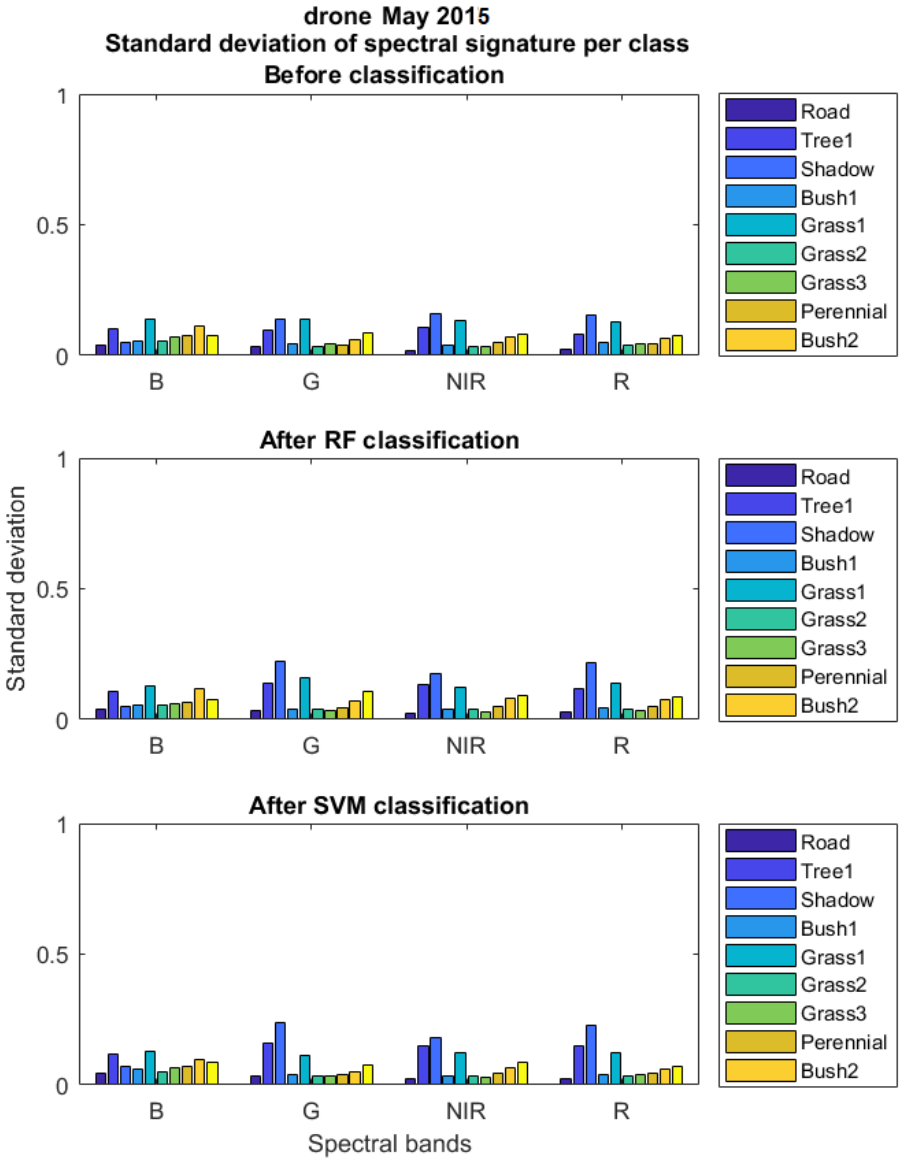

Figure 1: Standard deviation of spectral signature by class, drone May 2015

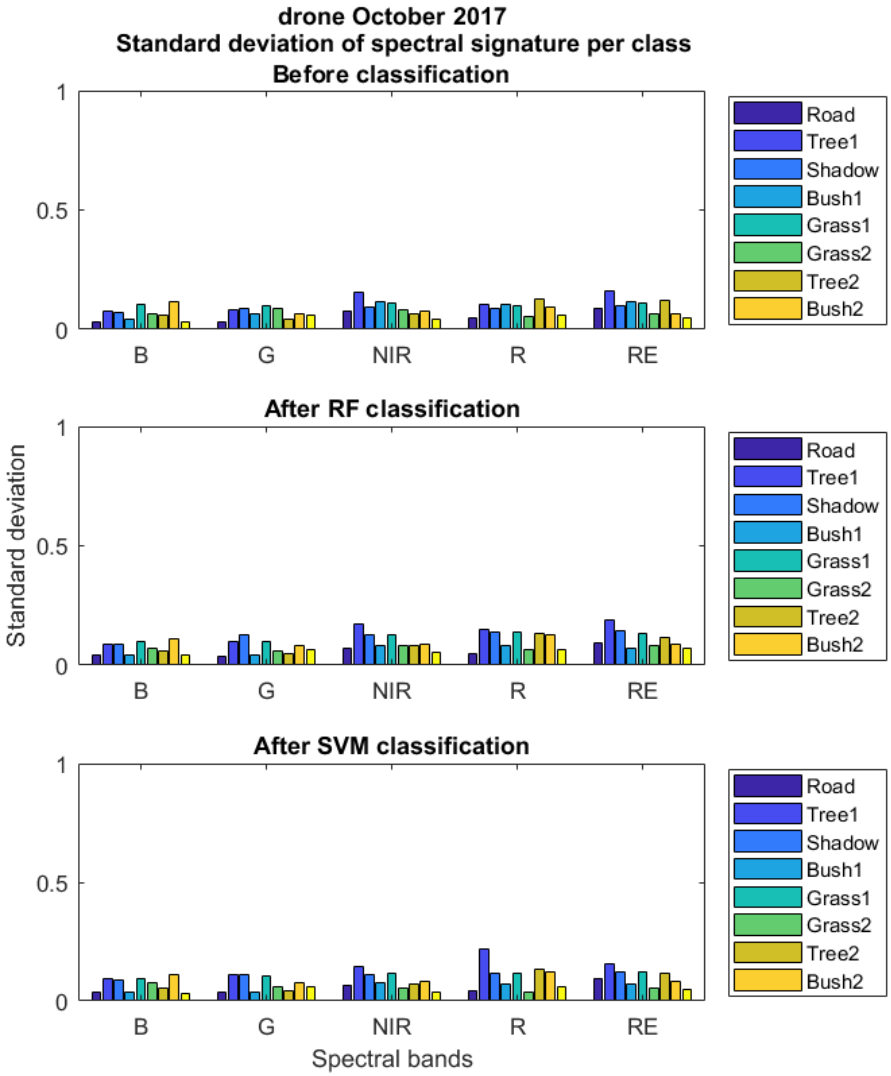

Figure 2: Standard deviation of spectral signature by class, drone October 2017

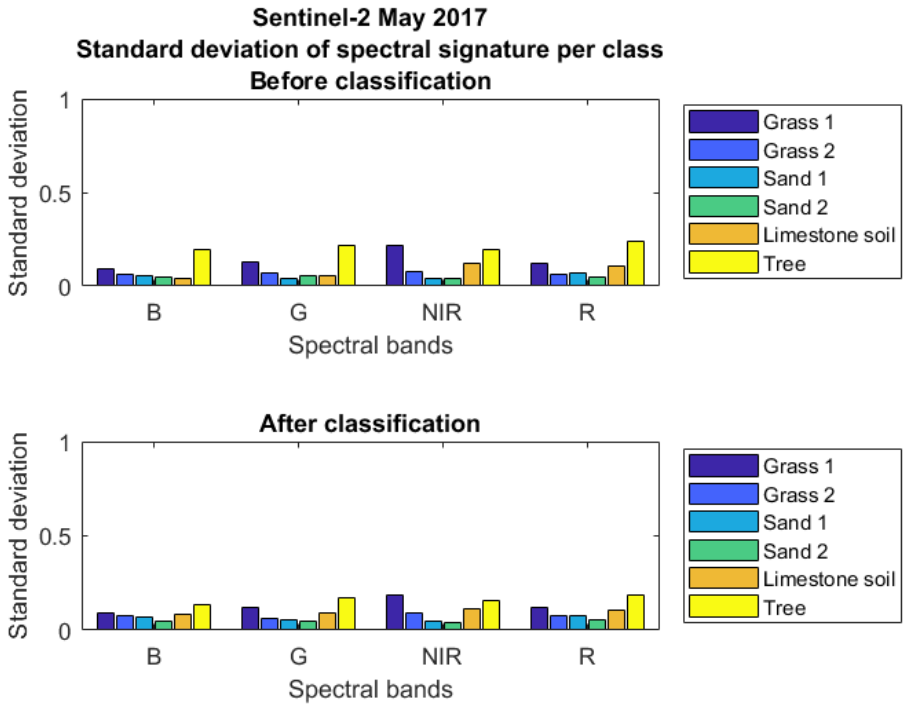

Figure 3: Standard deviation of spectral signature by class, Sentinel-2 May 2017

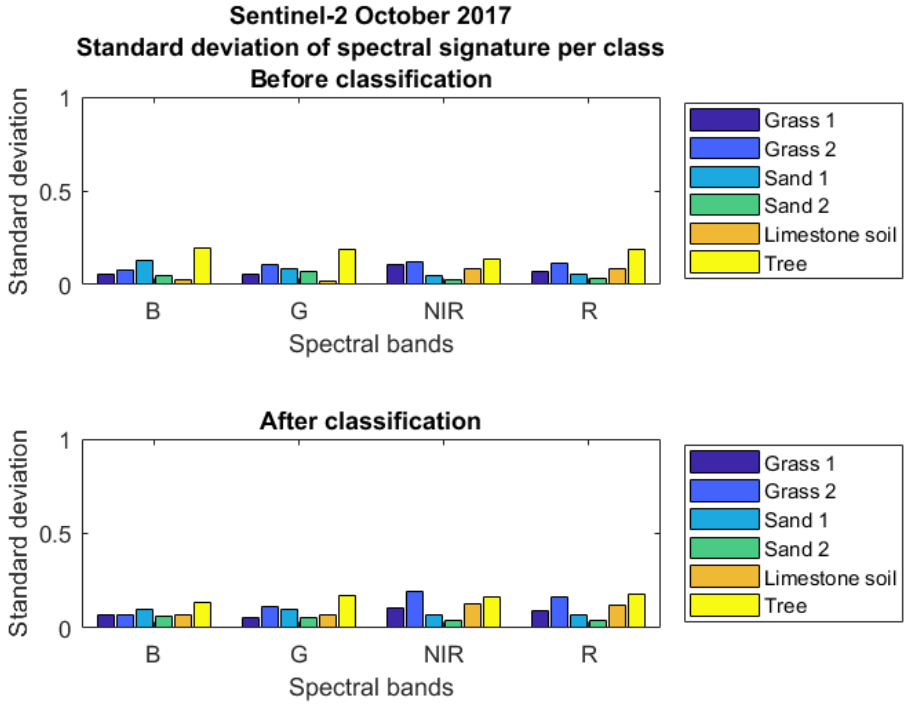

Figure 4: Standard deviation of spectral signature by class, Sentinel-2 October 2017

BIBLIOGRAPHY

R. Achanta, A. Shaji, K. Smith, A. Lucchi, P. Fua, and S. Süsstrunk. Slic superpixels compared to state-of-the-art superpixel methods. *IEEE Transactions on Pattern Analysis and Machine Intelligence*, 34(11):2274–2282, Nov 2012. ISSN 0162-8828. doi: 10.1109/TPAMI.2012.120.

B. Bacchilega. Personal photo, October 2017.

B. Bacchilega. Phenological stages of perennial and annual grasses. 2018.

C. A. Baldeck, M. S. Colgan, J.-B. Féret, Shaun R. Levick, R. E. Martin, and G. P. Asner. Landscape-scale variation in plant community composition of an African savanna from airborne species mapping. *Ecological Applications*, 24(1):84–93, 2014.

M. Belgiu and L. Drăguţ. Random forest in remote sensing: A review of applications and future directions. *ISPRS Journal of Photogrammetry and Remote Sensing*, 114:24–31, April 2016. ISSN 09242716. doi: 10.1016/j.isprsjprs.2016.01.011. URL http://linkinghub.elsevier.com/retrieve/pii/S0924271616000265.

Bluesky. How does LiDAR work?, 2017. URL http://www.lidar-uk.com/how-lidar-works/.

G. Boden. The Khwe and West Caprivi before Namibian independence: Matters of land, labour, power and alliance. *Journal of Namibian Studies: History Politics Culture*, 5:27–71, 2009.

T. Borowik, N. Pettorelli, L. Sönnichsen, and B. Jędrzejewska. Normalized difference vegetation index (NDVI) as a predictor of forage availability for ungulates in forest and field habitats. *European Journal of Wildlife Research*, 59(5):675–682, October 2013. ISSN 1612-4642, 1439-0574. doi: 10.1007/s10344-013-0720-0. URL http://link.springer.com/10.1007/s10344-013-0720-0.

J. du P. Bothma and J. G. du Toit, editors. *Game Ranch Management*. Van Schaik Publishers, Pretoria, 5th revised edition edition edition, January 2010. ISBN 978-0-627-02715-4.

P. Burai, B. Deák, O. Valkó, and T. Tomor. Classification of Herbaceous Vegetation Using Airborne Hyperspectral Imagery. *Remote Sensing*, 7(2):2046–2066, February 2015. ISSN 2072-4292. doi: 10.3390/rs70202046. URL http://www.mdpi.com/2072-4292/7/2/2046/.

M. Colgan, C. Baldeck, J-B. Féret, and G. Asner. Mapping Savanna Tree Species at Ecosystem Scales Using Support Vector Machine Classification and BRDF Correction on Airborne Hyperspectral and LiDAR Data. *Remote Sensing*, 4(12):3462–3480, November 2012. ISSN 2072-4292. doi: 10.3390/rs4113462. URL http://www.mdpi.com/2072-4292/4/11/3462/.

J. N. De Klerk. *Bush encroachment in Namibia: report on phase 1 of the Bush Encroachment Research, Monitoring, and Management Project*. Ministry of Environment and Tourism, Directorate of Environmental Affairs, Windhoek, Namibia, 2004. ISBN 978-0-86976-620-0.

F. de Morsier. Image processing for earth observation, EPFL, 2017.

DigitalGlobe. DigitalGlobe - See a Better World With High-Resolution Satellite Imagery, 2018. URL https://www.digitalglobe.com/.

ESA. Sentinel-2 - ESA Operational EO Missions - Earth Online - ESA, 2017a. URL https://earth.esa.int/web/guest/missions/esa-operational-eo-missions/sentinel-2.

ESA. Spatial - Resolutions - Sentinel-2 MSI - User Guides - Sentinel Online, 2017b. URL https://earth.esa.int/web/sentinel/user-guides/sentinel-2-msi/resolutions/spatial.

A. Ghosh and P.K. Joshi. A comparison of selected classification algorithms for mapping bamboo patches in lower Gangetic plains using very high resolution WorldView 2 imagery. *International Journal of Applied Earth Observation and Geoinformation*, 26:298–311, February 2014. ISSN 03032434. doi: 10.1016/j.jag.2013.08.011. URL http://linkinghub.elsevier.com/retrieve/pii/S0303243413000974.

D. Girardeau-Montaut. CloudCompare - Open Source project, 2003. URL http://www.cloudcompare.org/.

C. Giri, B. Pengra, J. Long, and T.R. Loveland. Next generation of global land cover characterization, mapping, and monitoring. *International Journal of Applied Earth Observation and Geoinformation*, 25:30–37, December 2013. ISSN 03032434. doi: 10.1016/j.jag.2013.03.005. URL http://linkinghub.elsevier.com/retrieve/pii/S0303243413000342.

R. Hijmans. Global Administrative Areas, January 2018. URL http://www.gadm.org/country.

DnI Institute. CART Decision Tree: Gini Index Explained, July 2015a. URL http://dni-institute.in/blogs/cart-decision-tree-gini-index-explained/.

DnI Institute. GINI Index: Work out Example, July 2015b. URL http://dni-institute.in/blogs/gini-index-work-out-example/.

V. Jagannath. Random Forest Template for TIBCO Spotfire® - Wiki page | TIBCO Community, March 2017. URL https://community.tibco.com/wiki/random-forest-template-tibco-spotfirer-wiki-page.

H. G. Jones and R. A. Vaughan. *Remote Sensing of Vegetation: Principles, Techniques, and Applications*. OUP Oxford, July 2010. ISBN 978-0-19-920779-4. Google-Books-ID: sTmcAQAAQBAJ.

R. Joshi. Accuracy, Precision, Recall & F1 Score: Interpretation of Performance Measures, September 2016. URL http://blog.exsilio.com/all/accuracy-precision-recall-f1-score-interpretation-of-performance-measures/.

D.F. Joubert, A. Rothauge, and G.N. Smit. A conceptual model of vegetation dynamics in the semiarid Highland savanna of Namibia, with particular reference to bush thickening by Acacia mellifera. *Journal of Arid Environments*, 72(12):2201–2210, December 2008. ISSN 01401963. doi: 10.1016/j.jaridenv.2008.07.004. URL http://linkinghub.elsevier.com/retrieve/pii/S0140196308001900.

A. Juel, G. B. Groom, J-C. Svenning, and R. Ejrnæs. Spatial application of Random For-

est models for fine-scale coastal vegetation classification using object based analysis of aerial orthophoto and DEM data. *International Journal of Applied Earth Observation and Geoinformation*, 42:106–114, October 2015. ISSN 03032434. doi: 10.1016/j.jag.2015.05.008. URL http://linkinghub.elsevier.com/retrieve/pii/S0303243415001178.

N. Juergens. Photo Guide to Plants of Southern Africa, October 2005. URL http://www.southernafricanplants.net/plantdata_sub.php?Mspec_ID=6030.

N. Keshava. A survey of spectral unmixing algorithms. *Lincoln Laboratory Journal*, 14(1):55–78, 2003.

Kuzikus. Visible Biodiversity of Kuzikus (Fauna & Flora), 2017. OCLC: 591659441.

Kuzikus. Kuzikus - Wildlife Reserve Namibia, 2018. URL http://www.kuzikus-namibia.de/xe_index.html.

Leskovec, Rajaraman, and Ullman. The k Means Algorithm | Stanford University, 2016. URL https://www.youtube.com/watch?v=RD0nNK51Fp8.

R. Lösch. How to compute impurity using Gini Index?, 2017. URL https://www.researchgate.net/post/How_to_compute_impurity_using_Gini_Index.

M. Mafanya, P. Tsele, J. Botai, P. Manyama, B. Swart, and T. Monate. Evaluating pixel and object based image classification techniques for mapping plant invasions from UAV derived aerial imagery: Harrisia pomanensis as a case study. *ISPRS Journal of Photogrammetry and Remote Sensing*, 129:1–11, July 2017. ISSN 09242716. doi: 10.1016/j.isprsjprs.2017.04.009. URL http://linkinghub.elsevier.com/retrieve/pii/S0924271616304944.

MathWorks. MATLAB - MathWorks, 1984. URL https://ch.mathworks.com/products/matlab.html.

MathWorks. MATLAB fitcecoc, 2017a. URL https://ch.mathworks.com/help/stats/fitcecoc.html#inputarg_Coding.

MathWorks. imhistmatchn, 2017b. URL https://ch.mathworks.com/help/images/ref/imhistmatchn.html.

MathWorks. MATLAB superpixels, 2017c. URL https://ch.mathworks.com/help/images/ref/superpixels.html?s_tid=doc_ta.

MathWorks. Create bag of decision trees - MATLAB, 2017d. URL https://ch.mathworks.com/help/stats/treebagger.html?requestedDomain=www.mathworks.com.

M. L. McHugh. Interrater reliability: the kappa statistic. *Biochemia Medica*, 22(3):276–282, October 2012. ISSN 1330-0962. URL https://www.ncbi.nlm.nih.gov/pmc/articles/PMC3900052/.

A. Michez, H. Piégay, L. Jonathan, H. Claessens, and P. Lejeune. Mapping of riparian invasive species with supervised classification of Unmanned Aerial System (UAS) imagery. *International Journal of Applied Earth Observation and Geoinformation*, 44:88–94, February 2016. ISSN 03032434. doi: 10.1016/j.jag.2015.06.014. URL http://linkinghub.elsevier.com/retrieve/pii/S0303243415300040.

N. Moleele, S. Ringrose, W. Arnberg, B. Lunden, and C. Vanderpost. Assessment of vegetation indexes useful for browse (forage) prediction in semi-arid rangelands. *International Journal of Remote Sensing*, 22(5):741–756, January 2001. ISSN 0143-1161, 1366-5901. doi: 10.1080/01431160051060147. URL http://www.tandfonline.com/doi/abs/10.1080/01431160051060147.

Berkeley University of California. Random forests - classification description, 2017. URL https://www.stat.berkeley.edu/~breiman/RandomForests/cc_home.htm.

F. Ofli, P. Meier, M. Imran, C. Castillo, D. Tuia, N. Rey, J. Briant, P. Millet, F. Reinhard, M. Parkan, and S. Joost. Combining Human Computing and Machine Learning to Make Sense of Big (Aerial) Data for Disaster Response. *Big Data*, 4(1):47–59, March 2016. ISSN 2167-6461, 2167-647X. doi: 10.1089/big.2014.0064. URL http://online.liebertpub.com/doi/10.1089/big.2014.0064.

M. Parkan. Digital-Forestry-Toolbox: A collection of digital forestry tools for Matlab, August 2017. URL https://github.com/mparkan/Digital-Forestry-Toolbox. original-date: 2016-05-13T07:30:11Z.

M. C. Peel, B. L. Finlayson, and T. A. McMahon. Updated world map of the Köppen-Geiger climate classification. *Hydrology and Earth System Sciences*, 11(5):1633–1644, 2007. doi: 10.5194/hess-11-1633-2007. URL https://www.hydrol-earth-syst-sci.net/11/1633/2007/.

Pix4D. Generate 2d and 3d information, purely from images with Pix4d, 2017. URL https://pix4d.com/.

A. Ramoelo, M. A. Cho, R. SA Mathieu, A. K. Skidmore, M. Schlerf, and I. M. A. Heitkönig. Estimating grass nutrients and biomass as an indicator of rangeland (forage) quality and quantity using remote sensing in Savanna ecosystems. 2012.

S. Ray. Understanding Support Vector Machine algorithm from examples (along with code), September 2017. URL https://www.analyticsvidhya.com/blog/2017/09/understaing-support-vector-machine-example-code/.

F. Reinhard. Personal conversation, September 2017.

N. Rey, M. Volpi, S. Joost, and D. Tuia. Detecting animals in African Savanna with UAVs and the crowds. *Remote Sensing of Environment*, 200:341–351, October 2017. ISSN 00344257. doi: 10.1016/j.rse.2017.08.026. URL http://linkinghub.elsevier.com/retrieve/pii/S0034425717303942.

J. G. Robinson and E. L. Bennett. Having your wildlife and eating it too: an analysis of hunting sustainability across tropical ecosystems. *Animal Conservation*, 7(4):397–408, November 2004. ISSN 1469-1795. doi: 10.1017/S1367943004001532. URL http://onlinelibrary.wiley.com/doi/10.1017/S1367943004001532/abstract.

S. L. Savage, R. L. Lawrence, and J. R. Squires. Predicting relative species composition within mixed conifer forest pixels using zero-inflated models and Landsat imagery. *Remote Sensing of Environment*, 171:326–336, December 2015. ISSN 00344257. doi: 10.1016/j.rse.2015.10.013. URL http://linkinghub.elsevier.com/retrieve/pii/S0034425715301644.

SAVMAP. SAVMAP | LASIG, October 2017. URL http://lasig.epfl.ch/savmap.

senseFly. senseFly, 2017a. URL https://sensefly.com.

senseFly. senseFly - eBee Plus, 2017b. URL https://sensefly.com/drone/ebee-plus-survey-drone.

G. Sherman. QGIS project, 2002. URL https://www.qgis.org/en/site/.

M. O. Smith, S. L. Ustin, J. B. Adams, and A. R. Gillespie. Vegetation in deserts: I. A regional measure of abundance from multispectral images. *Remote sensing of Environment*, 31(1):1–26, 1990.

B Strohbach. Photo Guide to Plants of Southern Africa, April 2014. URL http://www.southernafricanplants.net/plantdata_sub.php?Mspec_ID=567.

Z. K. Tessema, W. F. de Boer, and H. H.T. Prins. Changes in grass plant populations and temporal soil seed bank dynamics in a semi-arid African savanna: Implications for restoration. *Journal of Environmental Management*, 182:166–175, November 2016. ISSN 03014797. doi: 10.1016/j.jenvman.2016.07.057. URL http://linkinghub.elsevier.com/retrieve/pii/S0301479716304947.

A. Trevino. Introduction to K-means Clustering, 2017. URL https://www.datascience.com/blog/k-means-clustering.

N. M. Trodd and A. J. Dougill. Monitoring vegetation dynamics in semi-arid African rangelands: Use and limitations of Earth observation data to characterize vegetation structure. *Applied Geography*, 18(4):315–330, 1998.

USGS. EarthExplorer, 2017. URL https://earthexplorer.usgs.gov/.

G. Vaglio Laurin, Q. Chen, J. A. Lindsell, D. A. Coomes, F. Frate, L. Del Guerriero, F. Pirotti, and R. Valentini. Above ground biomass estimation in an African tropical forest with lidar and hyperspectral data. *ISPRS Journal of Photogrammetry and Remote Sensing*, 89:49–58, March 2014. ISSN 09242716. doi: 10.1016/j.isprsjprs.2014.01.001. URL http://linkinghub.elsevier.com/retrieve/pii/S0924271614000045.

F. van Langevelde, Z. K. Tessema, W. F. de Boer, and H. H.T. Prins. Soil seed bank dynamics under the influence of grazing as alternative explanation for herbaceous vegetation transitions in semi-arid rangelands. *Ecological Modelling*, 337:253–261, October 2016. ISSN 03043800. doi: 10.1016/j.ecolmodel.2016.07.013. URL http://linkinghub.elsevier.com/retrieve/pii/S0304380016302551.

B. H. Walker, D. Ludwig, C. S. Holling, and R. M. Peterman. Stability of Semi-Arid Savanna Grazing Systems. *The Journal of Ecology*, 69(2):473, July 1981. ISSN 00220477. doi: 10.2307/2259679. URL http://www.jstor.org/stable/2259679?origin=crossref.

S. Yee and T. Chu. A visual introduction to machine learning, 2017. URL http://www.r2d3.us/visual-intro-to-machine-learning-part-1/.

Q. Yu, P. Gong, N. Clinton, G. Biging, M. Kelly, and D. Schirokauer. Object-based detailed vegetation classification with airborne high spatial resolution remote sensing imagery. *Photogrammetric Engineering & Remote Sensing*, 72(7):799–811, 2006.

C. Zey. Principal Components, 2017. URL http://www.itl.nist.gov/div898/handbook/pmc/section5/pmc55.htm.

Q. Zhang, R. Qin, X. Huang, Y. Fang, and L. Liu. Classification of Ultra-High Resolution Orthophotos Combined with DSM Using a Dual Morphological Top Hat Profile. *Remote Sensing*, 7(12):16422–16440, December 2015. ISSN 2072-4292. doi: 10.3390/rs71215840. URL http://www.mdpi.com/2072-4292/7/12/15840.